NASA CR-159639
R79AEG366

CF6 JET ENGINE PERFORMANCE IMPROVEMENT

NEW FRONT MOUNT

Final Report

December 1979

W.A. Fasching

General Electric Company
Aircraft Engine Group
Cincinnati, Ohio 45215

Prepared for

NATIONAL AERONAUTICS AND SPACE ADMINISTRATION
LEWIS RESEARCH CENTER
21000 BROOKPARK ROAD
CLEVELAND, OHIO 44135

Contract: NAS3-20629

FOREWORD

The work was performed by the CF6 Engineering Department of General Electric's Aircraft Engine Group, Aircraft Engine Engineering Division, Cincinnati, Ohio. The program was conducted for the National Aeronautics and Space Administration, Lewis Research Center, Cleveland, Ohio, under Subtask 2.4 of the CF6 Jet Engine Performance Improvement Program, Contract Number NAS3-20629. The Performance Improvement Program is part of the Engine Component Improvement (ECI) Project, which is part of the NASA Aircraft Energy Efficiency (ACEE) Program. The NASA Project Engineer for the New Front Mount Program was D.C. Reemsnyder. The program was initiated in February 1978 and was completed in March 1979.

The report was prepared by W.A. Fasching, General Electric Program Manager, with the assistance of H.J. Pinsent, D.F. Beatty, and W.R. Chiaramonte.

TABLE OF CONTENTS

1.0 SUMMARY

As part of the NASA-sponsored Engine Component Improvement Program a new engine thrust mount has been developed which reduces fuel consumption and performance degradation in current CF6 turbofan engines. This new front mount reduces the induced point loads in the high pressure compressor (HPC) casing, resulting in a decrease in localized case distortion. This in turn allows the compressor to operate with reduced blade-to-case tip clearances, which improves the compressor efficiency and, consequently, overall engine performance.

Maximum radial deflection at each stage of the high pressure compressor (HPC) case was reduced up to 42% with the new front mount under simulated takeoff loads. The predicted HPC performance improvement due to the new front mount was not fully realized. Initial tests of the original front mount were conducted with a relatively flexible engine configuration and indicated large local HP Compressor radial deflection. Subsequent tests of the original front mount with the DC-10 wing pylon, inlet, and fan reverser provided a stiffer and more realistic baseline engine installation and reduced the measured maximum radial deflection. This decreased the available or potential improvement that could be accomplished with the new front mount. Consequently, the demonstrated performance improvement was 0.1% in cruise sfc as compared to a predicted value of 0.3%. The new front mount provides a 1.5° C reduction in EGT at takeoff (predicted 3.5° C), a 16% improvement in HPC stall margin, and a 10% improvement in compressor stator angle margin. Improvements in the stall and stator angle margins are significant for a new compressor and are even greater for a deteriorated engine.

Low cycle fatigue testing demonstrated a life capability of the new front mount system hardware in excess of 35,000 simulated flight cycles. Factory engine and flight test results have indicated trouble-free operation with the new front mount, and showed that the link loads agree closely with the calculations. Improved roundness in the HPC case due to the new front mount will provide reduced operating and maintenance costs for all CF6 turbofan aircraft engines.

The New Front Mount Performance Improvement concept offers an annual fuel savings per aircraft of 18,500 to 77,500 liters (4900 to 20,500 gal.) depending on the aircraft application and mission range, plus reduced maintenance costs resulting from higher stall margins which will reduce unscheduled removals. Following the successful completion of component qualification static tests and factory engine testing the new front mount system has been certified and is now being incorporated into all new CF6-50 production engines.

2.0 INTRODUCTION

National energy demand has outpaced domestic supply creating an increased U.S. dependence on foreign oil. This increased dependence was dramatized by the OPEC oil embargo in the winter of 1973 to 1974. In addition, the embargo triggered a rapid rise in the cost of fuel which, along with the potential of further increases, brought about a changing economic circumstance with regard to the use of energy. These events, of course, were felt in the air transport industry as well as other forms of transportation. As a result of these experiences, the Government, with the support of the aviation industry, has initiated programs aimed at both the supply and demand aspects of the problem. The supply problem is being investigated by looking at increasing fuel availability from such sources as coal and oil shale. Efforts are currently underway to develop engine combustor and fuel systems that will accept fuels with broader specifications.

Reduced fuel consumption is the other approach to deal with the overall problem. A long-range effort to reduce consumption is to evolve new technology which will permit development of a more energy efficient turbofan or the use of a different propulsive cycle such as a turboprop. Although studies have indicated large reductions in fuel usage are possible (e.g., 15 to 40 percent), the impact of this approach in any significant way would be 15 or more years away. In the short term, the only practical propulsion approach is to improve the fuel efficiency of current engines. Examination of this approach has indicated that a 5 percent fuel reduction goal starting in the 1980 to 1982 time period is feasible for the CF6 engine. This engine is, and will continue to be, a significant fuel user for the next 15 to 20 years.

Accordingly, NASA is sponsoring the Aircraft Energy Efficient (ACEE) Program (based on a comgressional request), which is directed at reduced fuel consumption of commercial air transports. The Engine Component Improvement (ECI) Program is the element of the ACEE Program directed at reducing fuel consumption of current commercial aircraft engines. The ECI Program consists of two parts: Engine Diagnostics and Performance Improvement. The Engine Diagnostics effort is to provide information to identify the sources and causes of engine deterioration. The Performance Improvement effort is directed at developing engine components having performance improvement and retention characteristics which can be incorporated into new production and existing engines.

The initial Performance Improvement effort consisted of a Feasibility Analysis which was conducted in cooperation with the Boeing and Douglas Aircraft Companies and American and United Airlines, and is reported in Reference 1. This study identified engine component modifications which had fuel savings potential over current CF6 engines and provided a technical and economic assessment of these modifications. This assessment included a determination of airline acceptability, the probability of introducing the concepts into production by the 1980 to 1982 time period, and their retrofit potential.

In the Feasibility Analysis, the New Front Mount performance improvement concept was selected for development and evaluation in ground test facilities,

because of its fuel savings potential and high payback. The objective of the New Front Mount Program was to develop technology and to verify the predicted reductions in compressor case distortions by component tests. Reduced case distortions allow closer compressor blade and vane clearances which improve compressor efficiency, thus resulting in lower fuel consumption. Improvement in cruise sfc due to the reduction in compressor running clearance was estimated to amount to about 0.3 percent.

The New Front Mount Program was a 13-month effort of component structural tests and monitoring of engine tests. The structural tests consisted of stress, deflection/distortion, and low cycle fatigue tests. The stress test served to verify and determine critical stress areas of the new front mount. The deflection/distortion test consisted of three phases. The first phase was conducted to compare engine casing deflection, distortion and structural stresses for the original and the new front mount. The second phase tested the new front mount to failsafe load conditions, and the third phase examined stresses induced by thermal growth and assembly stackup conditions. The Low Cycle Fatigue (Endurance) Test was conducted to demonstrate the cyclic load capability of the new front mount system.

3.0 DESCRIPTION OF NEW FRONT MOUNT CONCEPT

General Electric has previously recognized the performance impact of local engine deflections and has conducted analytical and component tests to assess the problem and define potential solutions. The work, related to the compressor, has progressed to the point where a new front mount design, having the potential for reducing local compressor case deflections, was defined and prototype mounts were fabricated. Analytical predictions of the potential reduction in deflections were translated into a compressor performance improvement. This improvement was estimated to offer a reduction in engine specific fuel consumption of 0.3 percent and a reduction in exhaust gas temperature of 3.5° C. A modest increase in engine weight of 4.5 kg (10 lb) was predicted for the new front mount.

3.1 OVERALL DESIGN APPROACH

The mounting system for the CF6 engine is illustrated by the typical wing installation shown in Figure 3.1. The engine and nacelle are attached to the wing pylon by a front and rear mount; the front mount is designed to carry all thrust and axial inertia loads together with side and vertical loads, while the rear mount carries side load, vertical load, and rolling moment. The front mount to pylon joint is fully clamped, which results in secondary redundant moments about the pitch, roll, and yaw axes.

Analysis and component testing of the original front mount system has shown that the major portion of the axial thrust load is carried by the pin-ended rigid link which connects the front mount to the fan frame 12 o'clock midstrut casting (Figure 3.2). It was also shown that the clevis support beams, which connect the clevis to the HPC case flange, transmit large radial and axial point loads to the compressor casing. These point loadings result in localized compressor case distortions which, when combined with the engine casing "backbone" bending deflections, require larger-than-desired compressor blade-to-case clearances in order to eliminate rotor rubs. Further, aircraft certification of the higher thrust 244,650 N (55,000 lb) CF6-50C1 and CF6-50E engine configurations has indicated more extensive compressor rotor rubs through Stage 11 than previously observed. The original front mount system, at these higher rated thrust loads, would require a further increase in blade clearances with attendant losses in performance and stall margin, in order to eliminate rotor rubs.

General Electric performed component static load tests with the original front mount installation during which simulated flight loads were applied to the engine shell structure to induce loads on the front mount. Deformation of the high pressure compressor casing cross section relative to the rotor axis was recorded by deflection potentiometers mounted radially from the rotor shaft and swept through 360° to record the radial deflection of the casing. A typical result is shown in Figure 3.3. The maximum inward radial deflection (reduction in clearance) occurs at the top vertical (12 o'clock) centerline, and is the combined effect of local deflections due to vertical and axial punch loads and the overall bending of the compressor casing in the vertical plane.

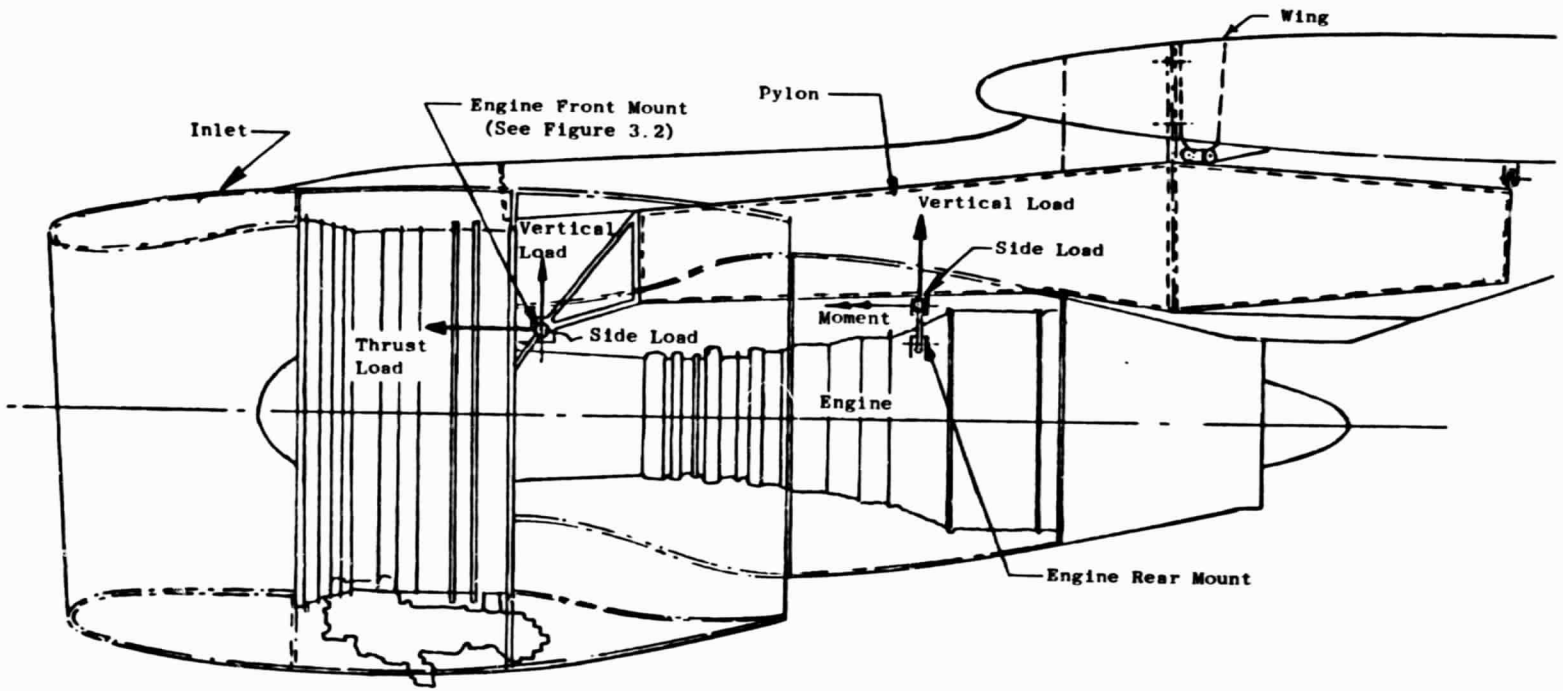

Figure 3.1. Typical Engine-Nacelle-Pylon-Wing Installation Showing Front and Rear Engine Mounts and Load Paths.

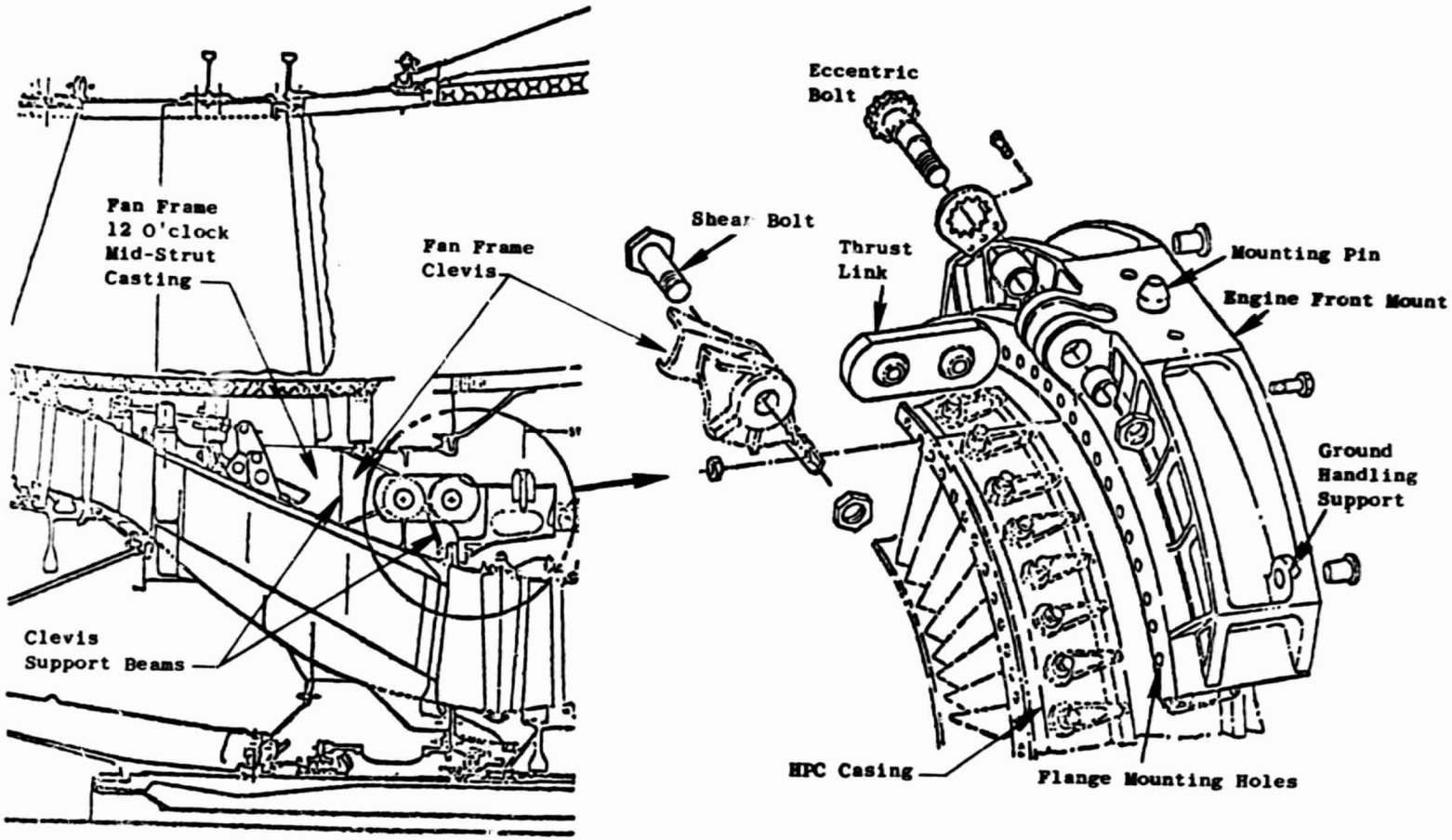

Figure 3.2. Original Front Mount System.

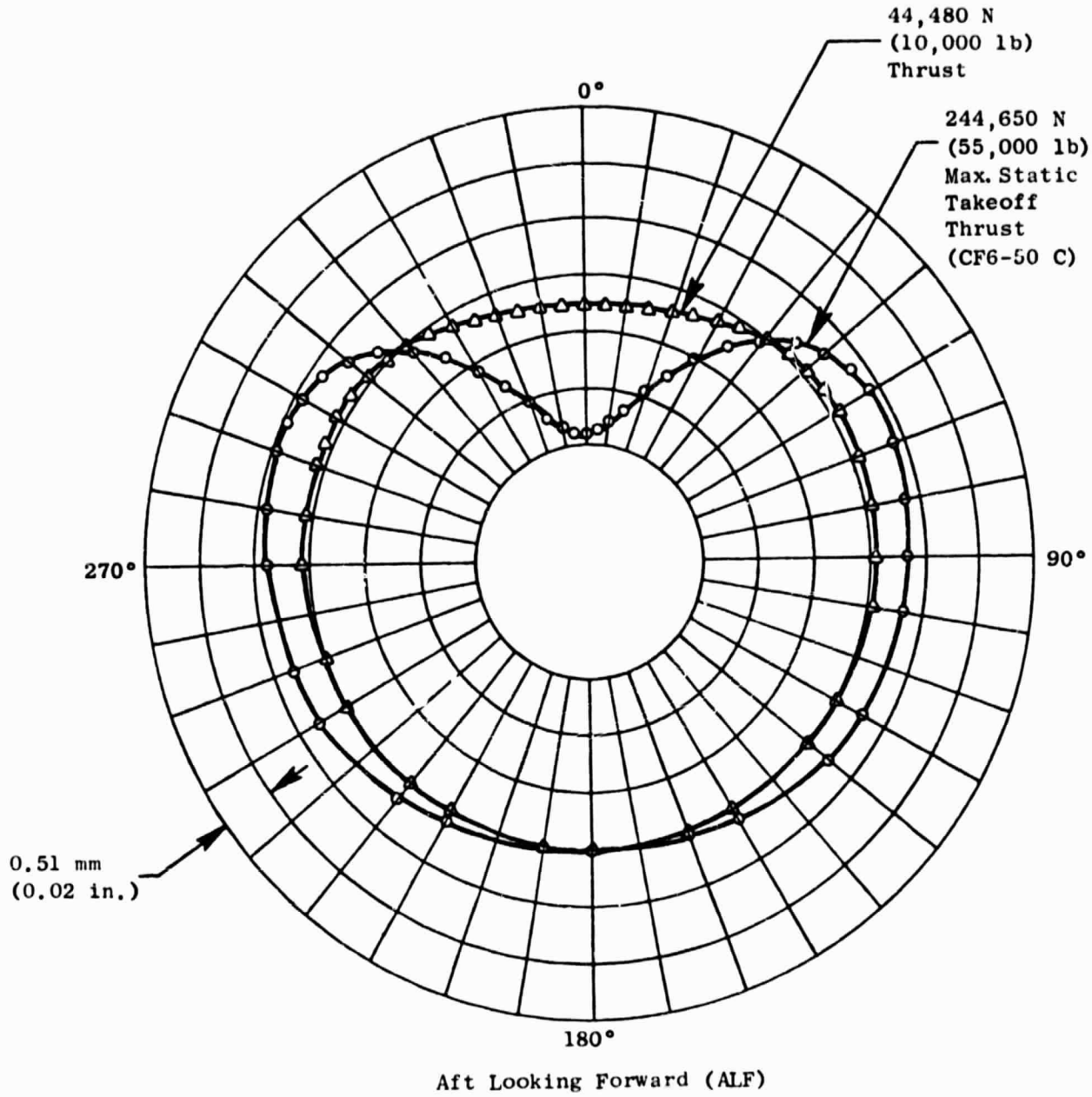

Figure 3.3. Typical HP Compressor Casing Distortion.

If the maximum radial deflection at each compressor stage is plotted versus the axial location of the stage, an upper backbone deflection curve is obtained. Figure 3.4 shows the upper backbone deflection obtained during a series of tests conducted to separate front mount individual load effects. Curve (a) shows the deflection for the simulated maximum static thrust condition with the engine weight supported (Zero G); Curve (b) shows the deflection for the same simulated maximum static thrust with the vertical reaction caused by the above-center applied thrust force reacted elsewhere; and Curve (c) shows the deflection when only the vertical load due to the simulated maximun thrust was induced on the mount.

Overall casing bending deflection was calculated from a harmonic analysis of the total deflection curve. The N=1 component of the Fourier Series obtained is the vertical translation of the section due to the overall bending of the casing. The final separation of individual effects is shown in Figure 3.5. The calculated total deflection due to simulated maximum static thrust is the sum of the experimental deflection values of the single point thrust load and the vertical reaction load, plus the calculated beam bending deflection. These results were used to correlate and fine tune the finite element computer structural model of the engine structure. A comparison between the resulting calculation of casing deflection and test measurement is shown in Figure 3.6. Very good agreement was obtained.

In addition to the distortion observed at the maximum static takeoff thrust condition, more severe bending deflection occurs during aircraft rotation at takeoff. This is caused by large vertical lift loads on the forward portion of the nacelle. A comparison between the HPC casing backbone deflection for these two conditions simulated during a static test with the original front mount is shown in Figure 3.7.

The basis of the reduction in deflection due to the local effect is illustrated in Figure 3.8. Curve (a) shows a typical exaggerated cardiod deflection curve obtained from a single point load application typical of the single center link original front mount; and Curve (b) illustrates the effect of splitting the single point into two loads of half the intensity located at 30° on each side of the center point. Combining these deflection curves results in the single curve of greatly reduced deflection amplitude shown by the dotted line.

Based on this effort a new front mount system was designed. The new front mount applies the engine thrust reaction at two points ±30° from the top vertical and reacts engine vertical and side forces with a series of links connected tangentially to the compressor casing forward flange (Figure 3.9). A prototype new front mount (Figure 3.10) was component tested and showed an appreciable reduction in compressor deflection. Figure 3.11 presents the predicted improvement in compressor deflection with the new front mount for the most severe takeoff at rotation loading condition. Also presented for comparison is the calculated core engine beam bending, which is the minimum distortion possible without major stiffening of the compressor case.

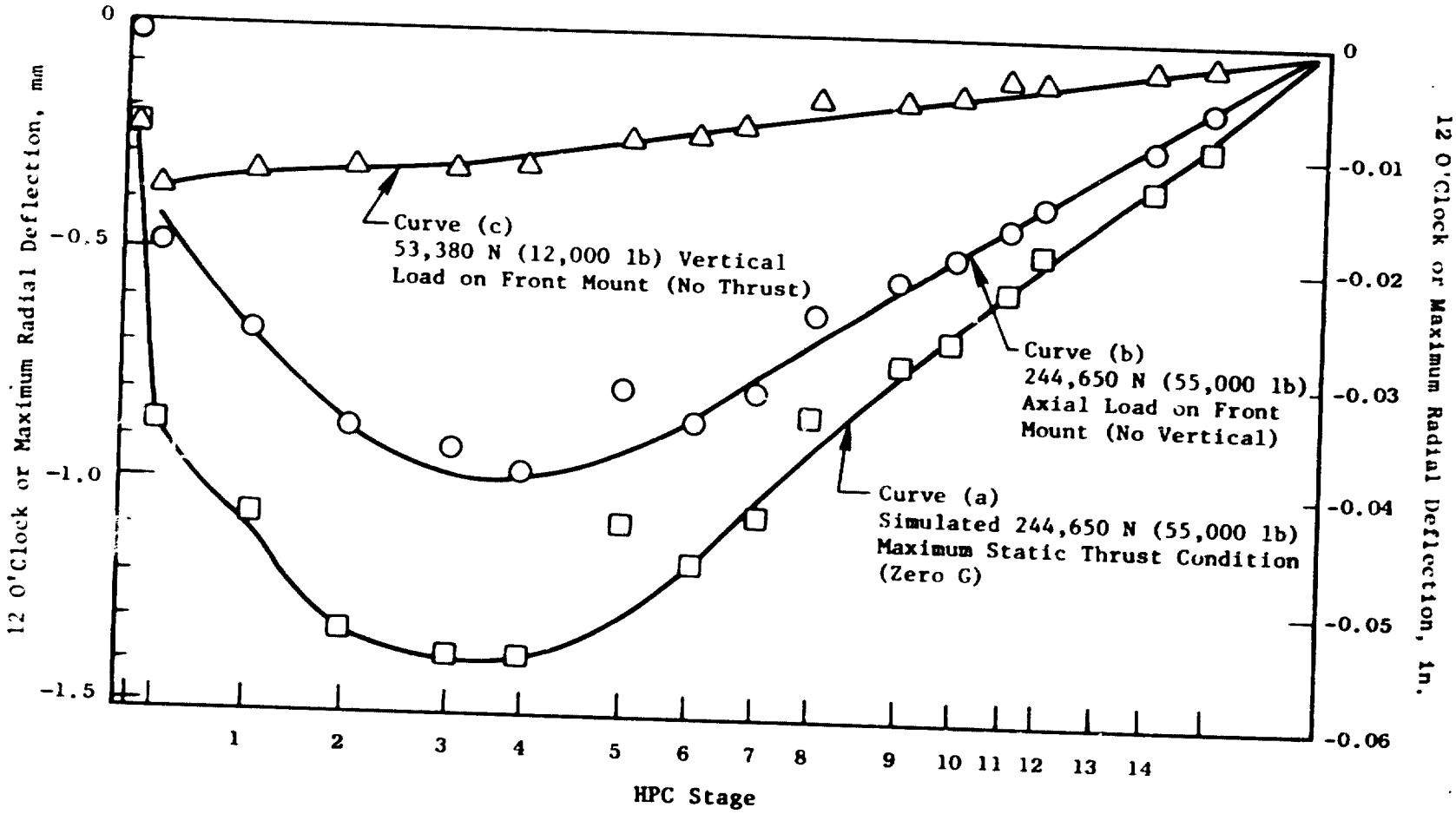

Figure 3.4. CF6-50 Original Front Mount - HPC Casing Backbone Radial Deflection, Effect of Vertical Reaction Due to Maximum Static Thrust.

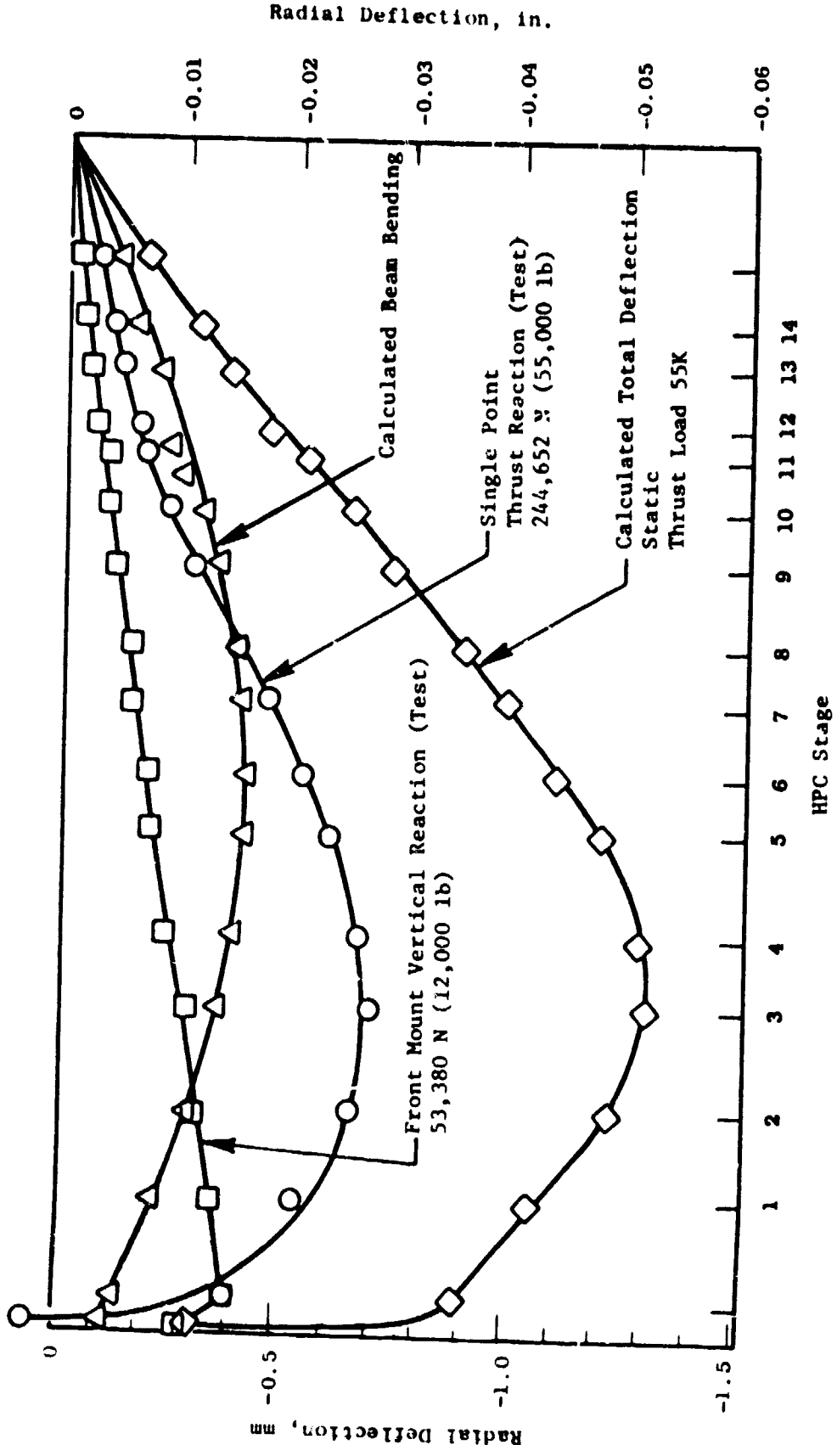

Figure 3.5. CF6-50 Original Front Mount – HPC Casing Backbone Radial Deflection, Individual Contributions to Total Deflection Due to Maximum Static Thrust.

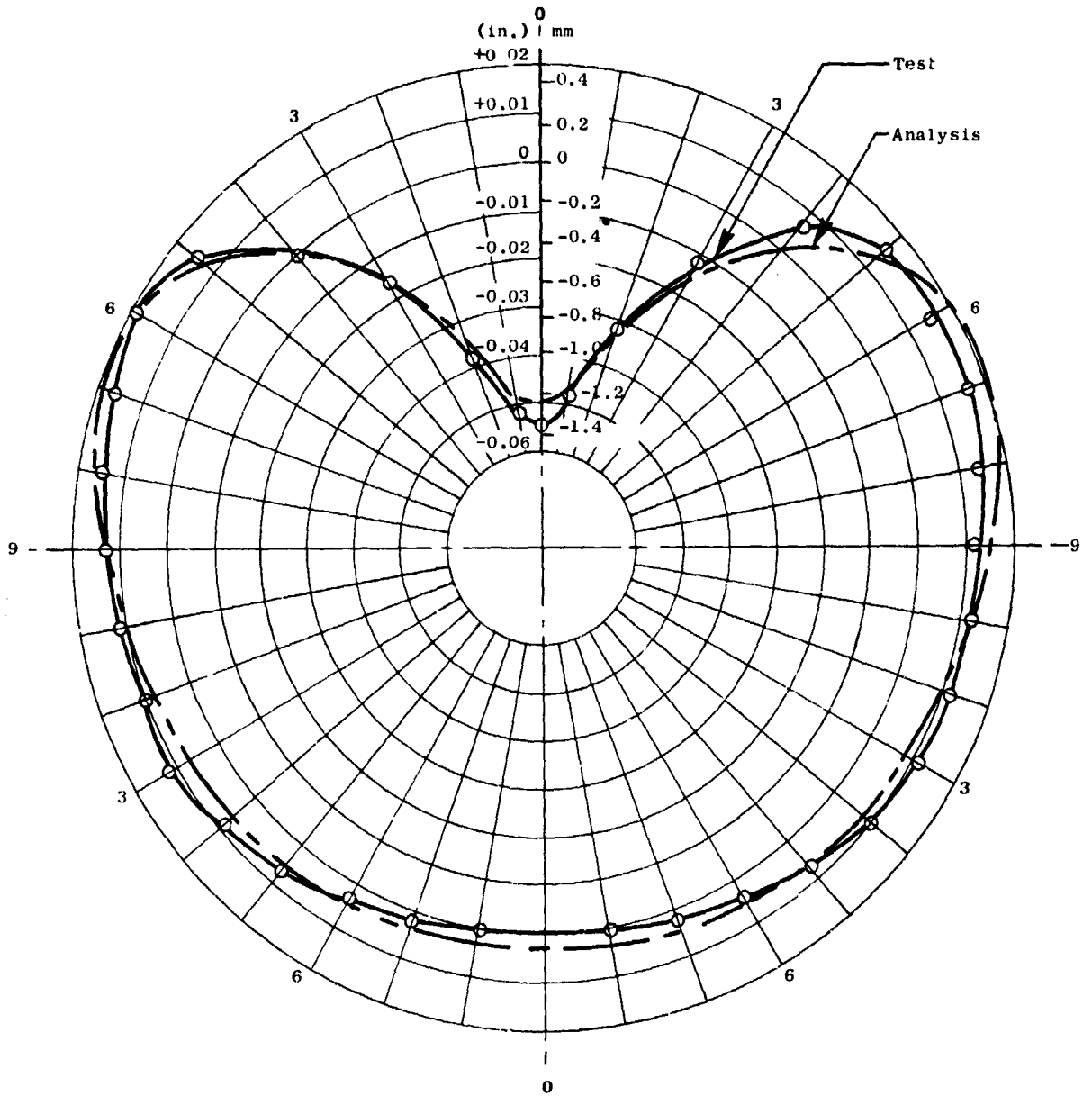

Figure 3.6. CF6-50 Original Front Mount; Maximum Static Thrust, Comparison Between Calculated and Measured HPC Casing Radial Deflection at Stage 3.

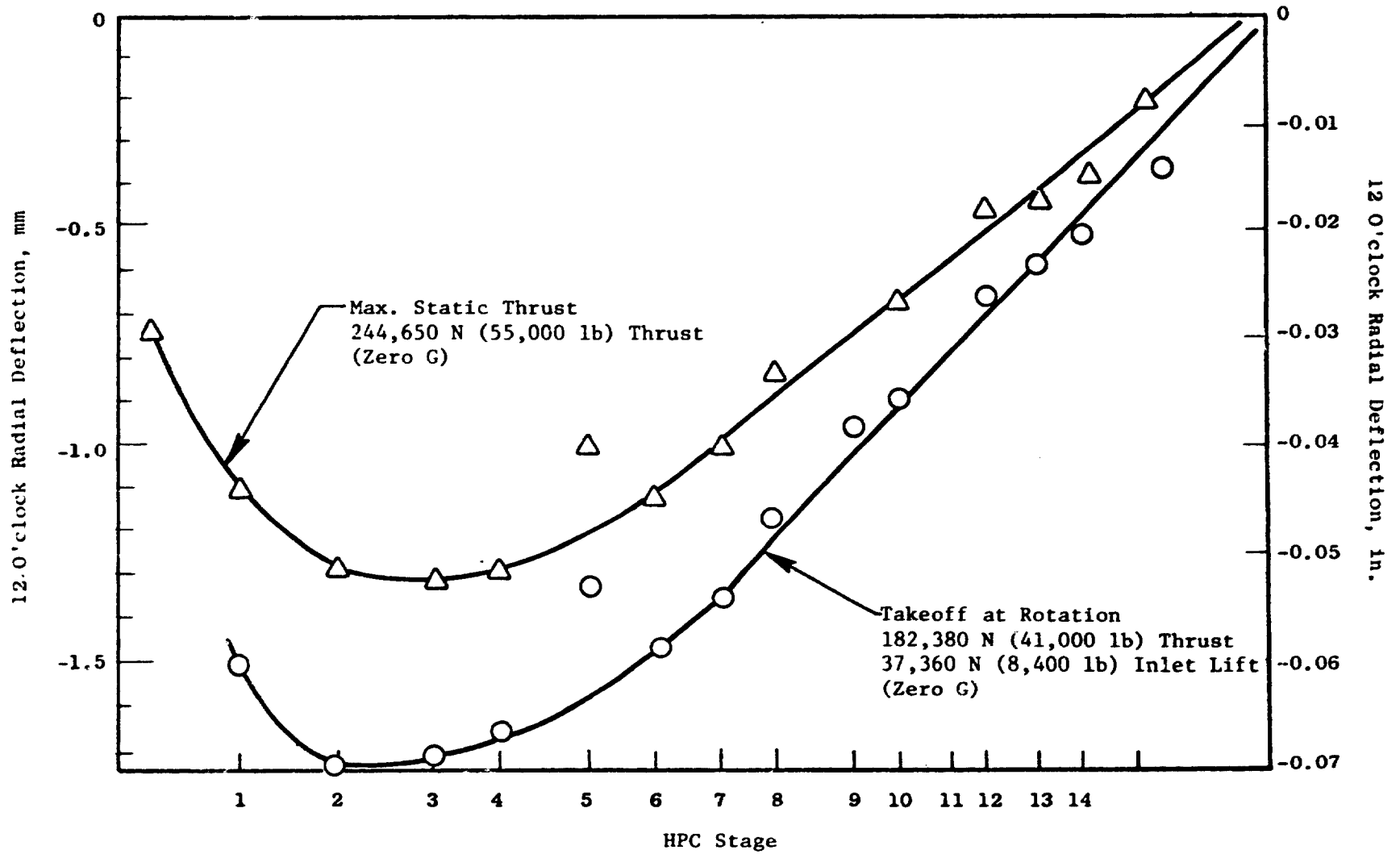

Figure 3.7. CF6-50 Wing Engine - Original Front Mount, HPC Backbone Radial Deflection for Maximum Static Thrust and Takeoff at Rotation Conditions.

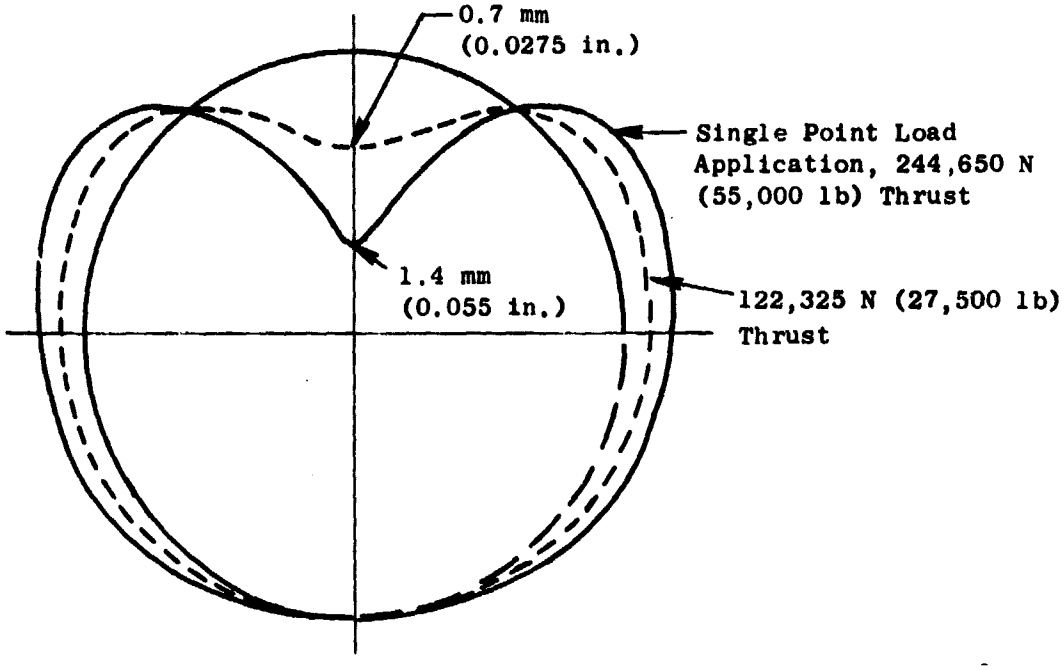

(a) Original Front Mount with Single Point Load Application

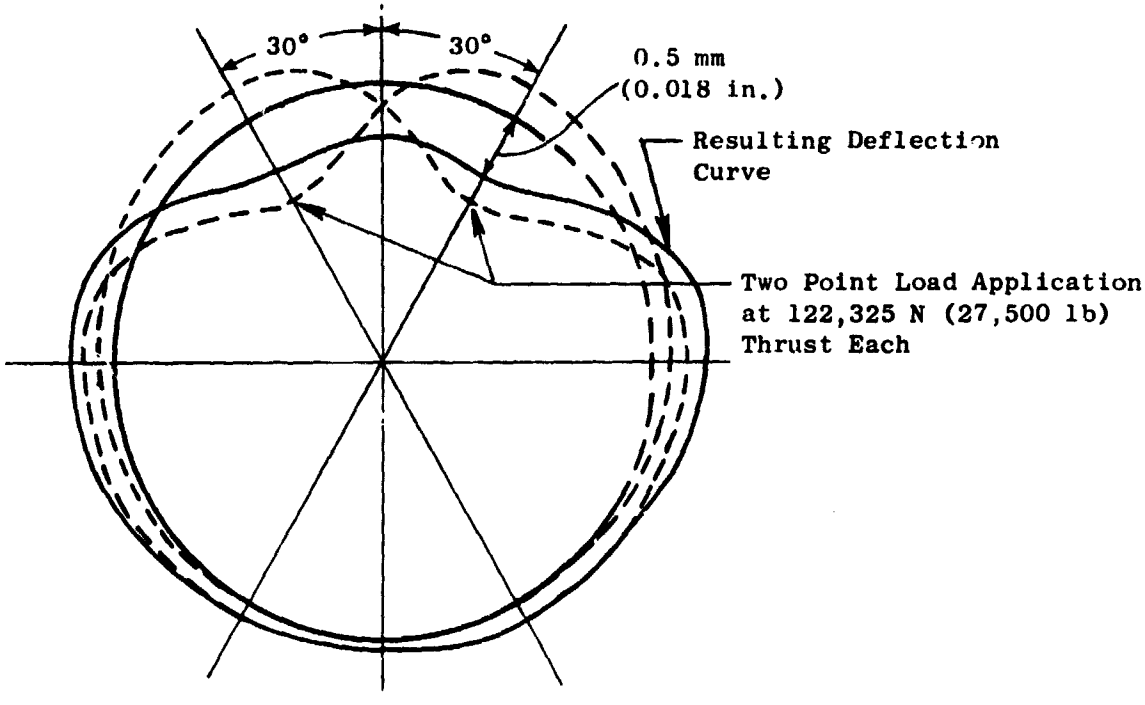

(b) New Front Mount with Two Point Load Application

Figure 3.8. Original and New Front Mounts, HPC Casing Radial Deflection Estimated Effect of Two Point Load Application at Max. Static Thrust (Zero G).

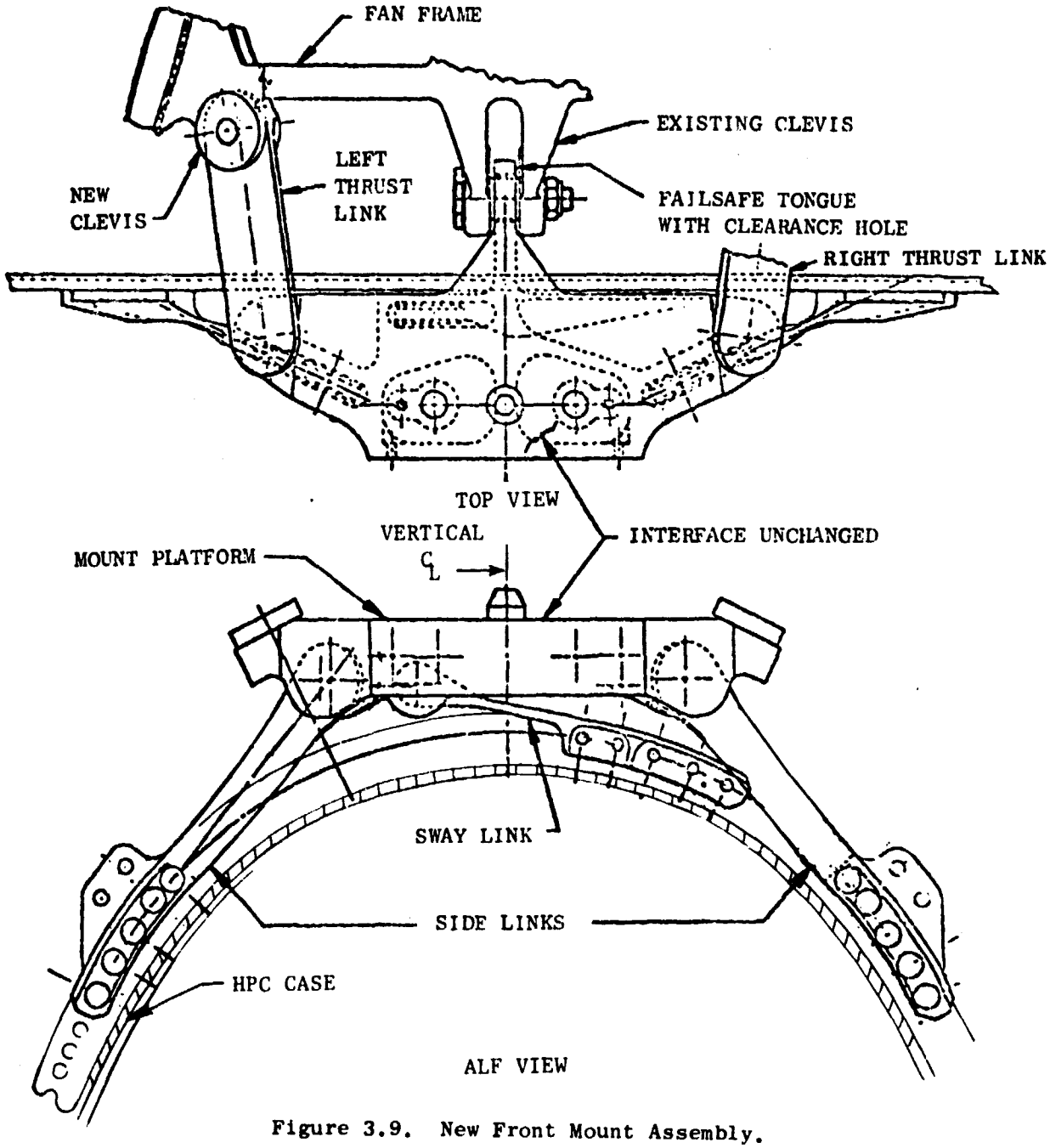

Figure 3.9. New Front Mount Assembly.

Figure 3.10. New Front Mount Prototype.

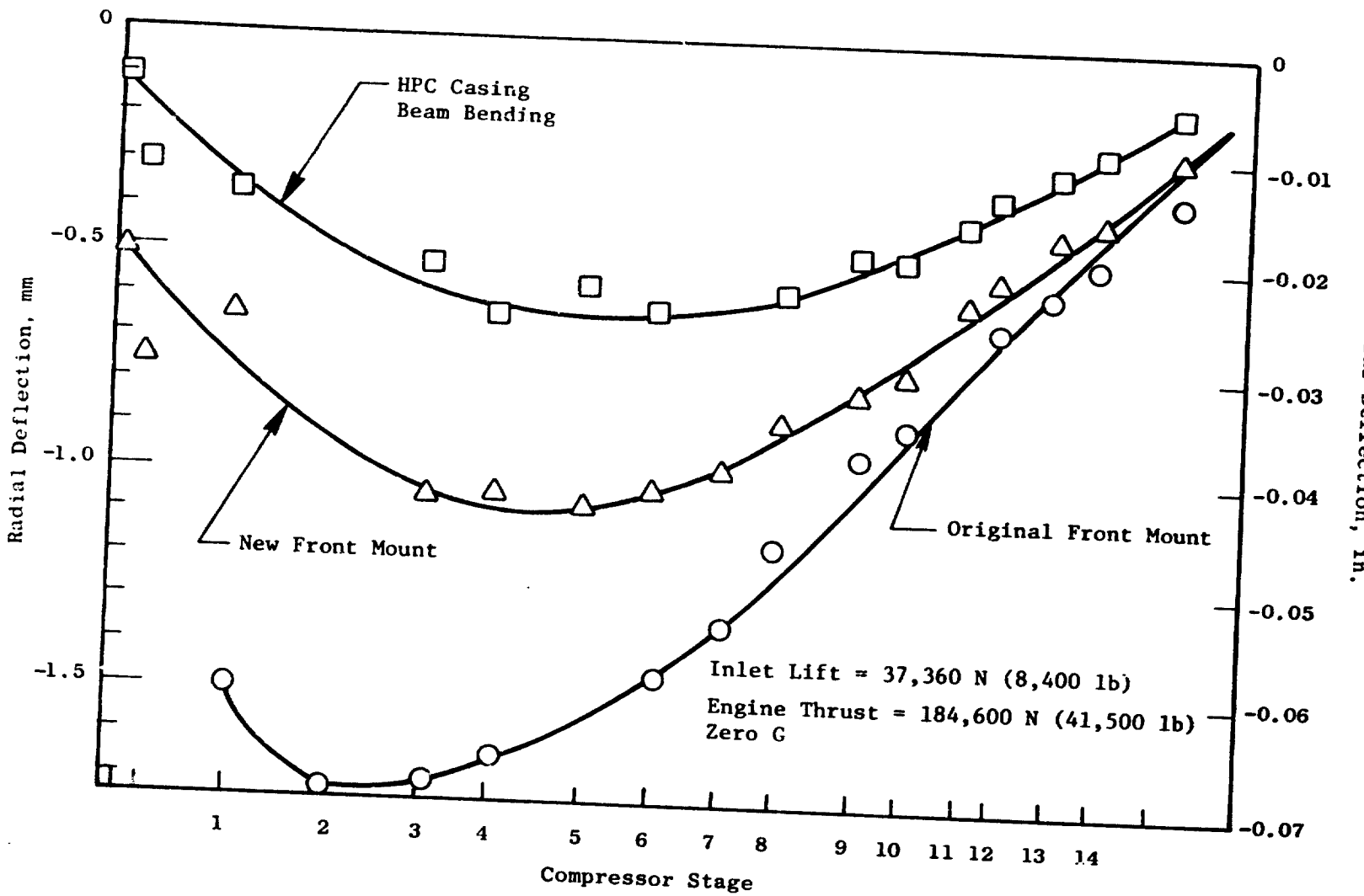

Figure 3.11. CF6-50 Original and New Front Mount - HPC Casing Backbone Bending Radial Deflection, Takeoff at Rotation Condition (Zero G).

3.2 DESIGN CRITERIA

The CF6-50 new front mount was designed to achieve a total useful life of at least 35,000 flight cycles or 50,000 aircraft operating hours, whichever occurs first. It was designed for operation to power settings and within the flight envelope defined in CF6-50 Model Specification E2162. Maneuver limit load factors for flight and landing conditions, and ultimate or crash conditions were already established for the original front mount design and have been adhered to for the new front mount. Failsafe loads and failure criteria were established in conjunction with airframe manufacturers and the requirements of FAR 25.

Simulated low cycle fatigue loads were established to represent 35,000 flight cycles plus the cumulative effect of all flight maneuver and gust conditions. All engine/airframe interfaces were required to be identical to those of the original front mount.

3.3 DESIGN DESCRIPTION AND CHARACTERISTICS

The new front mount platform is a 6Al-4Va titanium forging which provides a front mount to airframe interface which is identical to the original design. The platform contains five clevises for the attachment of links which distribute the loads into the fan frame and compressor casing such that the compressor casing distortions are reduced.

The supporting members, two thrust links, two side links, and one sway link are manufactured from 18% nickel maraging steel; grade 300. (The low cycle fatigue test of this material is described in Appendix B). Corrosion protection for the links is provided by a sealed aluminum spray coating. All attachment bolts are of tensilized Inco 718 material. Figures 3.9 and 3.10 show the assembled front mount components.

A failsafe feature is provided as an integral part of the mount platform, in the form of a tongue with an oversized and elongated hole for the bolt which connects it to the fan frame 12 o'clock clevis. In the original engine mount design this clevis carried all the axial thrust loads. In the new design the tongue and clevis provide an additional axial, vertical, and side load path in the event of failure of any of the supporting links or attachment hardware.

The fan frame is modified locally to provide additional attachment clevises for the new thrust links together with local reinforcement to the one o'clock and eleven o'clock strut root castings for the new clevis loads.

Maintainability

Compared with the original front mount, maintainability of the new front mount is unchanged. Major interface surfaces have again been shot peened and coated with a dry film lubricant to prevent the occurrence of fretting.

Installation procedures at the new front mount pylon interface are unchanged from the original mount. Installation of the new front mount on the engine at the fan frame and compressor casing front flange does entail the use of an additional tool, a torque multiplier, to tighten the two bolts attaching the thrust links to the front mount.

Reliability

The new front mount was designed to achieve a total useful life of 35,000 flight cycles and to operate for power settings and maneuver load factors for flight and landing defined in the engine model specifications. Design limit and fatigue conditions were established in conjunction with the airframe designers, and a rigorous structural integrity test program of limit, ultimate, and fatigue loadings has been conducted. Front mount component loads and temperatures have been measured during factory engine and flight tests and were correlated with the design loads used for the analysis and component testing.

Safety

The new front mount was designed for engine operation within the power settings and load factors established for flight and landing levels for 35,000 flight cycles. All major load paths in the mount are redundant and an additional load path, in the form of the failsafe tongue which does not normally carry loads, has been incorporated.

Failsafe conditions have been established in conjunction with the airframe manufacturer in which failure of one or more of the front mount load paths has been assumed. Continuous operation of the aircraft under normal loading is possible with each of the stipulated failures. The ability of the structure to withstand a reduced flight maneuver spectrum was demonstrated by analysis and static load tests of the complete engine shell as described in Section 6.2.

4.0 APPARATUS AND PROCEDURE

Two separate test configurations and facilities were utilized for the New Front Mount Performance Improvement Concept structural test program. A vertically assembled, floor-mounted setup was used for the stress distribution and low cycle fatigue tests. A horizontal assembly of the engine shell and wing pylon was suspended from test facility structural frames for the compressor case deflection/distortion, failsafe, and assembly and thermal stress correlation tests. The tests were conducted in the Static Load Laboratory of Building 703 at the General Electric Evendale, Ohio facility.

4.1 STRESS AND LOW CYCLE FATIGUE TEST SETUP

Test hardware consisted of all the engine outer structure in the load paths provided to distribute the engine front mount loads into the fan frame and compressor forward casing. Figures 4.1 and 4.2 show the test setup and load nomenclature.

Included in the test assembly were the modified fan frame with the forward, mid and aft fan casings, the Stage 4 booster case and the number 1 and 3 bearing housings with test facility rings to simulate engine component stiffness. The fan frame and casings together with the new front mount components were assembled together with the high pressure compressor casing, which was in turn bolted to the test laboratory floor adapter plate.

Loads were applied to the front mount platform by means of a steel yoke plate on which five hydraulic loading cylinders were attached. Two cylinders applied loads parallel to the engine axis and were used to provide axial force and yawing moments to the mount. Loads normal to the engine axis in the vertical direction were applied by two cylinders which also provided the pitching moments. Side loads were applied by a single laterally mounted cylinder.

The cylinder loads were controlled by a hydraulic console and measured by means of electrical strain gage type load cells. During the low cycle fatigue tests, the takeoff and landing load cycles were applied at the rate of approximately six cycles per minute by a hydroelectronic mechanical sensor system. The loading schedule was programmed by a data track, and the load output of each loading cylinder was measured by load cells and continuously monitored on a strip chart recorder.

During each phase of the stress and low cycle fatigue tests, component stress levels were derived from calculations based on strain gage readings obtained from electrical resistance foil type strain gages installed on the front mount platform, supporting links and fan frame. Deflections of the mount platform relative to the fan frame rear flange plane were measured by electrical deflection potentiometers attached on a ring mounted from the rear

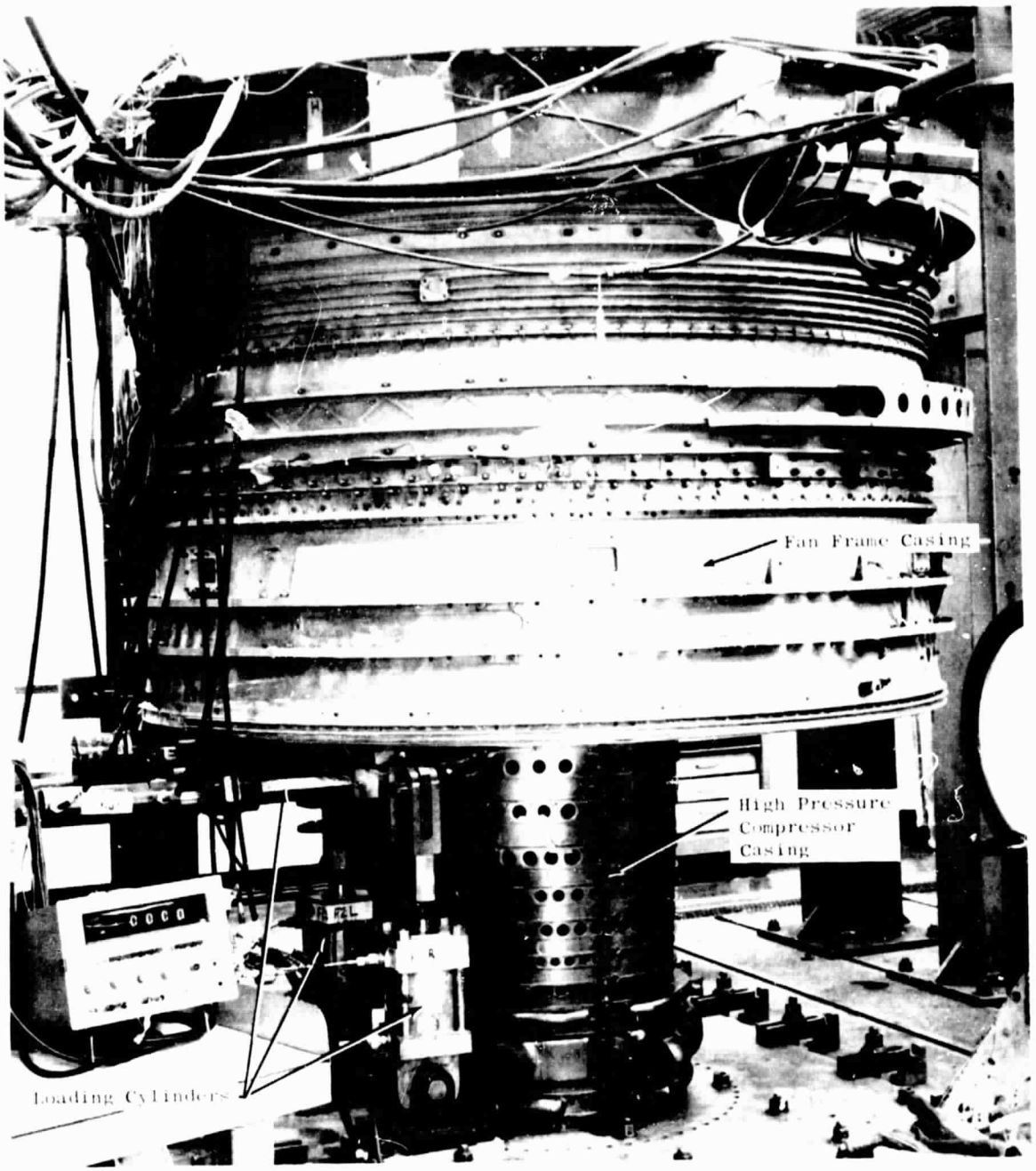

Figure 4.1. Stress and Low Cycle Fatigue Test Setup.

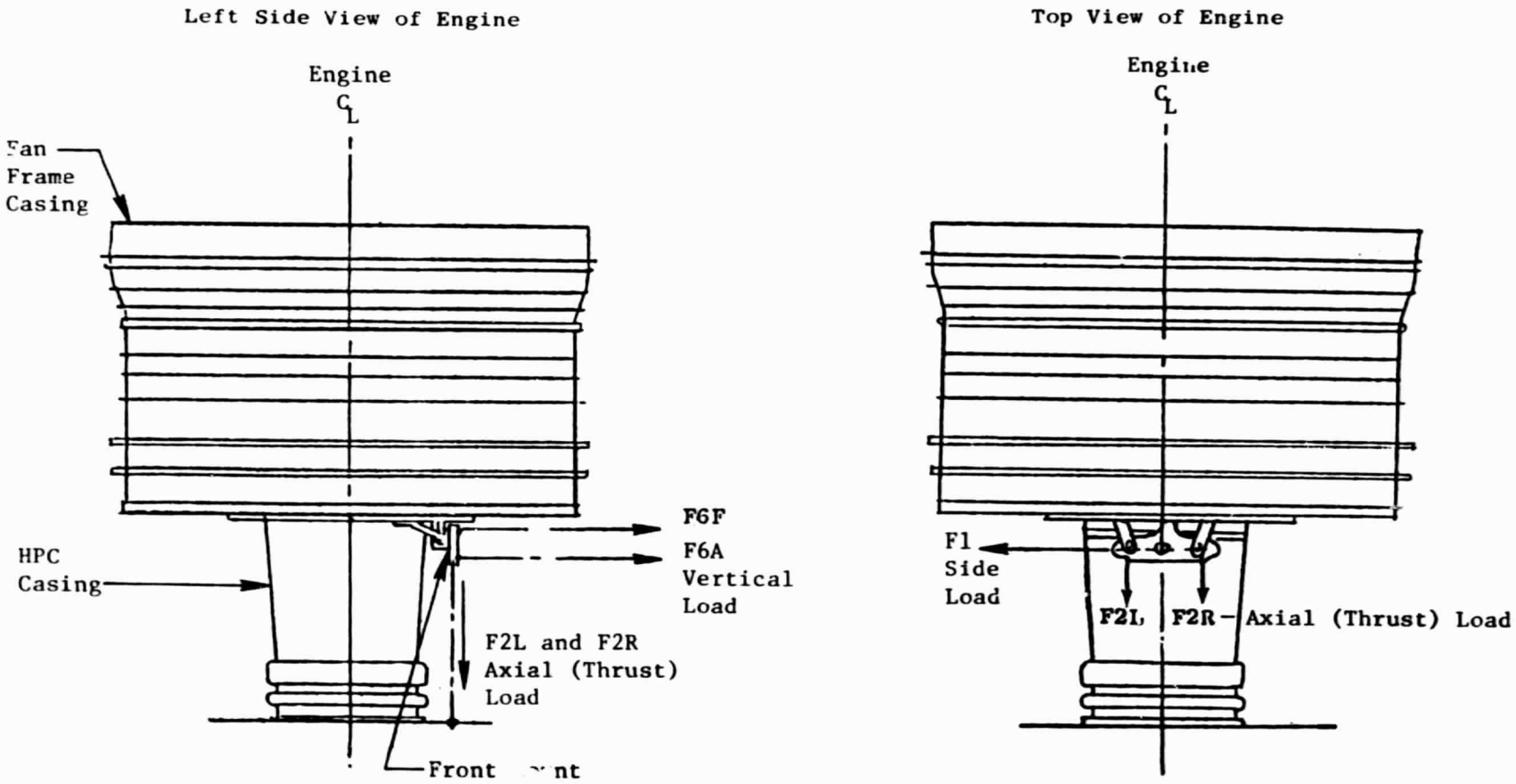

Figure 4.2. Stress and Low Cycle Fatigue Test Setup.

flange. Signals from the strain gages or deflection potentiometers were selected by a micro scan relay or crossbar selector and read out on an analog to digital converter. Permanent records of the data were stored on "floppy disk." The stored data were processed by the General Electric Evendale time sharing computer center into engineering units. The data were presented in tabular printout or, if required, by means of polar plots. Quick-look time sharing programs provided on-line data from selected gages to monitor the testing.

Locations of strain gages on each component are shown in Figures 4.4 through 4.8. Deflection gage locations for the new front mount are shown in Figure 4.3.

4.2 DEFLECTION/DISTORTION TEST SETUP

Deflection/distortion tests were conducted on a complete CF6-50 engine outer shell structure suspended from a DC-10 wing pylon as shown in Figures 4.9 to 4.11.

The engine shell assembly consisted of the modified fan frame with the forward, mid and rear fan casings, the Stage 4 booster casing, and the number 1 and 3 bearing housings. The core engine casings comprised the compressor forward and rear casing, the compressor rear frame, turbine midframe, low pressure turbine stator casing and the turbine rear frame complete with all bearing cones. A DC-10 wing engine inlet was attached to the fan frame.

The engine assembly was installed on a DC-10 wing engine pylon by attachment links at the rear mount which were strain gaged and calibrated, and by means of either the original front mount or the interchangeable new front mount.

Two steel arches, which supported the DC-10 wing pylon, were bolted to the laboratory T-slot floor which also provided anchor points for the hydraulic loading cylinders. Thrust loads were applied on the engine at the aft end of the core casing by means of a hydraulic cylinder attached to the pylon support frames. The inlet airload for the takeoff at rotation condition was simulated by loads applied by hydraulic loading cylinders attached to nylon belts wrapped around the lower circumference of the inlet. All hydraulic cylinder loads were controlled manually and measured by means of electric resistance strain gage type load cells.

Strain gages were installed on the front mount, supporing links, and fan frame as shown in Figures 4.4 through 4.8. Relative motion of the engine structure was measured using stationary mounted deflection potentiometers. Radial deflection of the core and fan casings were measured by means of deflection potentiometers mounted from facility shafts which were supported at the same bearing locations as the engine shafts. Slow rotation 360° "sweeps" were made with these shafts to measure radial distortion at 5° increments over the upper 120° of the casings, and 10° increments for the remainder of the circumference (Figures 4.12 through 4.19).

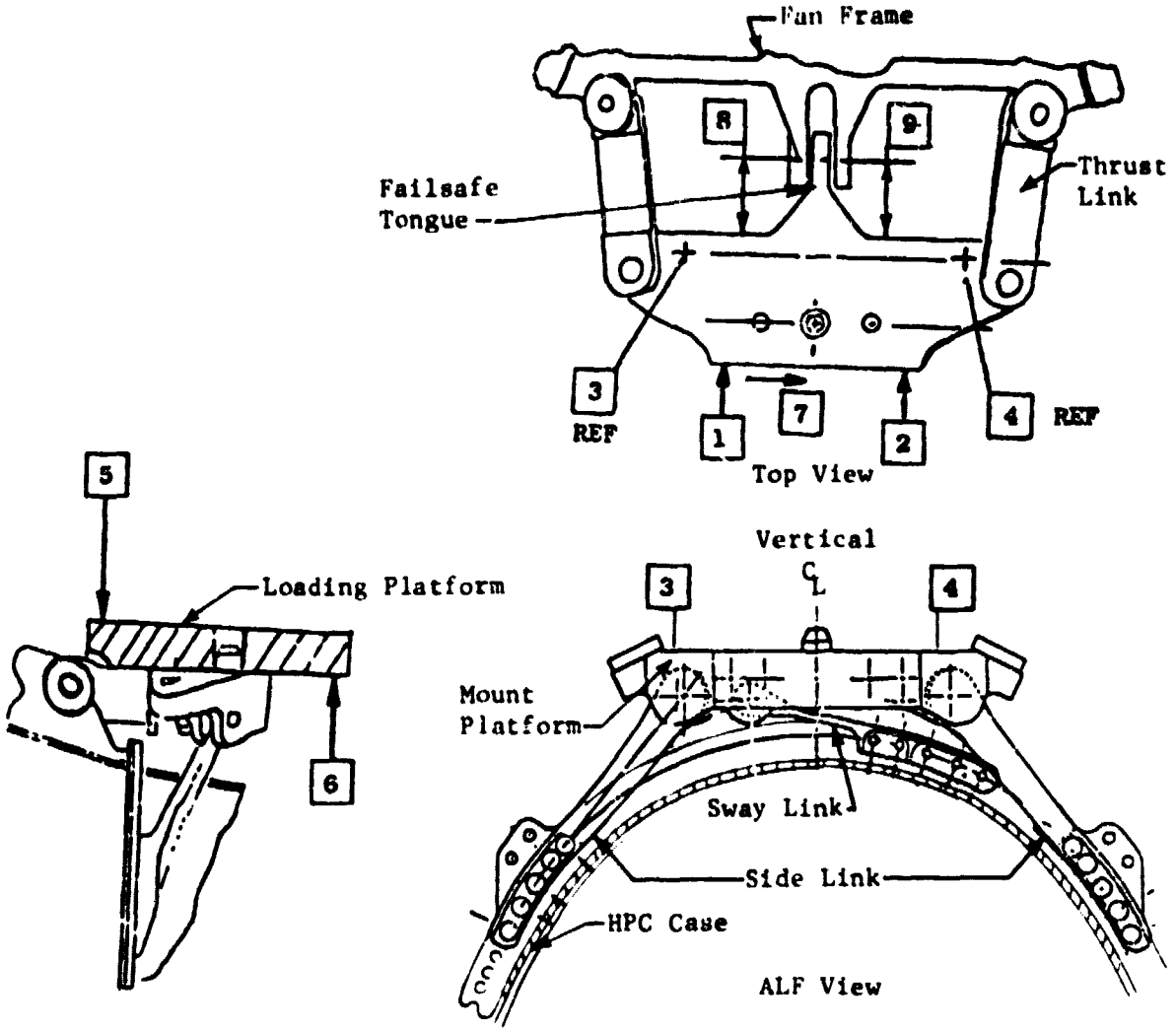

Deflection gages 1 through 7 were mounted on a ring mounted to the forward flange of the compressor case. Deflection gages 8 and 9 were mounted on the 12:00 fan frame clevis.

Figure 4.3. Front Mount Deflection Gage Locations.

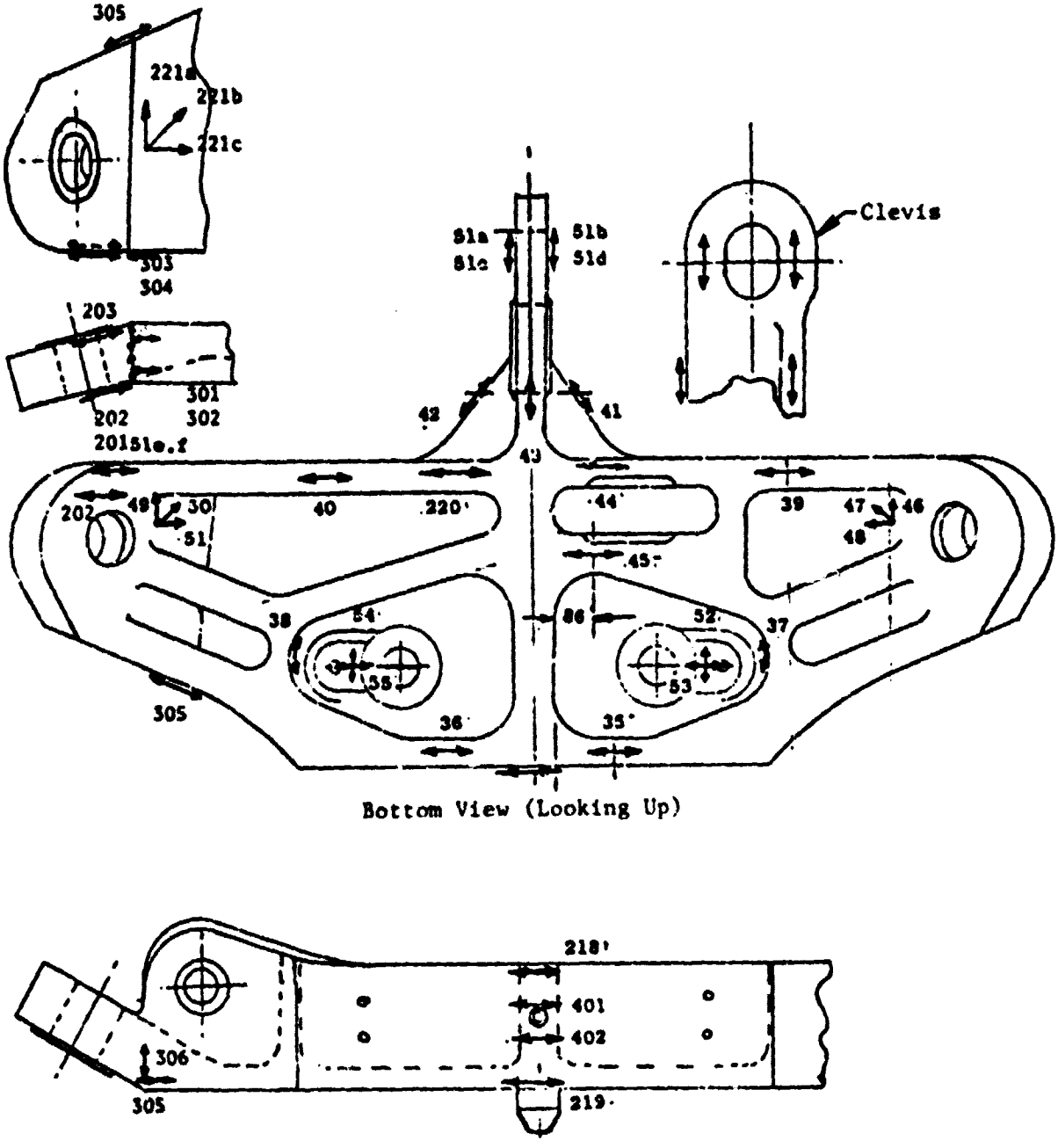

Bottom View (Looking Up)

Figure 4.4. Mount Platform Strain Gage Locations.

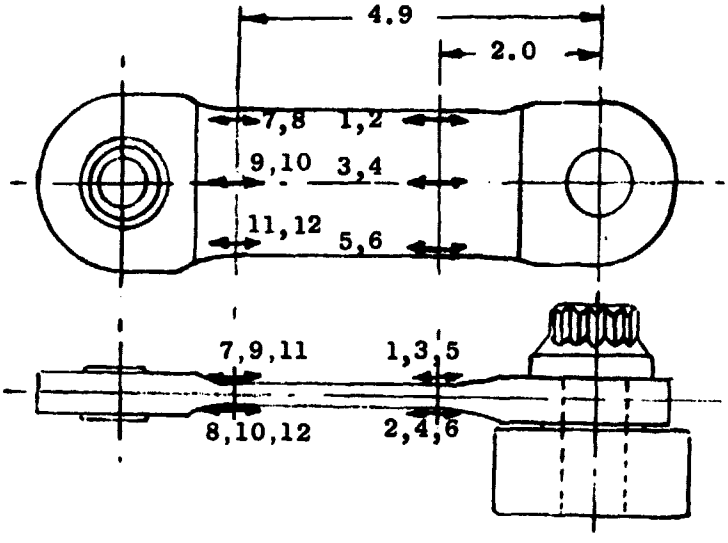

RIGHT THRUST LINK

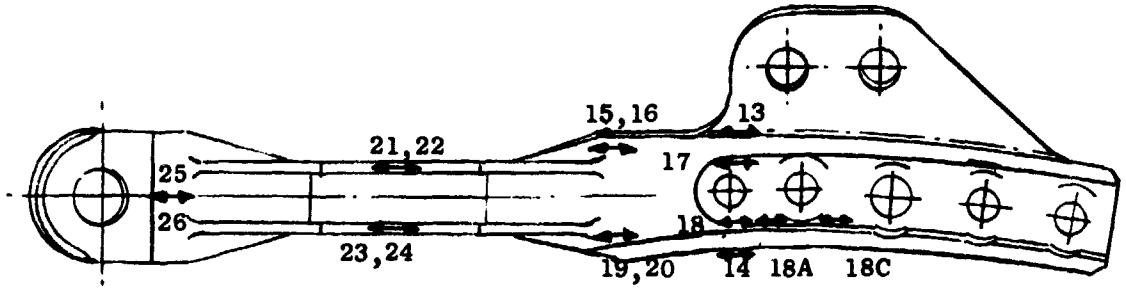

RIGHT SIDE LINK

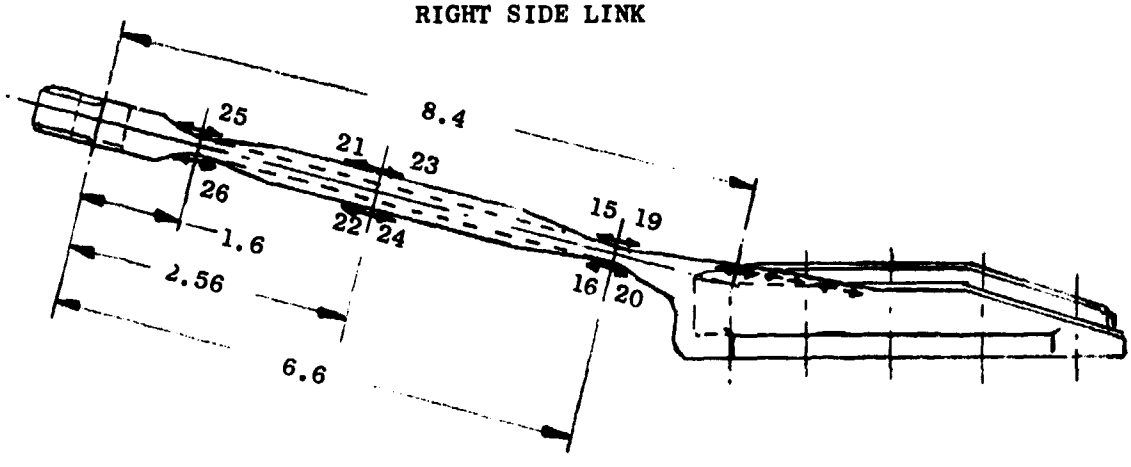

Figure 4.5. Thrust Link and Side Link Strain Gage Locations.

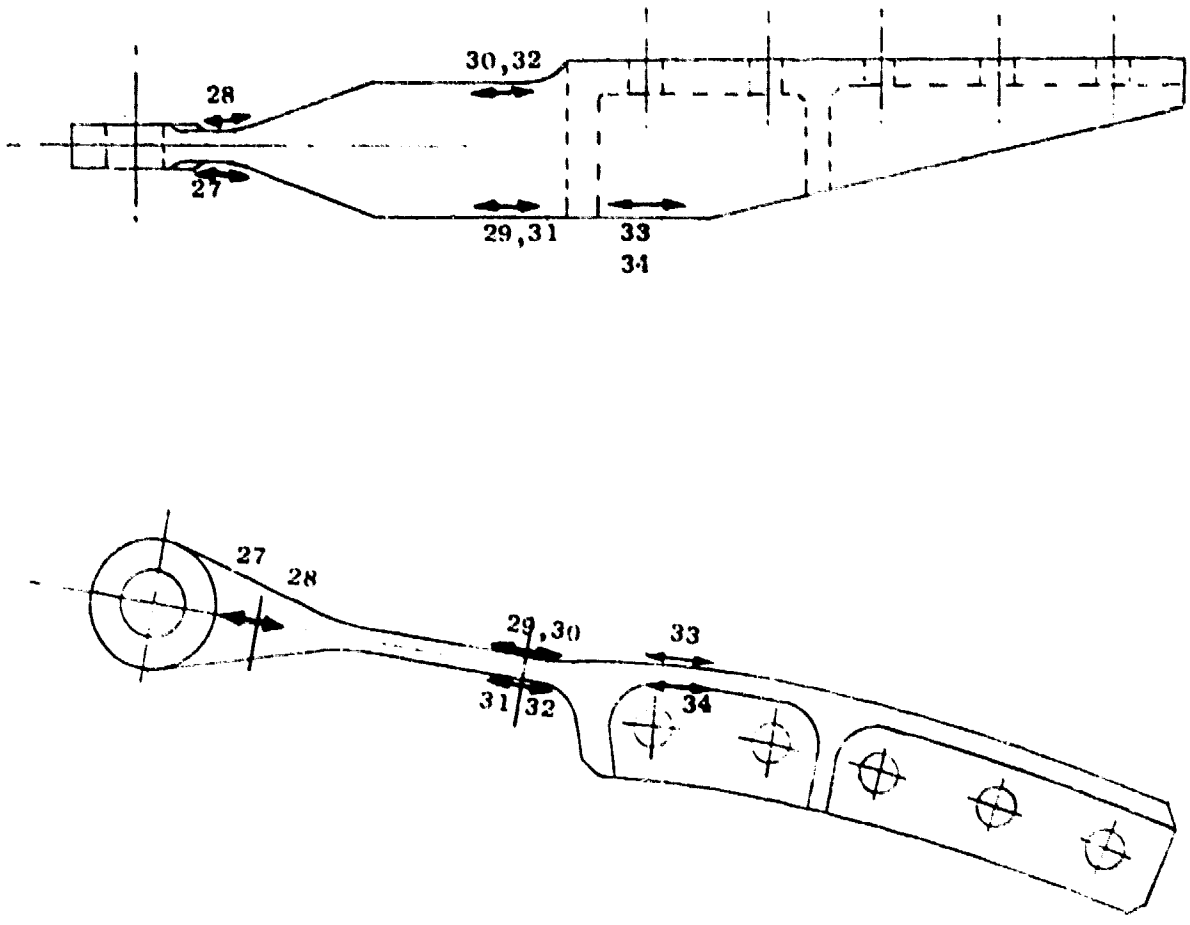

Figure 4.6. Sway Link Strain Gage Locations.

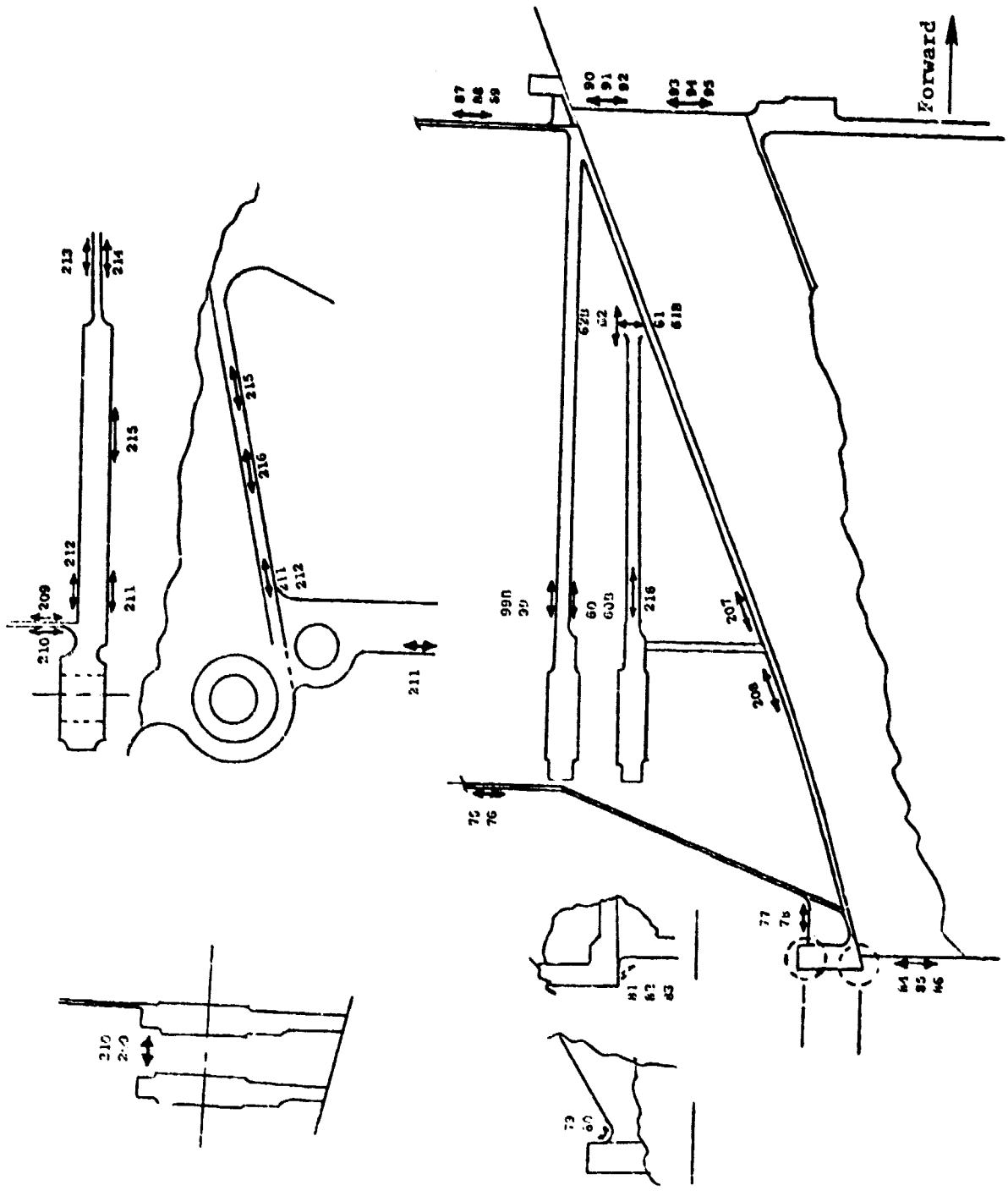

Figure 4.7a. Fan Frame Strain Gage Locations.

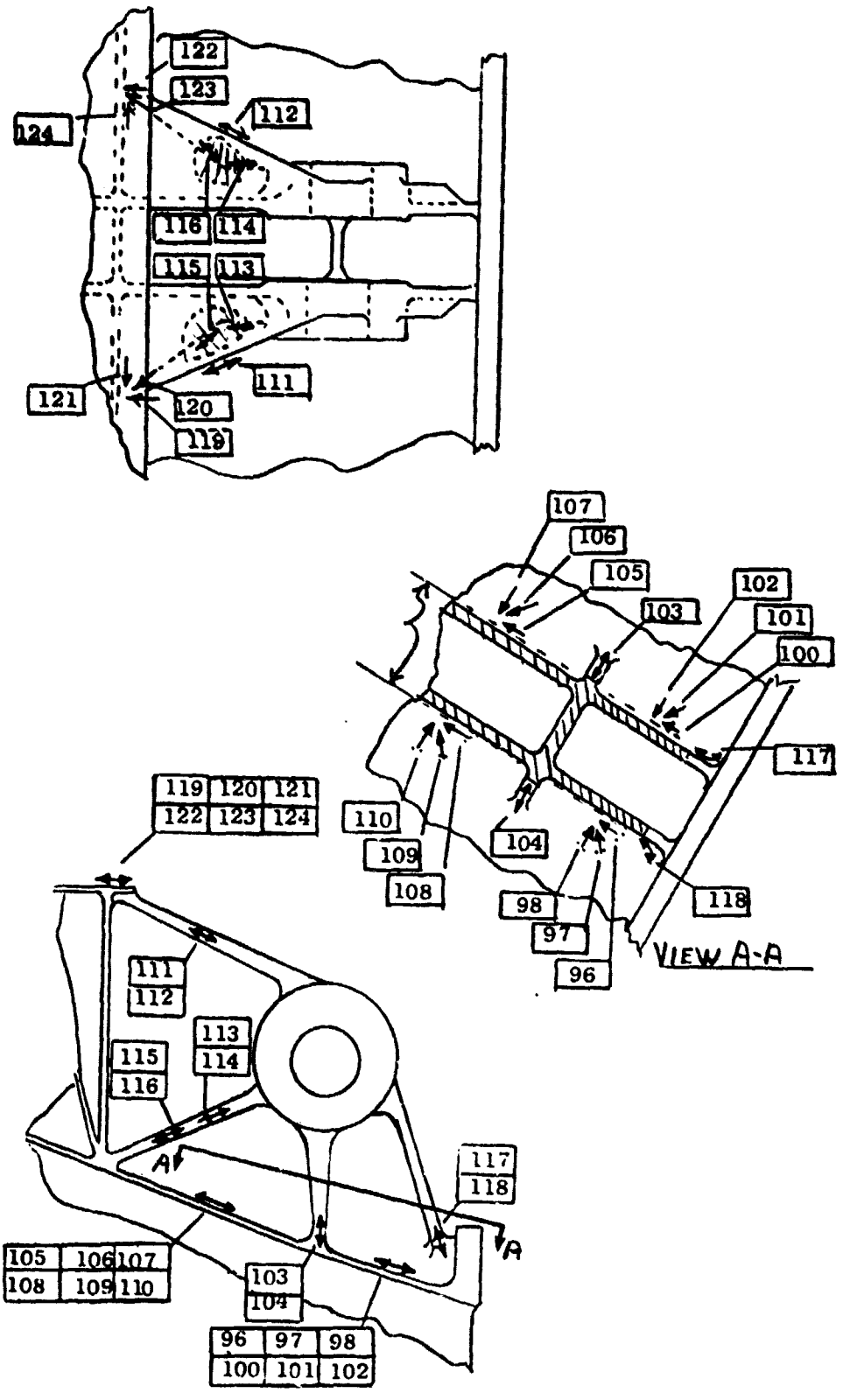

Figure 4.7b. Fan Frame Strain Gage Locations.

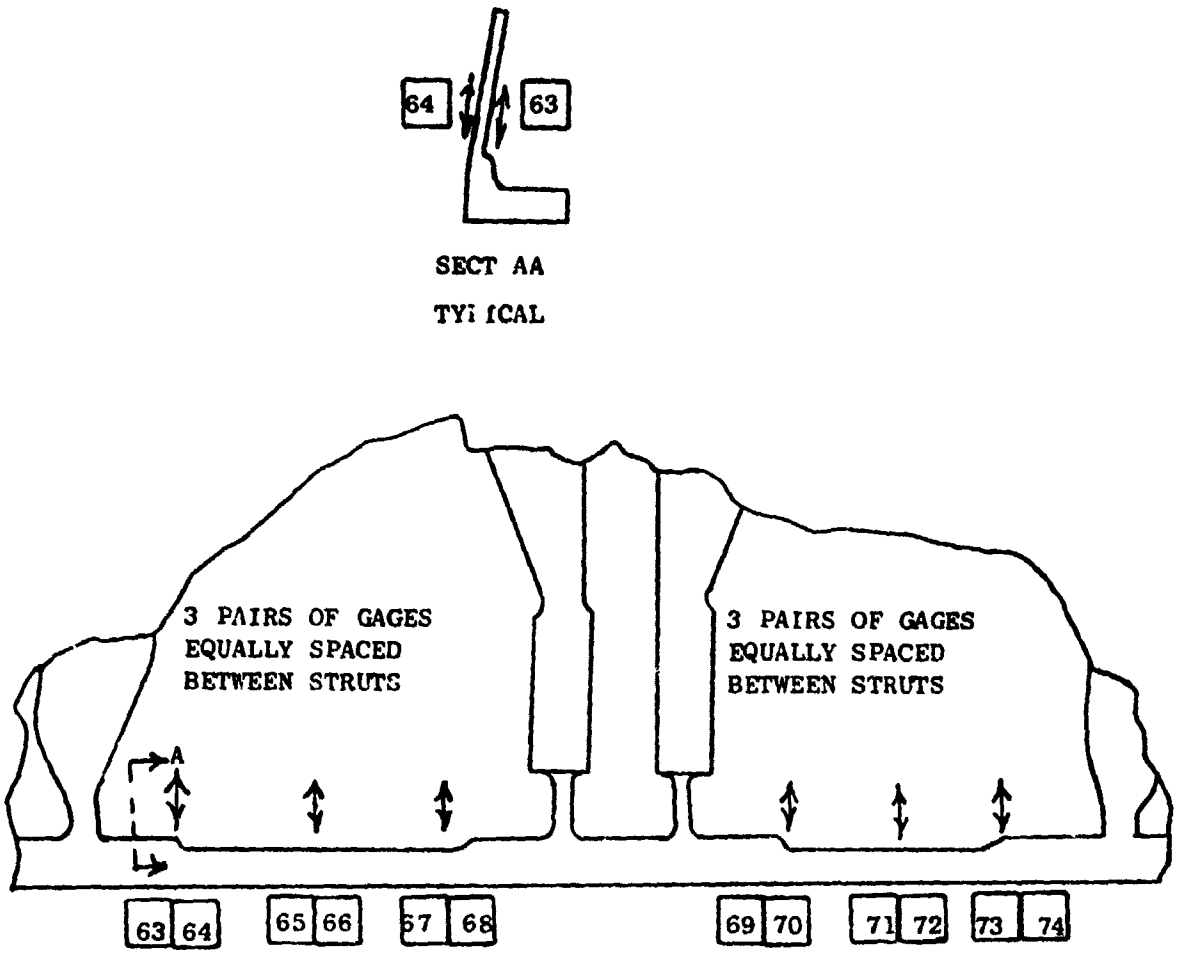

Figure 4.7c. Fan Frame Strain Gages Between Struts.

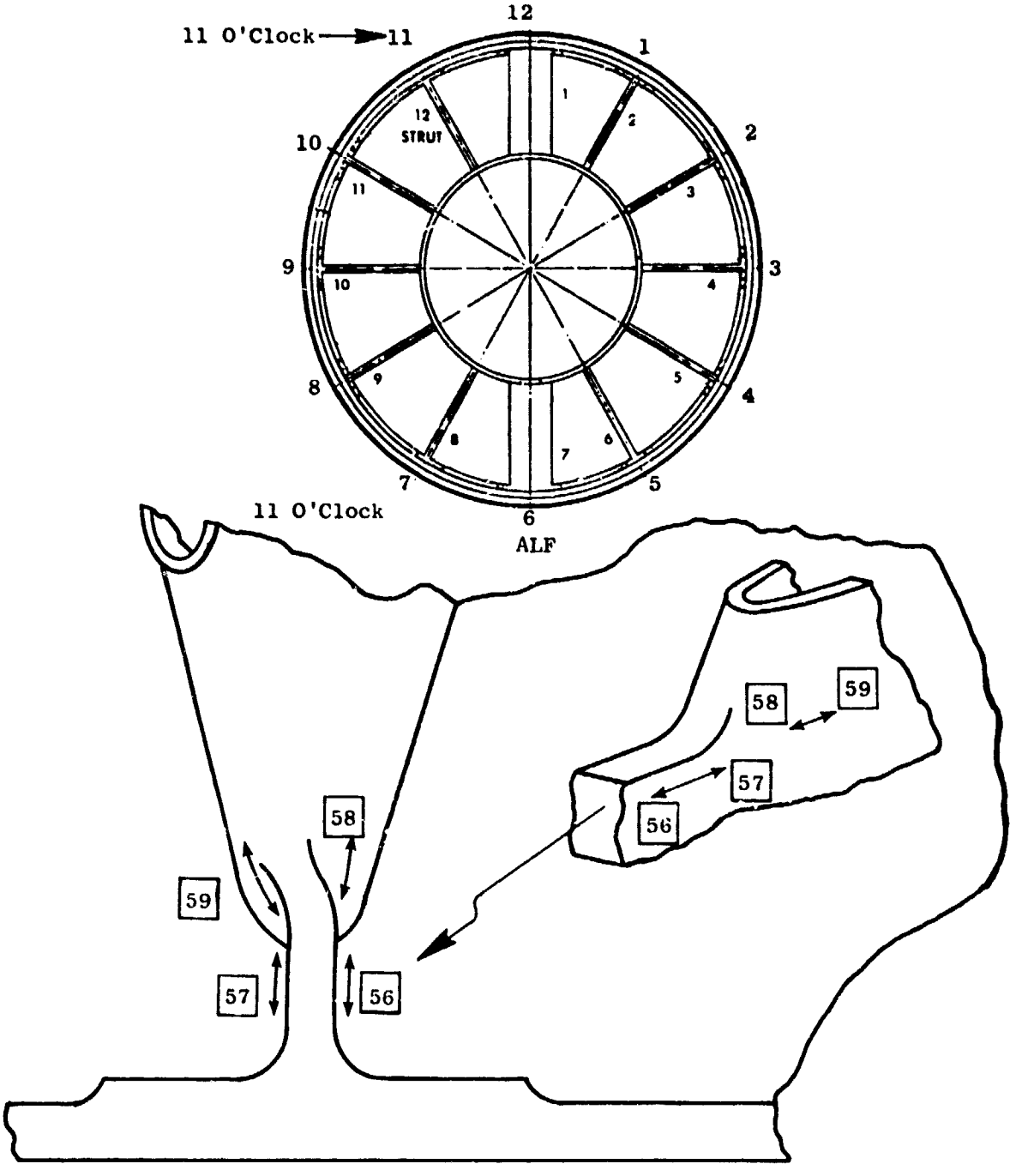

Figure 4.7d. Fan Frame Strain Gages on Strut 12 at 11 O'Clock.

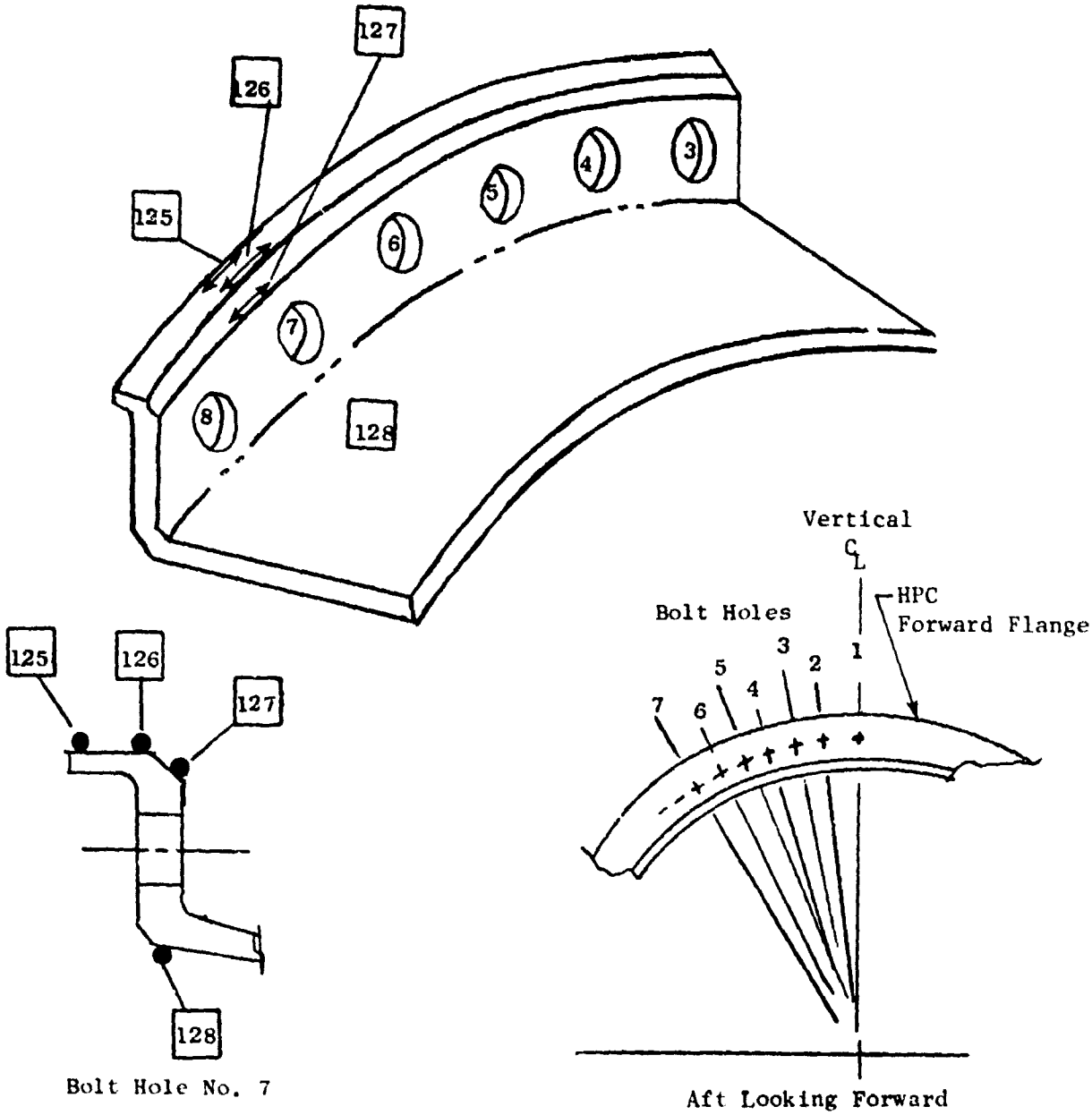

Figure 4.8. High Pressure Compressor Case Strain Gage Locations.

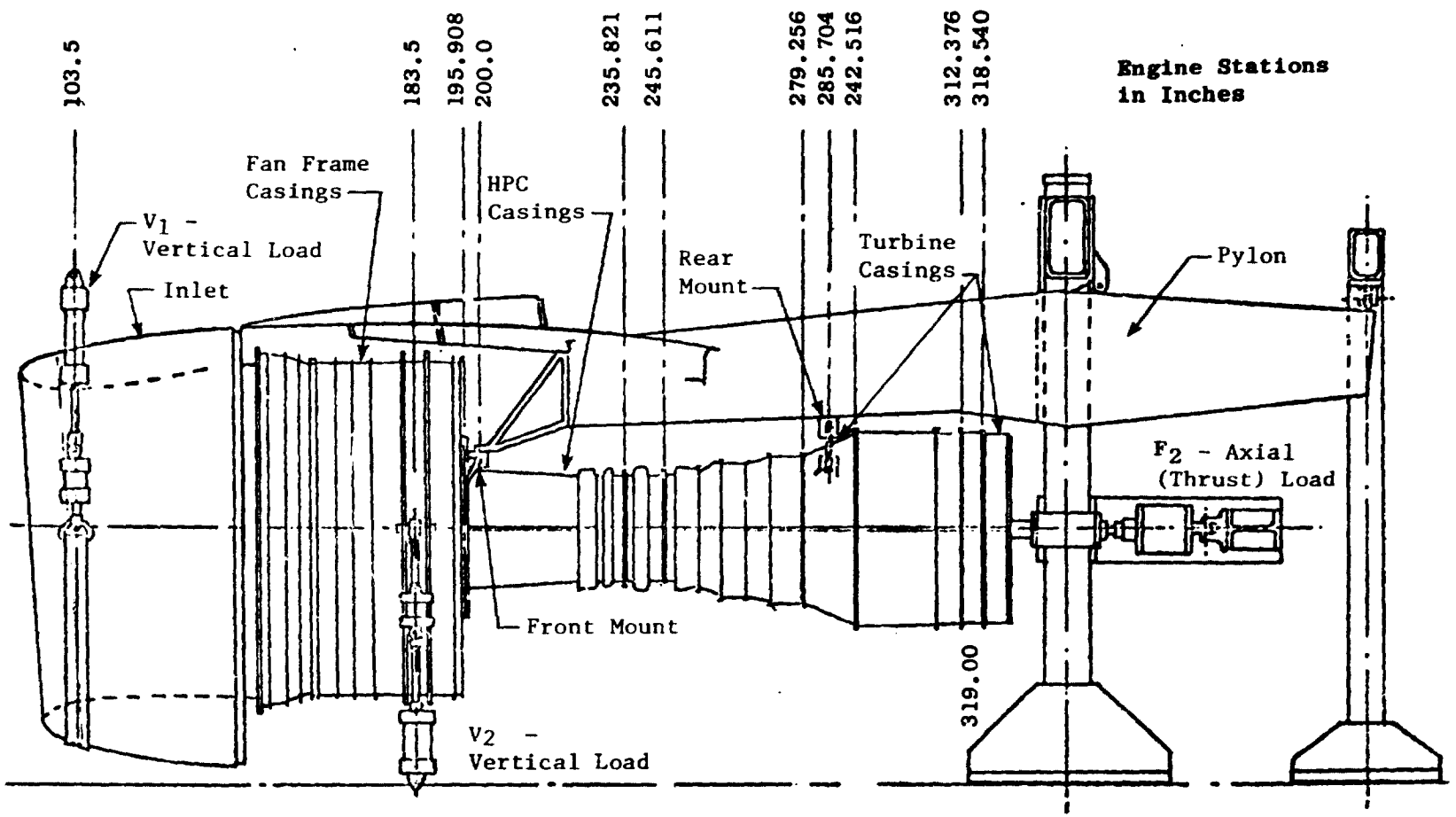

Figure 4.9. Deflection/Distortion Test Setup.

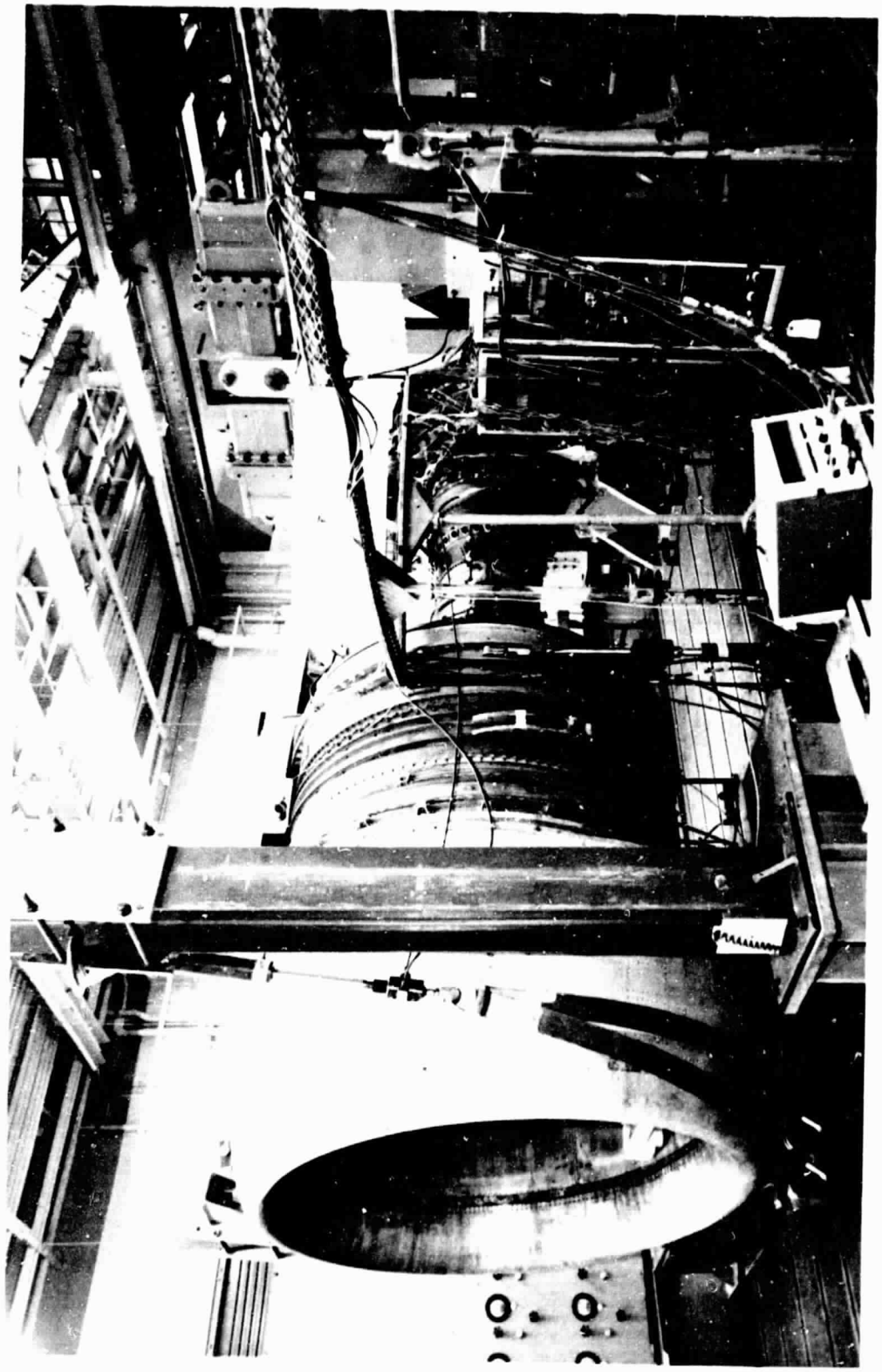

Figure 4.10. Deflection/Distortion Test Setup.

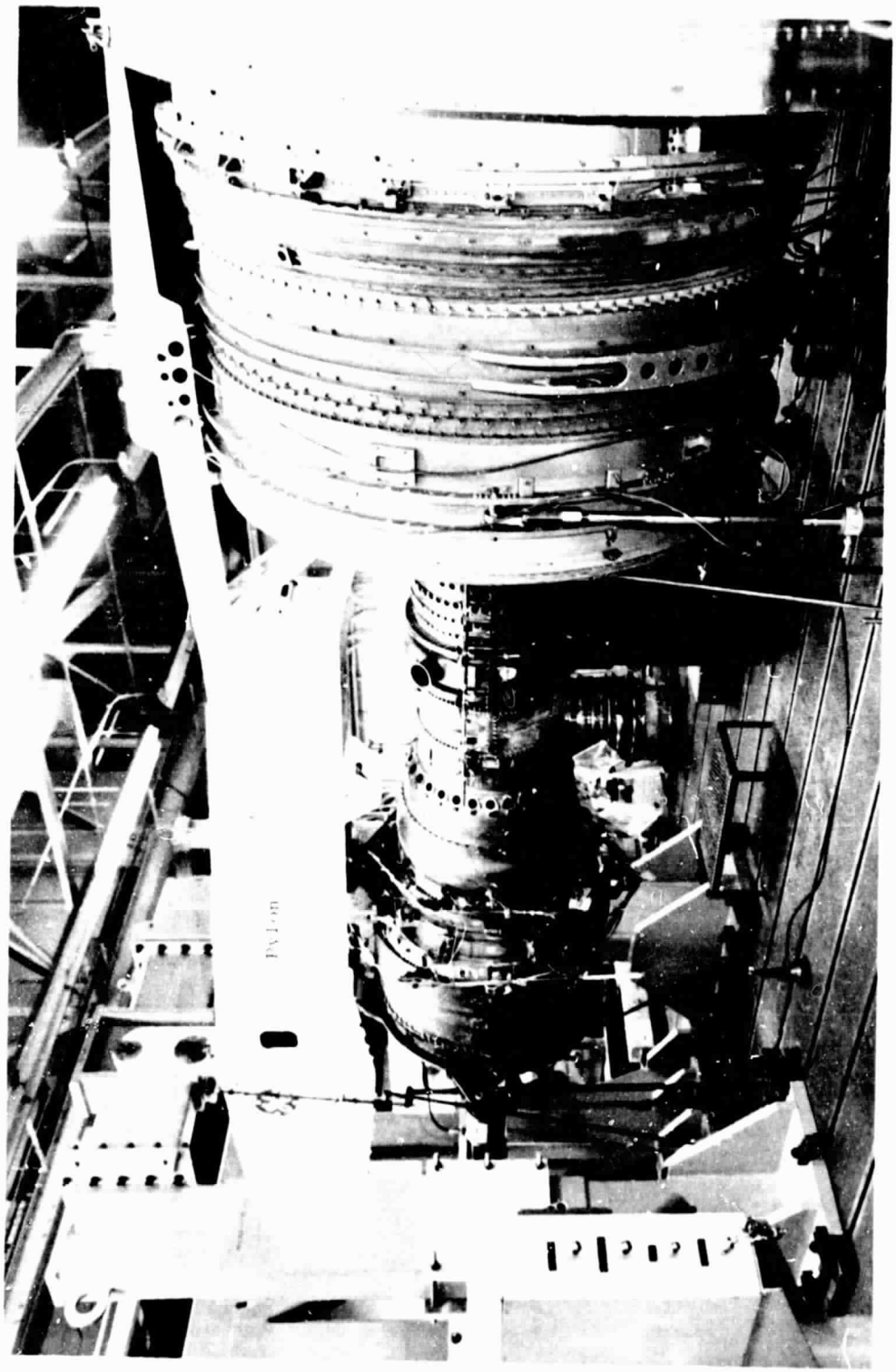

Figure 4.11. Deflection/Distortion Test Setup.

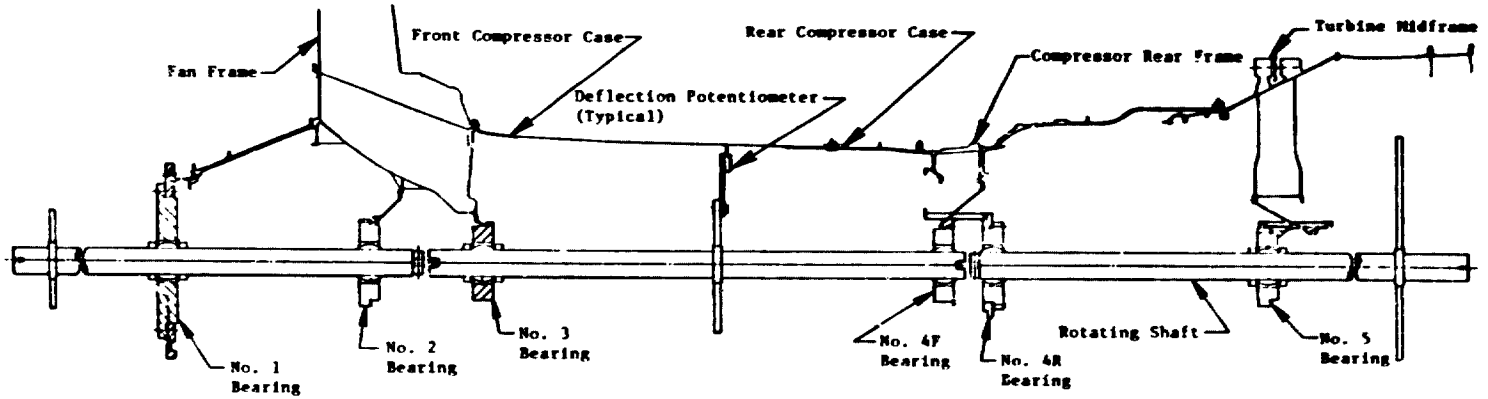

Figure 4.12. Compressor Case Radial Deflection Instrumentation Rotating Shaft and Bearings Locations.

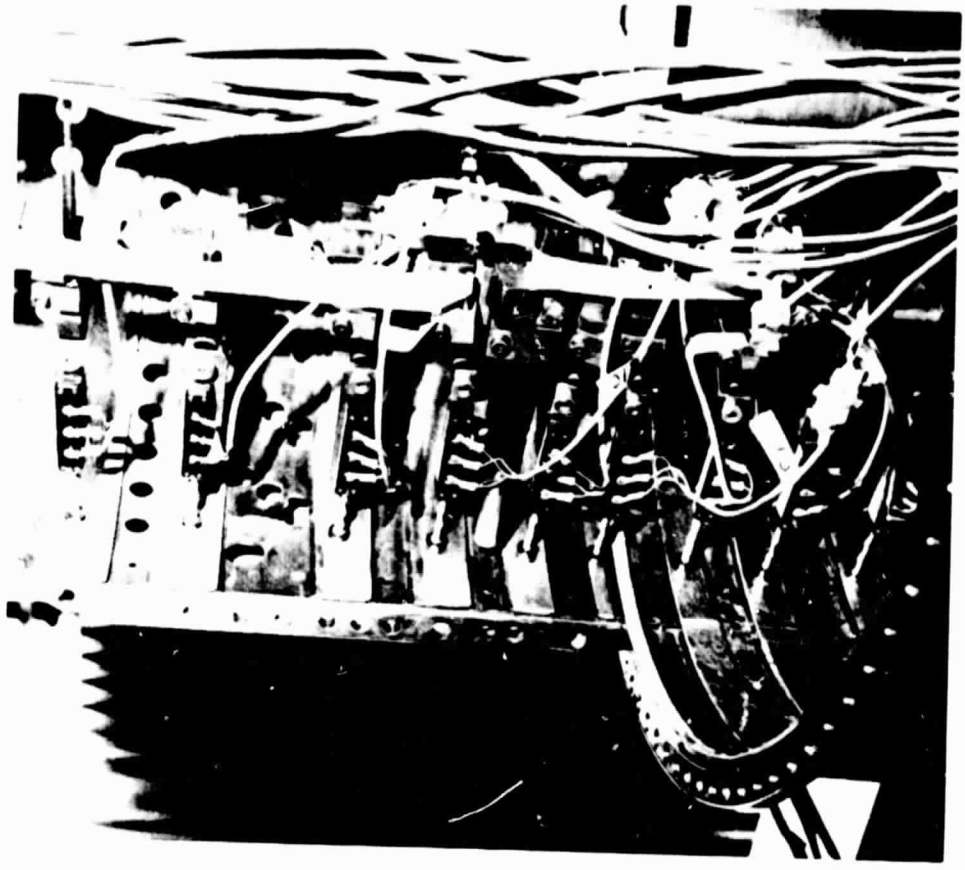

Figure 4.13. Compressor Casing Deflection Instrumentation.

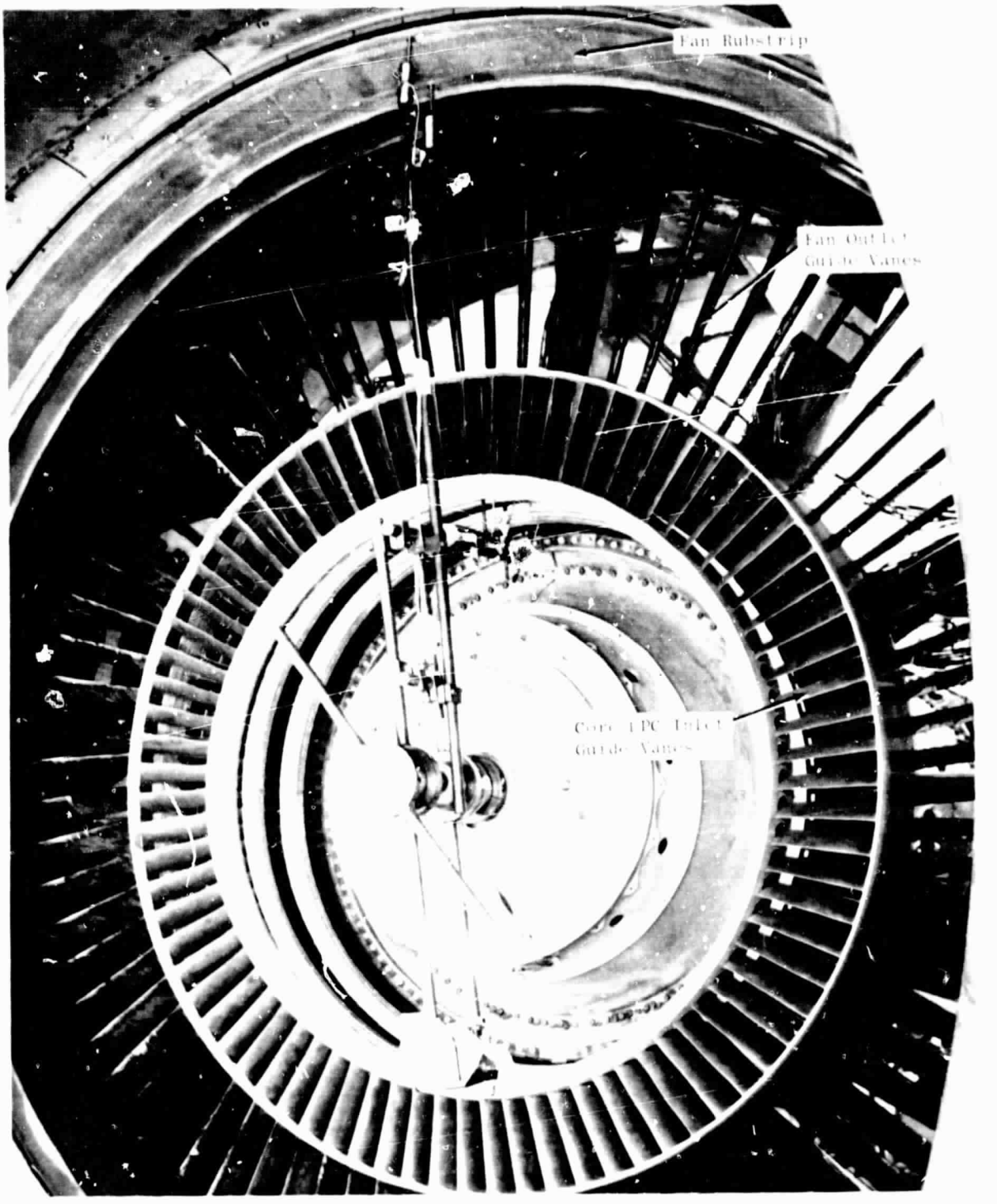

Figure 4.11. Fan Casing Deflection Instrumentation.

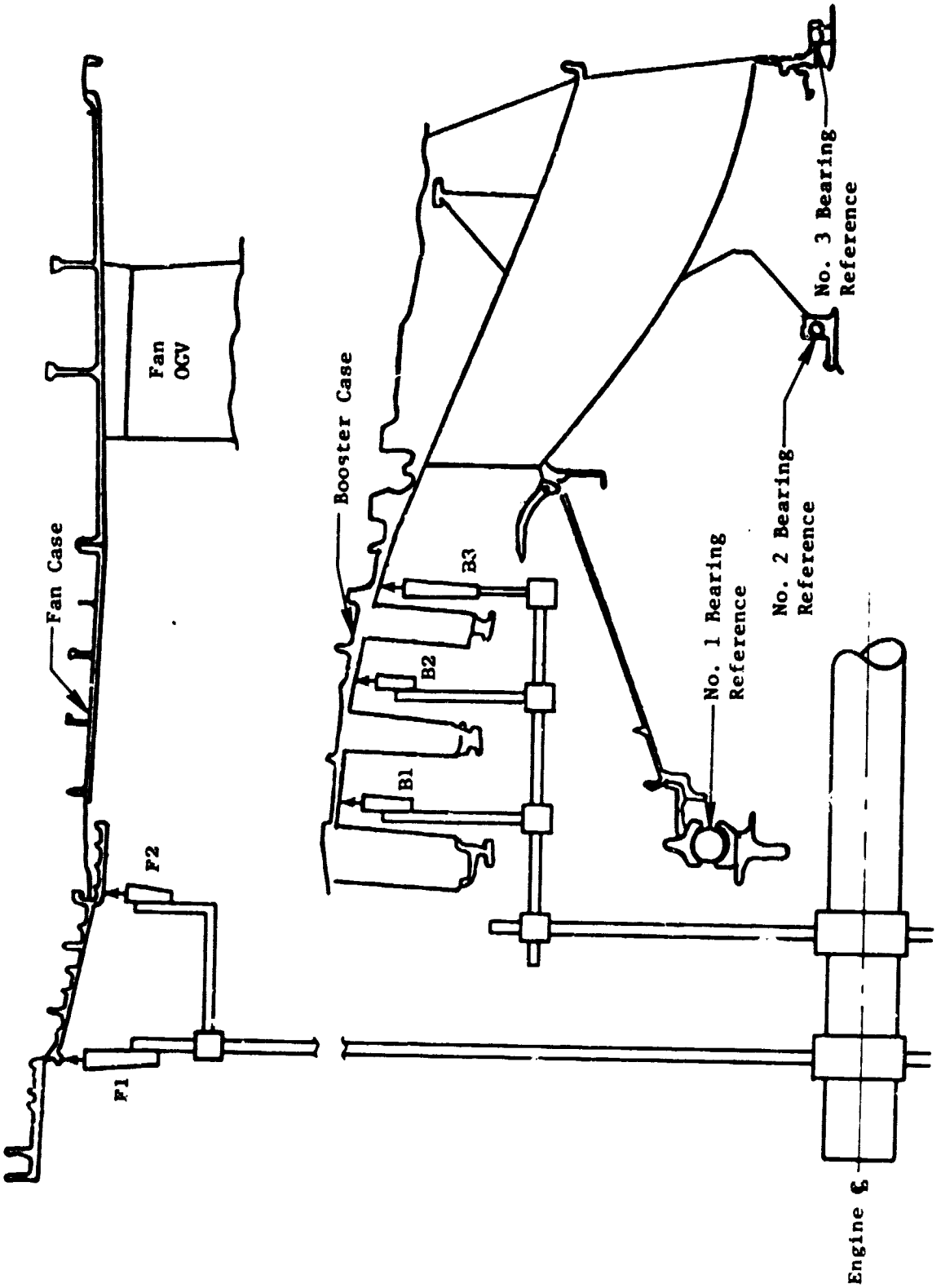

Figure 4.15 Fan Case and Booster Case Deflection Instrumentation.

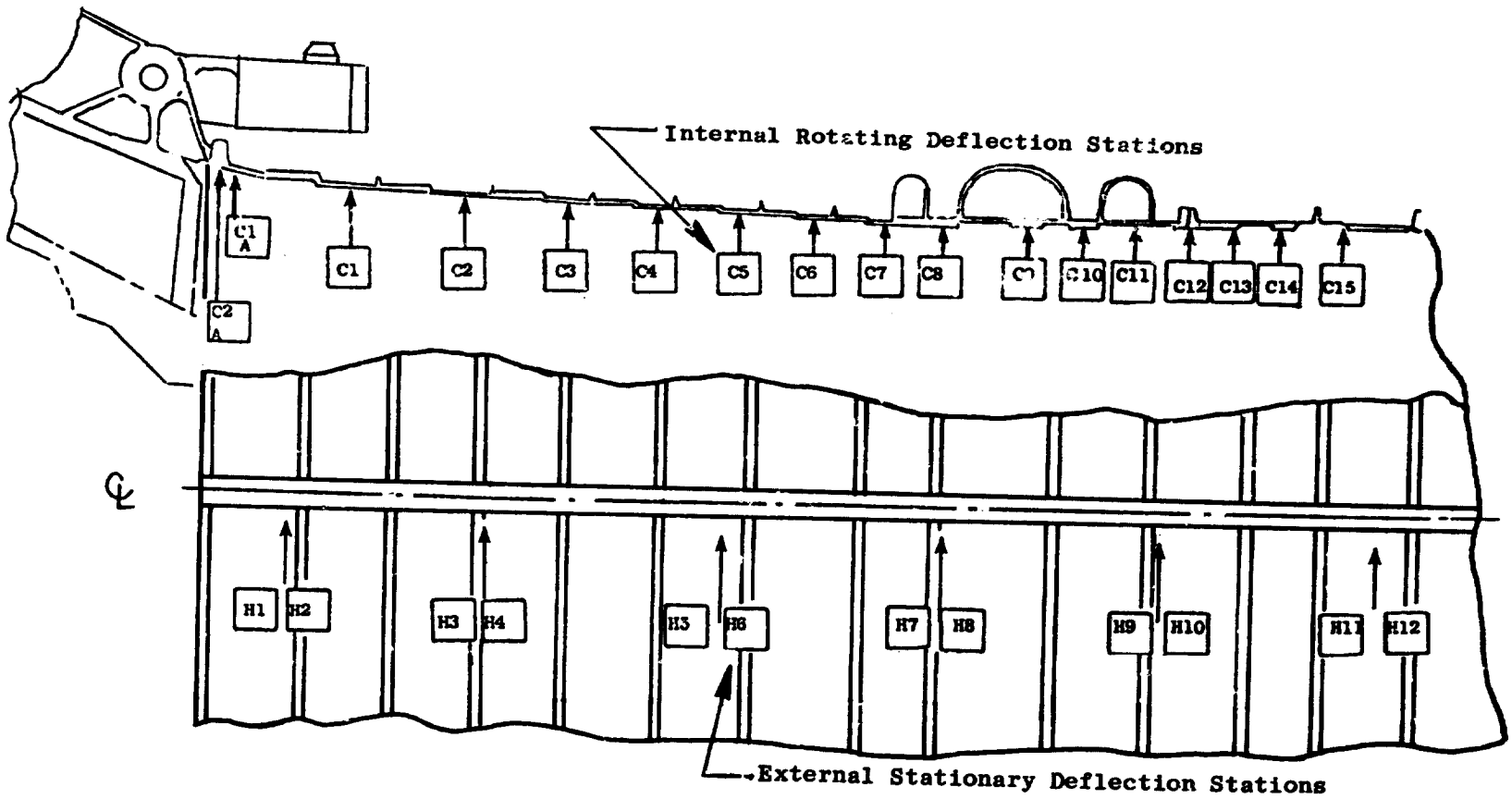

Figure 4.16. Compressor Case Deflection Instrumentation.

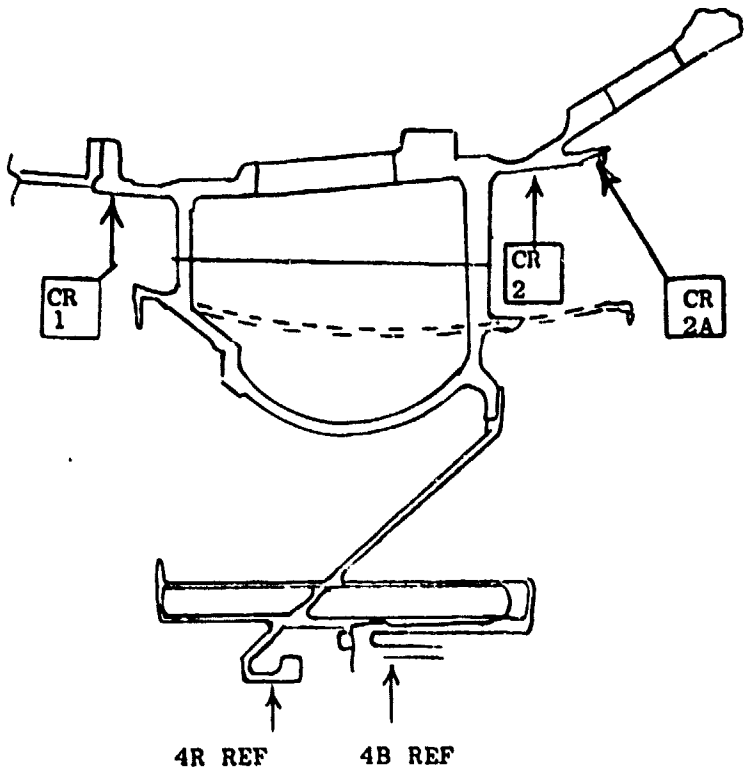

Figure 4.17. Compressor Rear Frame Deflection Instrumentation.

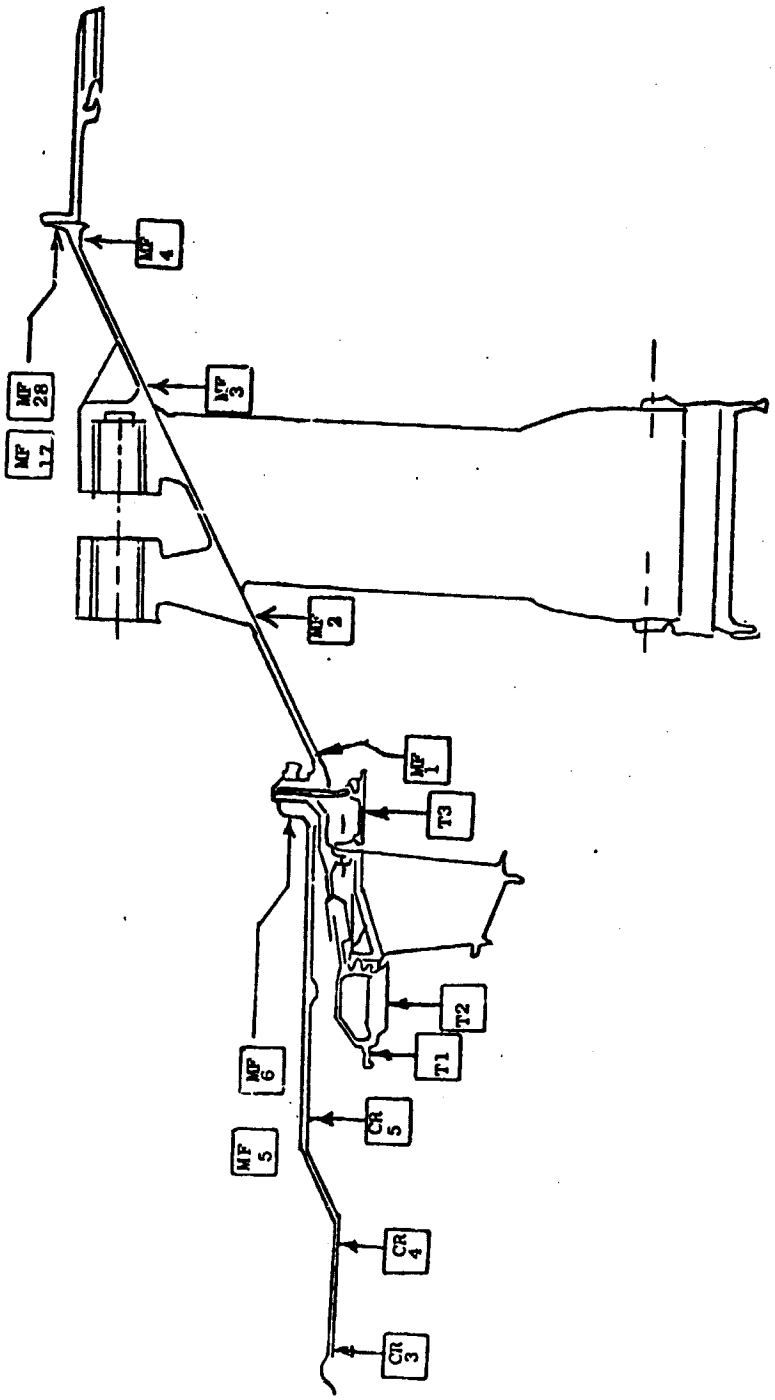

Figure 4.18. HP Turbine Shroud and Midframe Deflection Instrumentation.

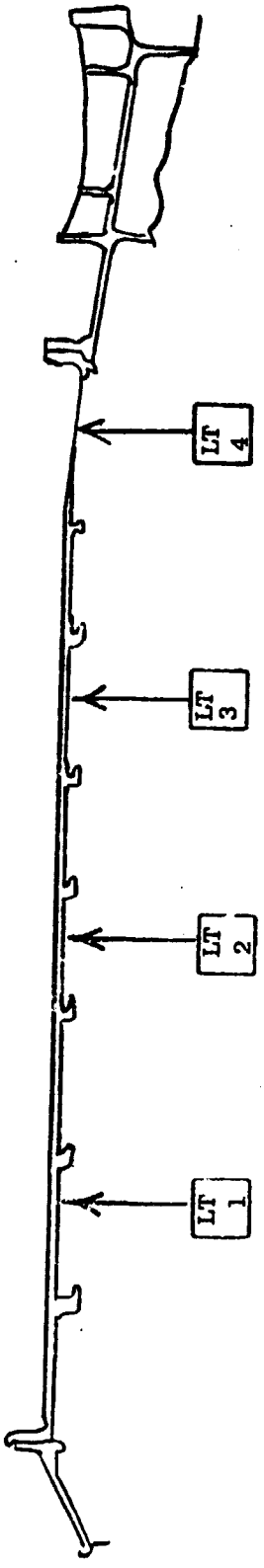

Figure 4.19. LP Turbine Case Deflection Instrumentation.

Potentiometer signals at each increment were recorded by the digital recording system and then transferred to the time sharing computer and plotting system. Stationary potentiometers were used to measure the overall deflection (Figures 4.3, 4.16 and 4.20).

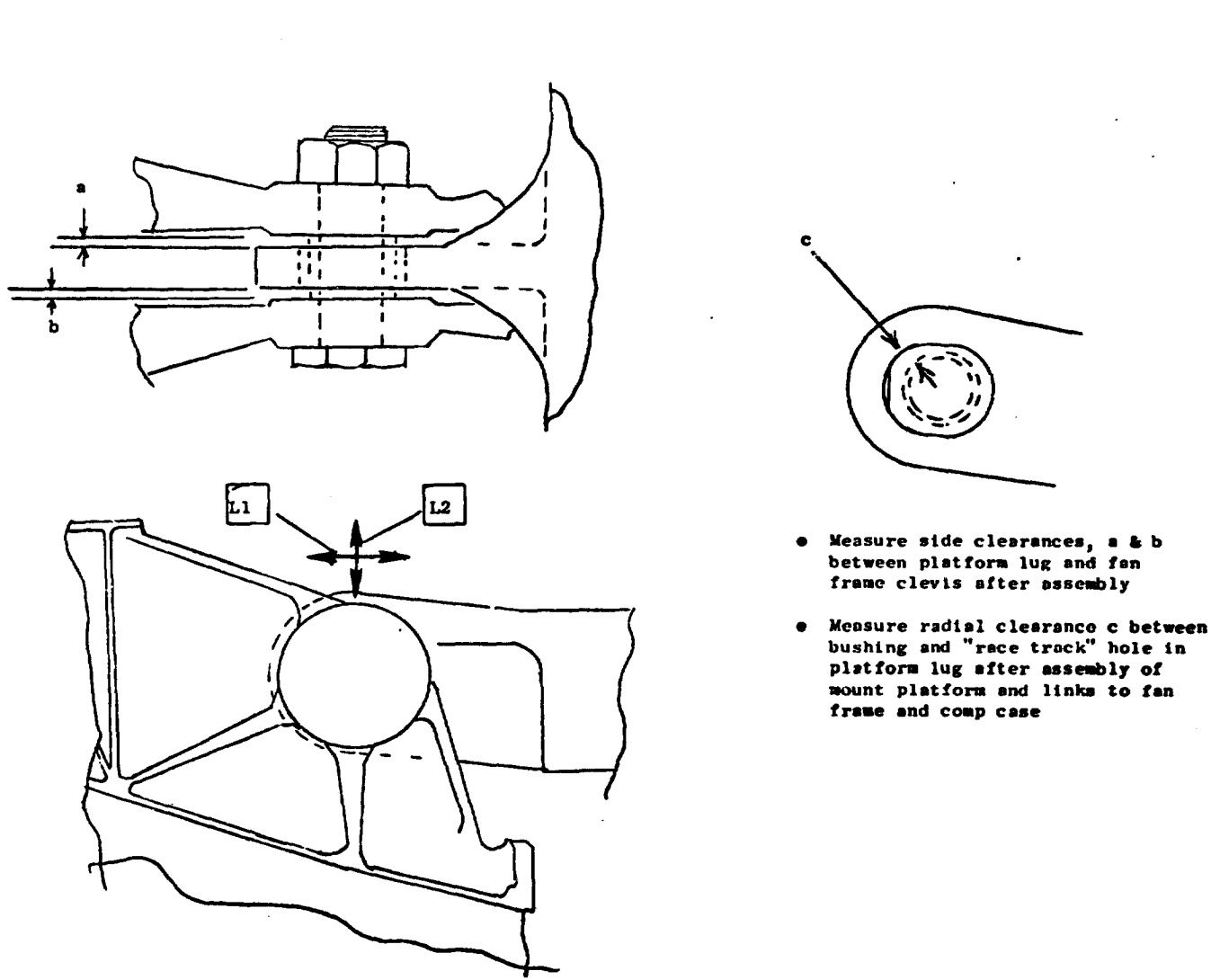

Figure 4.20. Mount Platform/Fan Frame Clevis Relative Motion Deflection Instrumentation.

5.0 STRESS TEST

The objective of the stress test was to use the Stresscote brittle lacquer technique to verify predicted highly stressed regions and to determine any other local stress concentrations in the new front mount, supporting links, and backup structure. Results of these tests were used to confirm the location of previously installed strain gages and indicate areas where additional strain gages should be located. A description of the stress test setup is presented in Section 4.1.

5.1 TEST PROCEDURE

Four tests were conducted to simulate side loads, forward and aft axial (thrust) loads, and vertical loads. Each test included either the maximum side, axial, or vertical load component. The corresponding 100% load conditions are defined in Figure 5.1.

Prior to the assembly of the individual test parts, electrical resistance strain gages had been installed at the locations shown in Figures 4.4 through 4.8. Test components were assembled using normal assembly procedures to the configuration shown in Figure 4.1. After torquing all attachment hardware, Stresscote brittle lacquer was applied. Specified areas of the fan frame, new front mount platform, supporting links, and compressor casing, together with standard calibration bars, were coated and allowed to dry until the crack sensitivity was within 0.005 to 0.009 mm/mm (in./in.). In each of the four tests, loads were applied in 20% increments to the 100% values, and for specific test runs, up to 120%. At each increment, strain gage readings were recorded and after unloading to zero, the Stresscote crack patterns were mapped and identified on each part.

5.2 TEST RESULTS AND DISCUSSION

Figures 5.2 through 5.8 show the Stresscote crack mapping on the respective components after completion of the four tests. Stresscote crack development determined the limiting stress areas. Details of the individual tests are as follows:

Side Loads Test

Maximum side load applied was 53,380 N (12,000 lb), which is 120% of the value specified in the load table (Figure 5.1). This maximum test load is approximately four times the typical design operating load and is approximately 29% of the design limit side load condition. Inspection of the Stresscote did not reveal any crack formation of the new front hardware and fan frame. The only Stresscote crack formation developed on the compressor

Test No.	Type of Load	Applied Test Loads, N (lb) (Figure 4.2)				
		Side	Axial (Thrust)		Vertical	
		F1	F2L	F2R	F6F	F6A
1	Side Load	44480 (10000)	0	0	0	0
2	Axial Load (Aft)	0	55600 (12500)	55600 (12500)	0	0
3	Vertical Load	0	0	0	33360 (7500)	33360 (7500)
4	Axial Load (Fwd)		-55600 (-12500)	-55600 (-12500)		

Figure 5.1. Stress Test 100% Load Conditions.

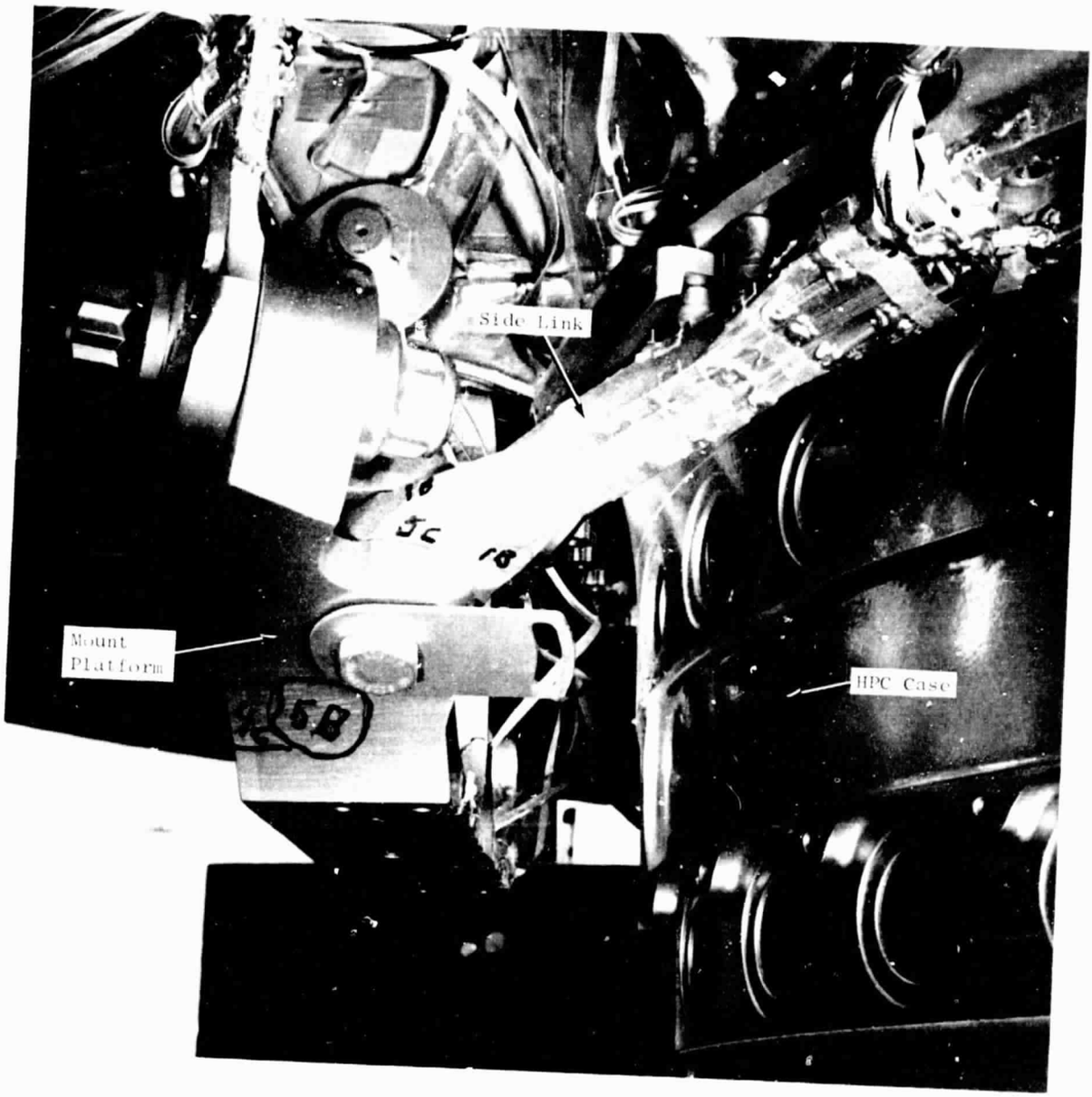

Figure 5.2. Photograph of Stresscoat Map Pattern.

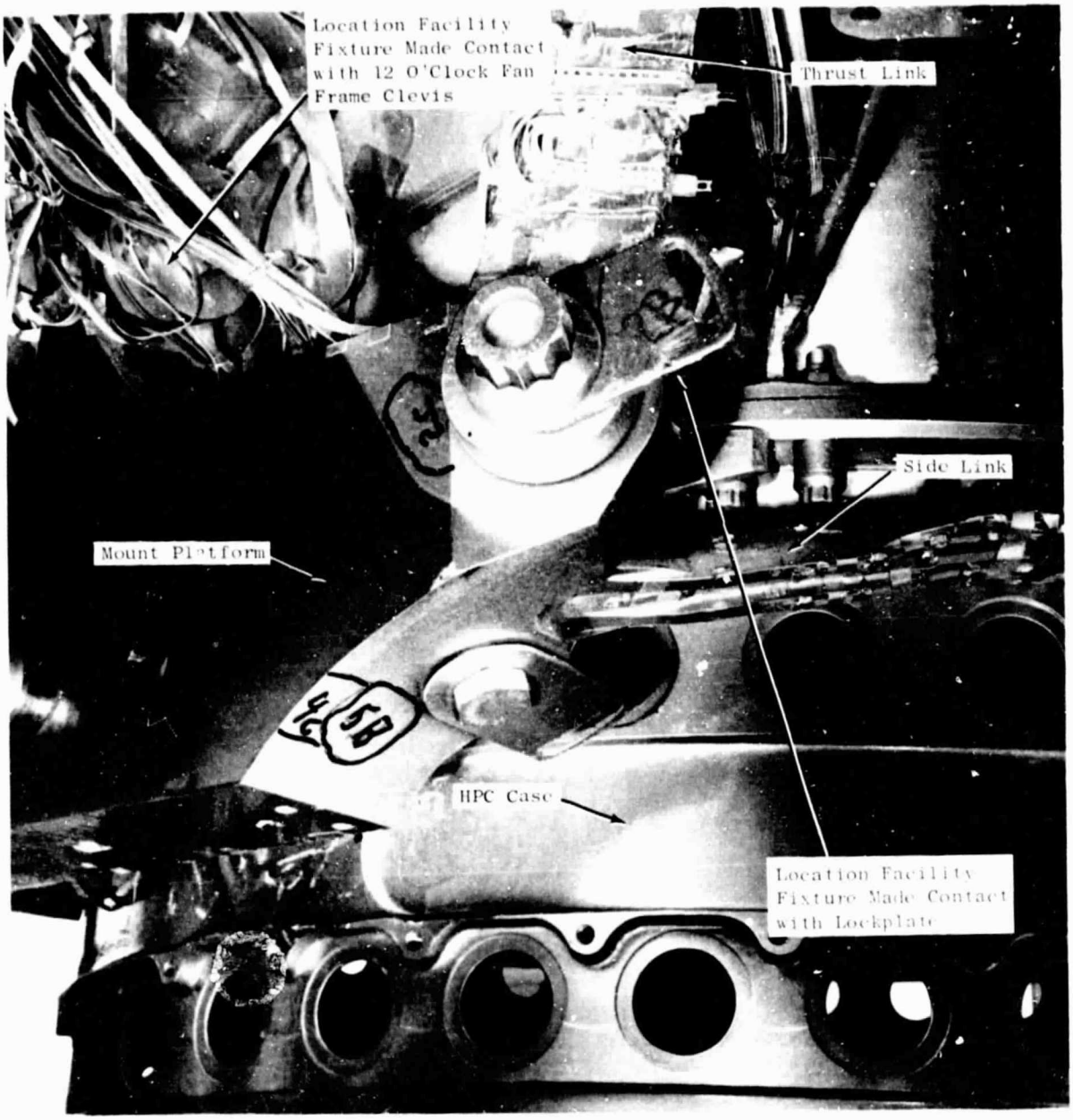

Figure 5.3. Photograph of Stresscoat Map Pattern.

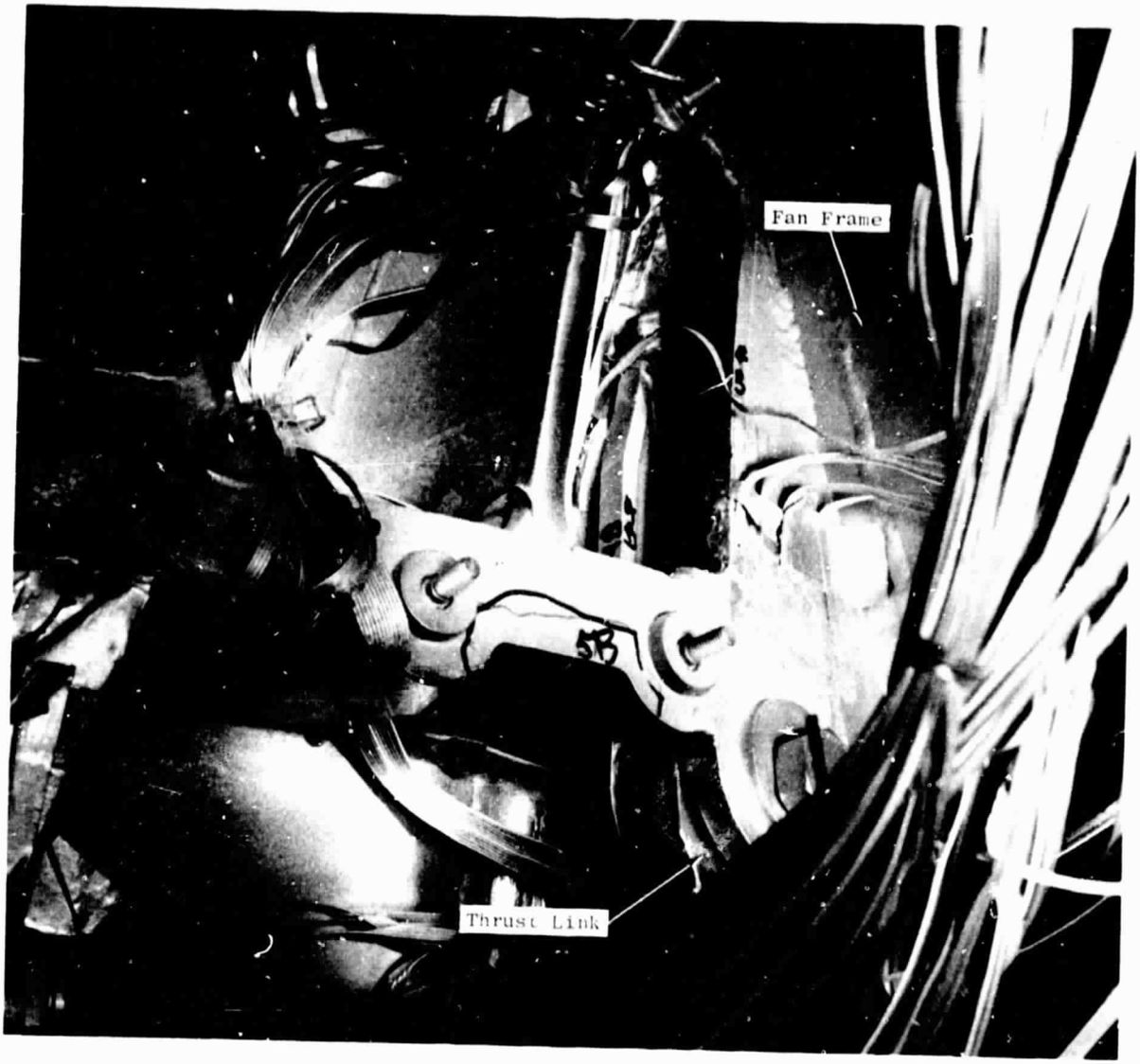

Figure 5.4. Photograph of Stresscoat Map Pattern.

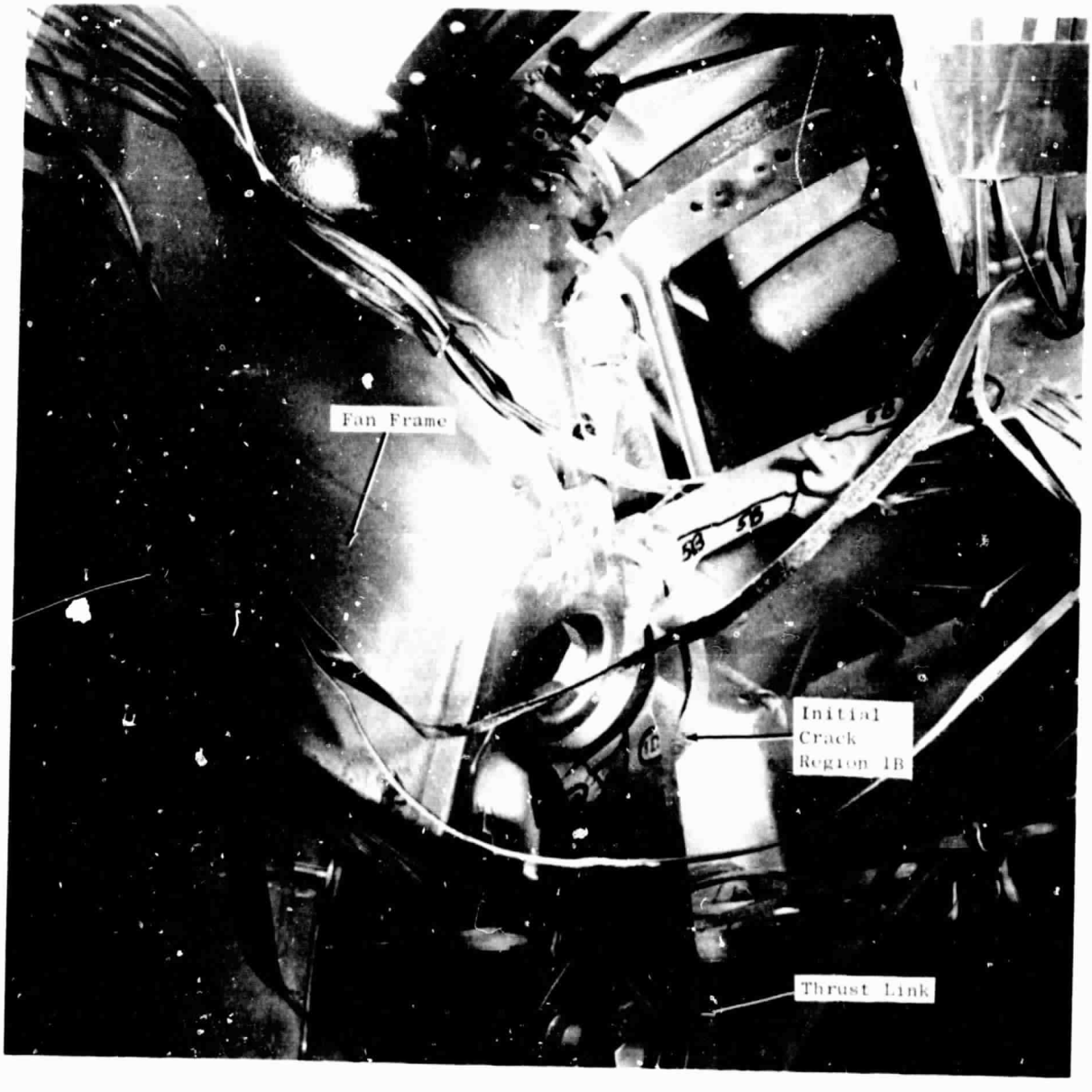

Figure 5.5. Photograph of Stresscoat Map Pattern.

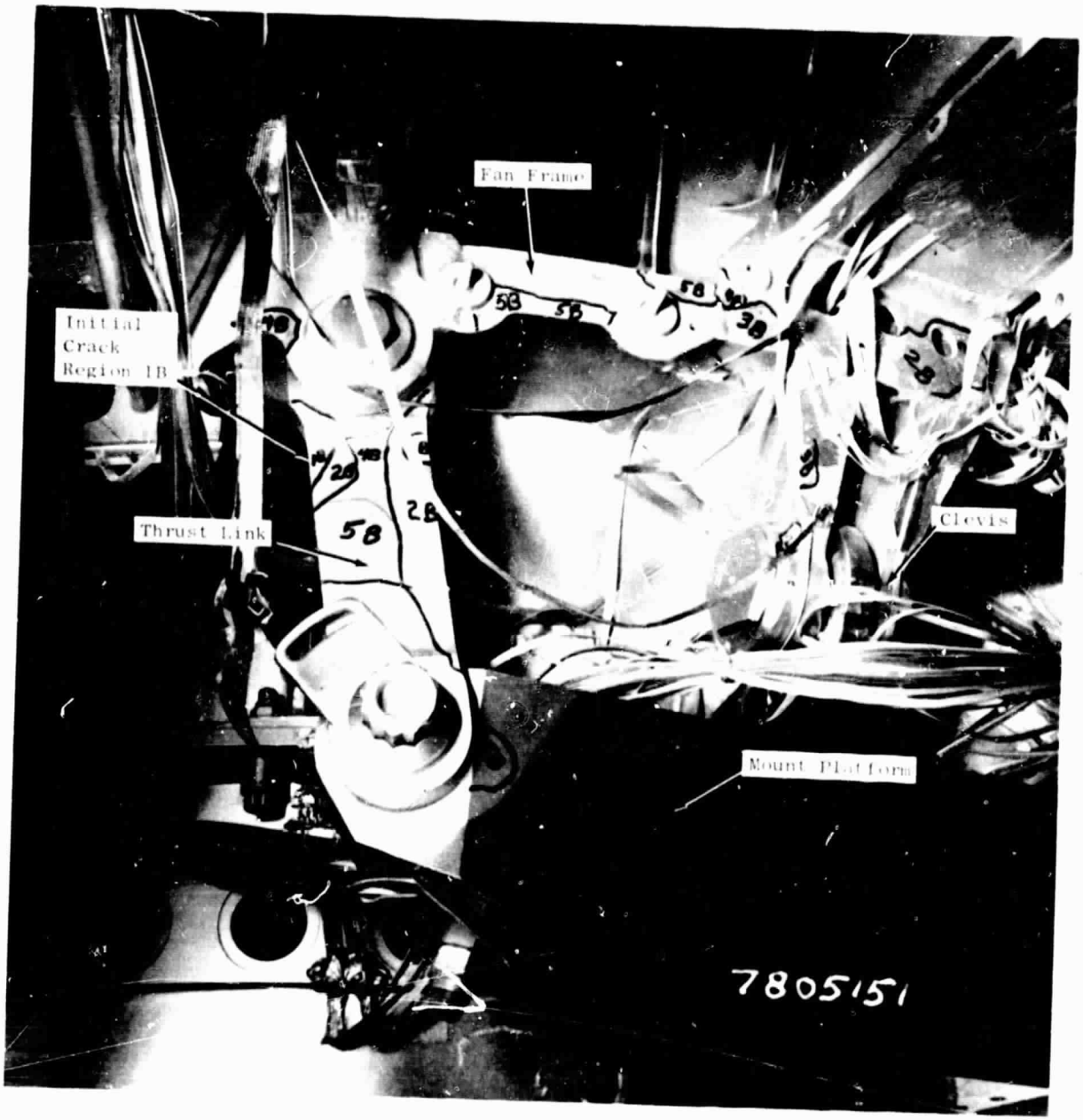

Figure 5.6. Photograph of Stresscoat Map Pattern.

Figure 5... Photograph of Stresscoat Map Pattern.

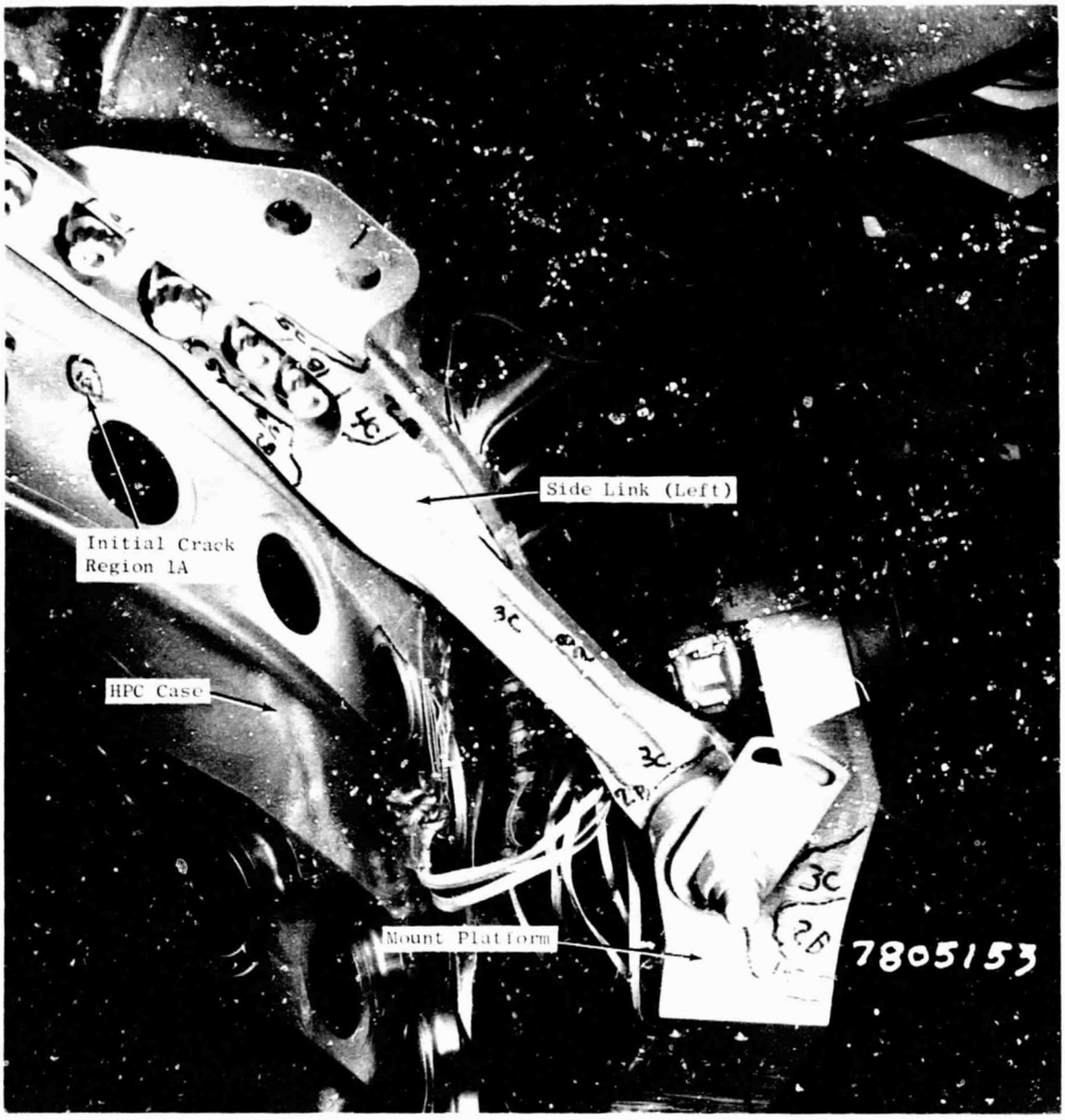

Figure 5.8. Photograph of Stresscoat Map Pattern.

case near the Stage 1 variable vane hole as shown on Figure 5.8, region 1A. A review of the strain gage readings confirmed that the primary load-carrying member for side loads is the center link. Inaccessibility of the center link limited the capability to inspect this component for Stresscote cracks. The absence of Stresscote cracks in other areas indicates a relative low stress condition in members outside the primary load path for a side load condition.

Axial Loads Test

The maximum axial (thrust) load applied was 133,450 N (30,000 lb), which is 120% of the value specified in Figure 5.1. This maximum load is 57% of the typical maximum thrust condition and 29% of the maximum limit load condition for axial loads.

Initial Stresscote cracks developed on the axial thrust link as shown on Figures 5.5 and 5.6, region 1B. Initial crack patterns developed at 66,720 N (15,000 lb) axial load. The thrust links are the primary load-carrying members for the axial load and initial crack formation on these links was anticipated. During this test run suspicious formation of Stresscote cracks developed on the fan frame and side link, region 2B, Figures 5.6 and 5.8. Subsequent investigation of strain gage data showed high strain readings on the fan frame and a side load pickup in the center link. A visual inspection of the test facilty detected that the mount facility loading fixture had rotated and made contact with the fan frame clevis at the 12 o'clock location and also with the lock plate on the right side (aft looking forward) thrust link at locations shown in Figure 5.3. It was determined that the rotation was caused because the right side actuator was not vented. After the hydraulic actuator was properly vented, the test facility fixture was reassembled. A checkout of the system was completed and the axial load test was repeated. Stresscote cracks that developed in the side link and fan frame from the test fixture movement are valid for indicating the critical stress areas on the fan frame, side link, and mount platform.

Initial Stresscote cracks in the fan frame clevises in line with the thrust links developed at 88,960 N (20,000 lb) axial load, Figures 5.4 and 5.5. The load was increased to 111,200 N (25,000 lb) and additional stress cracks developed in new areas on the fan frame and mount platform as shown on Figures 5.4 and 5.6, region 5B.

Vertical Loads Test

Maximum vertical load applied was 66,720 N (15,000 lb), which is 100% of the value specified in Figure 5.1. This maximum load is 100% of the typical flight condition vertical load and 22% of the maximum limit vertical load condition. The side links are the primary members for carrying vertical loads. Additional Stresscote crack formation on the mount platform was mapped for the 13,340 N (3,000 lb) vertical load. The Stresscote crack formation on the side links and mount platform generally appeared to broaden from previous crack

development. Figures 5.2, 5.7, and 5.8 show the pertinent Stresscote cracks for the vertical load. Visual inspection of the side links and mount platform Stresscote crack patterns did not reveal a change in the principal stress direction from preceding tests.

Reverse Axial Loads Test

This test was conducted to determine if additional Stresscote crack formations could be detected for a reverse thrust axial load condition, which simulates aircraft deceleration on landing. The test consisted of applying a reversed axial load in 22,240 N (5,000 lb) increments to 88,960 (20,000 lb). At each test point, the load was returned to zero for inspection. No additional Stresscote cracks were detected.

Discussion of Stress Test Results

Based on the four stress tests discussed in the previous paragraphs, nine additional strain gages were added on the mount platform for the deflection/distortion tests discussed in Section 6.0 (Figure 5.9). Strain gage 220 was selected to provide additional strain distribution information along the forward flange of the mount platform. The other eight strain gages were selected based on the exhibited Stresscote crack pattern development which indicated limiting stress areas not identified previously for strain gage instrumentation.

Limit Load Tests

Following the Stresscote tests, static limit load tests of the CF6-50 new front mount system and associated structures were conducted to demonstrate design limit load capability and structural integrity. Simulated key flight loads were applied. The engine new front mount and associated structure did not fail, malfunction, or permanently deform when tested to the defined limit load conditions. Sufficient strength margin was exhibited to substantiate the ultimate load capabilities to 150% of the certified limit load. The test results were submitted to the FAA for formal certification of the CF6-50 new front mount.

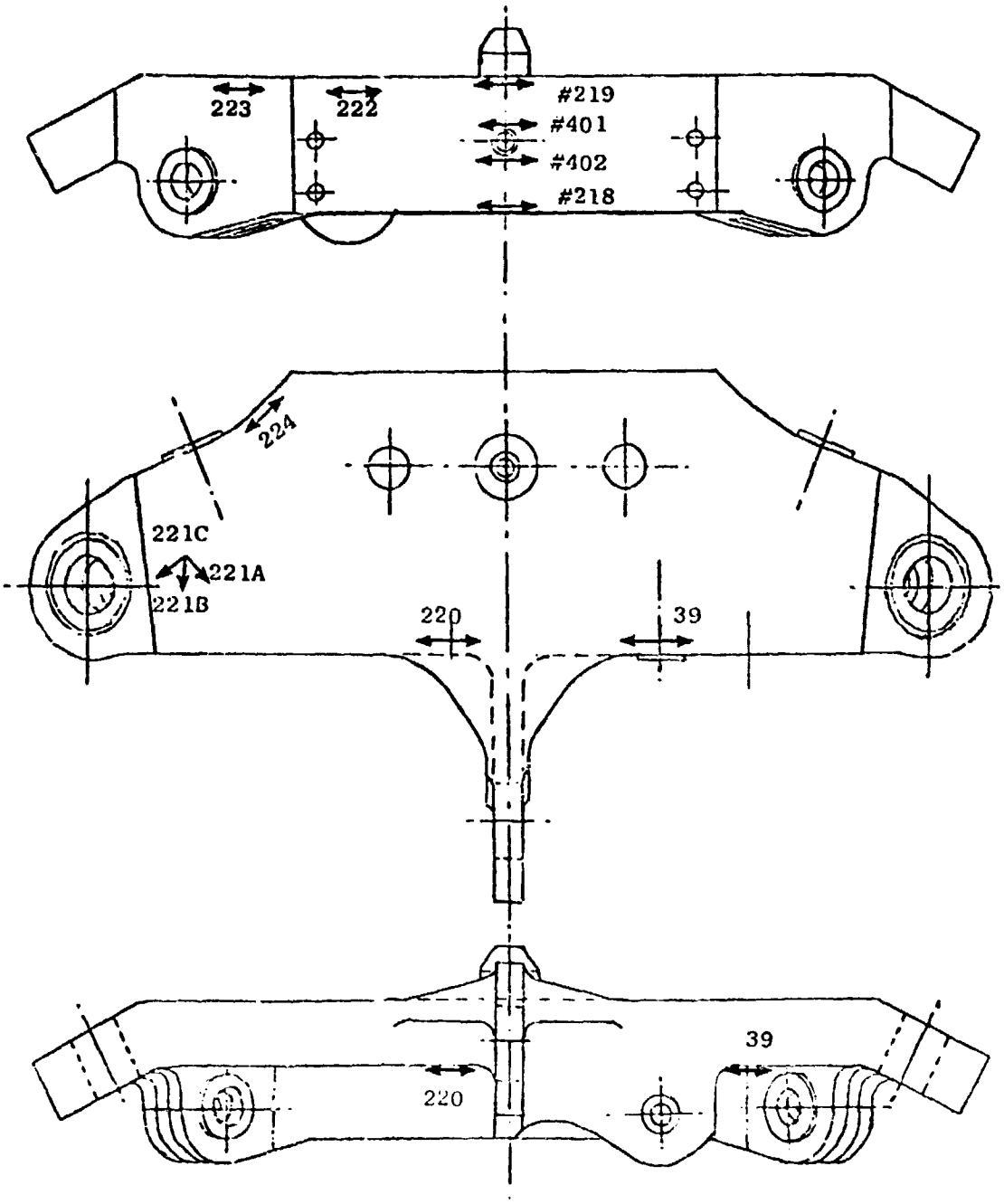

Figure 5.9. Additional Mount Platform Strain Gages Based on Stress Test Results.

6.0 DEFLECTION/DISTORTION TESTS

Three separate tests were conducted as a part of the deflection/distortion tests, and are listed below:

1. Engine casing deflection/distortion tests

2. Failsafe load tests of the new front mount with simulated element failures

3. Simulated thermal and assembly stress correlation tests.

In each of these tests, deflection of the mount system and distortion of the compressor casing cross section was recorded, and the stresses obtained from measured strain gage outputs were compared with calculated stresses. Deflection of the fan case, compressor rear frame, turbine midframe, and low pressure turbine case were also measured. A description of the deflection/distortion test setup with a complete CF6-50 engine outer shell structure suspended from a DC-10 wing pylon is presented in Section 4.2.

The first test was conducted to measure the compressor casing deflection and structural stresses induced for maximum power conditions by simulating maximum static thrust and takeoff at rotation load conditions, first with the original and then the new front mount. In the second test, failsafe load conditions, representing maximum axial, side, and vertical loads for the corresponding design maximum flight load condition were applied to the new front mount, on which component failures were simulated by removal of components from the assembly. The third test examined stresses induced in the new front mount system for simulated thermal growth of the supporting structure and simulated stackup assembly conditions.

6.1 Engine Casing Deflection/Distortion Test

The objective of the engine casing deflection/distortion test was to demonstrate, by back-to-back testing, the advantage of the new front mount system over the original front mount in reducing compressor casing distortion caused by the local reaction of thrust and vertical loads at the front mount. Overall deflection of the engine shell was also measured and strain gages, installed on each of the front mount components and fan frame, were read to confirm the calculated loads and stresses induced in the individual members.

6.1.1 Test Procedure

Comparison tests between the original and new front mount were conducted under two conditions of maximum axial loads. Engine runup on the wing and

ground engine tests were simulated by the maximum static thrust with a 1G down inertia load. Takeoff at rotation was simulated by the corresponding engine thrust plus an aerodynamic up-load on the inlet and the 1G down inertia load. These two loading conditions have been used consistently for all tests, and the associated loads and sign convention are shown in Figure 6.1.

Initially, a "zero" deflection reading was obtained with the engine inlet removed and the engine supported by the fan case ground handling points and the rear engine mount. This "zero" is very similar to the attitude of and support for the engine when the internal boring of the cases is conducted and represents closely the undeflected casing. After reconnecting the front mount to the pylon a 1G down load was applied and all strain gages and deflection potentiometers were recorded, and a 360° sweep made with the shaft-mounted deflection potentiometers to record casing radial distortion. The loading was then increased incrementally to the maximum test values and the stationary potentiometers and strain gages recorded at each step, and the 360° sweep of the shaft mounted deflection potentiometers was repeated. This procedure was repeated for the test conditions listed in Figure 6.1.

6.1.2 Test Results and Discussion

Compressor Casing Deflection

Of major interest in this test series was the reduction in HPC casing deflection which can be realized by the use of the new front mount system. The reduction in radial deflection relative to the rotor shaft bearings was obtained by comparing the radial deflection at each stage of the high pressure compressor (HPC) casing with the original and the new front mounts under identical loading conditions. In addition to these tests with a titanium HPC casing, a steel HPC casing was tested with the original and new front mount under General Electric funding.

Immediately following each test, polar plots of the radial deflection at various thrust load levels were obtained. Typical plots showing the titanium compressor case circumferential distortion from 0 to the maximum static thrust condition are shown in Figures 6.2 through 6.5. As noted, increasing the axial (thrust) load increases the circumferential distortion of the compressor case, and results in a cardiod-type shape. Both stages 2 and 3 of the compressor case show a significant reduction in maximum radial deflection at 12 o'clock with the new front mount as compared to the original. (Note the difference in radial deflection scales on the polar plots for the original and the new front mounts.) For the 55,000 lb. maximum static thrust plus 1G down applied load, the maximum radial deflection at Stage 3 decreased about 50% from 0.038 in. with the original to 0.018 in. with the new front mount.

In Figures 6.6 through 6.11 the compressor casing radial deflections with the original and the new front mount are compared for the maximum static thrust and the takeoff at rotation conditions. The original titanium HPC case was tested with the original and the new front mount, and a new steel HPC

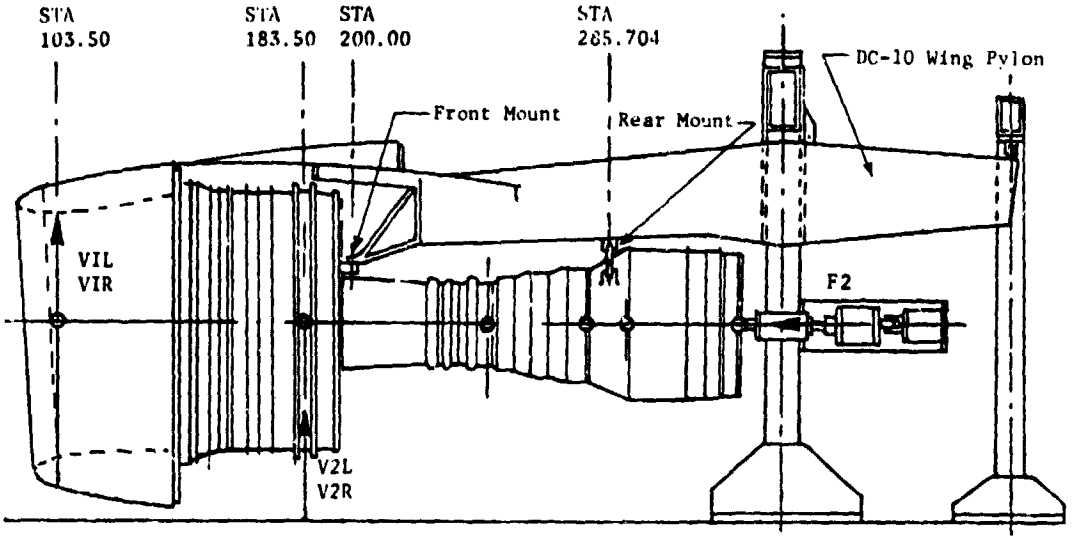

Test Condition	Applied Test Loads N - (lb)				
	Thrust	Inlet Air Load		Inertia Load	
	F2 Axial	V1L Vertical	V1R Vertical	V2L* Vertical	V2R* Vertical
Maximum Static Thrust	244,650 (55,000)	0	0	-9,150 (-2,058)	-9,150 (-2,058)
Takeoff at Rotation	184,601 (41,500)	19,570 (4,400)	19,570 (4,400)	- 9,150 (-2,058)	- 9,150 (-2,058)

*V2L & V2R plus the tare weight of the test engine assembly give the correct 1 'G' down reaction at the front mount and very close agreement with the compressor casing bending moment under vertical gravitational effects.

Figure 6.1. Test Loads for Deflection/Distortion Tests.

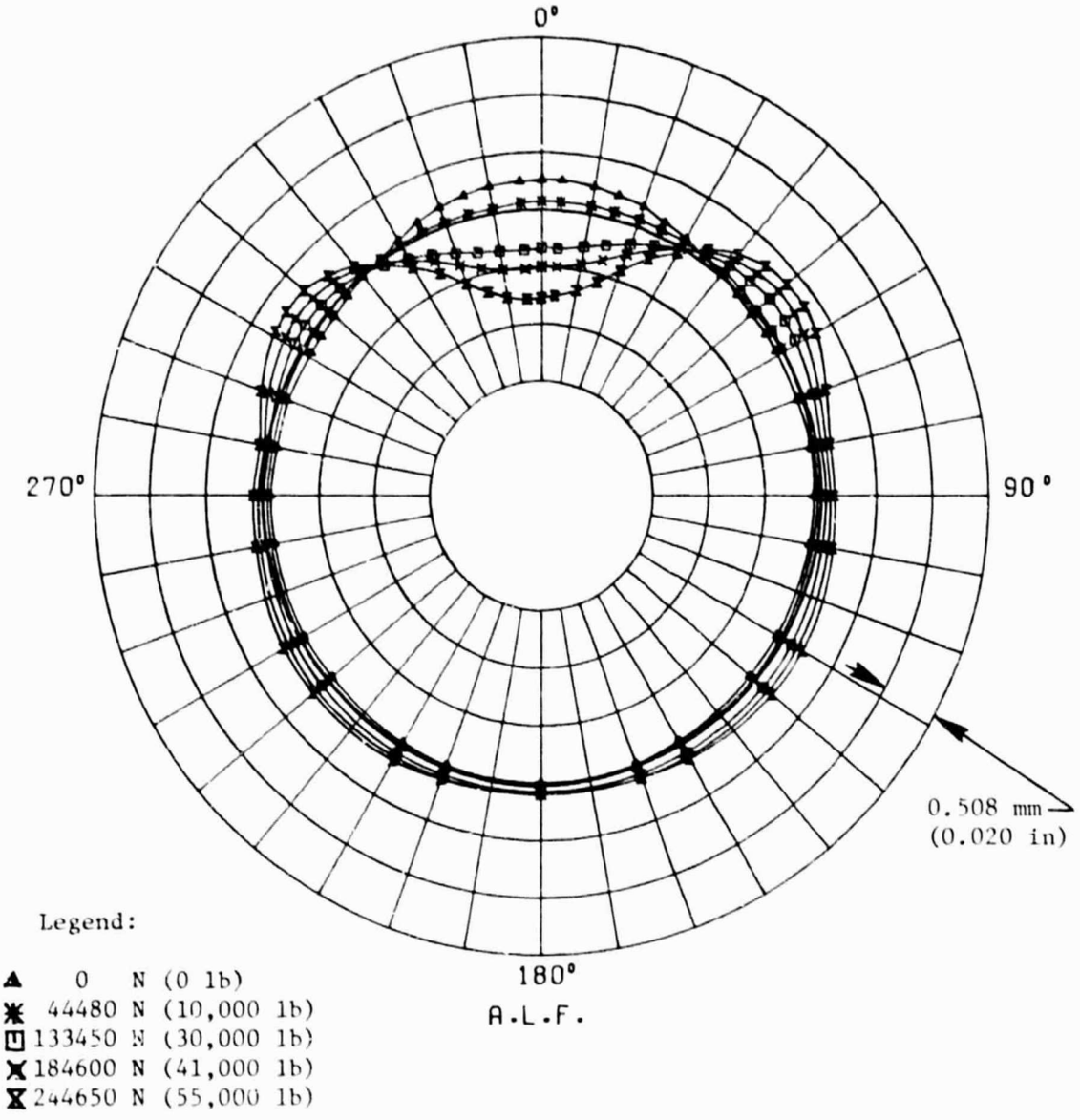

Figure 6.2. CF6-50 Original Front Mount - HPC Casing Stage 2 Radial Deflection, 0 to Maximum Static Thrust Condition (Including 1 G Down).

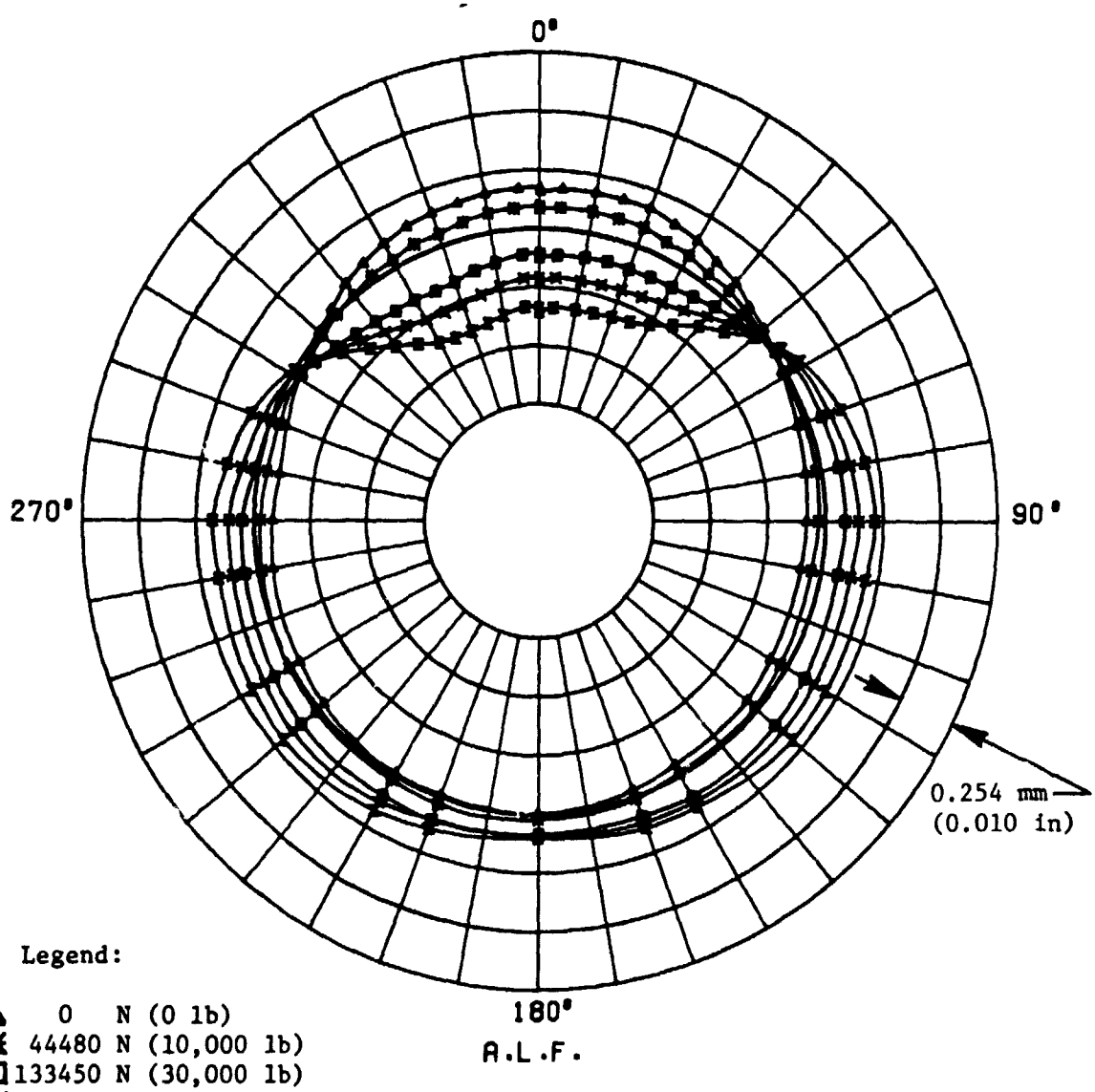

Figure 6.3. CF6-50 New Front Mount - HPC Casing Stage 2 Radial Deflection, 0 to Maximum Static Thrust Condition (Including 1 G Down).

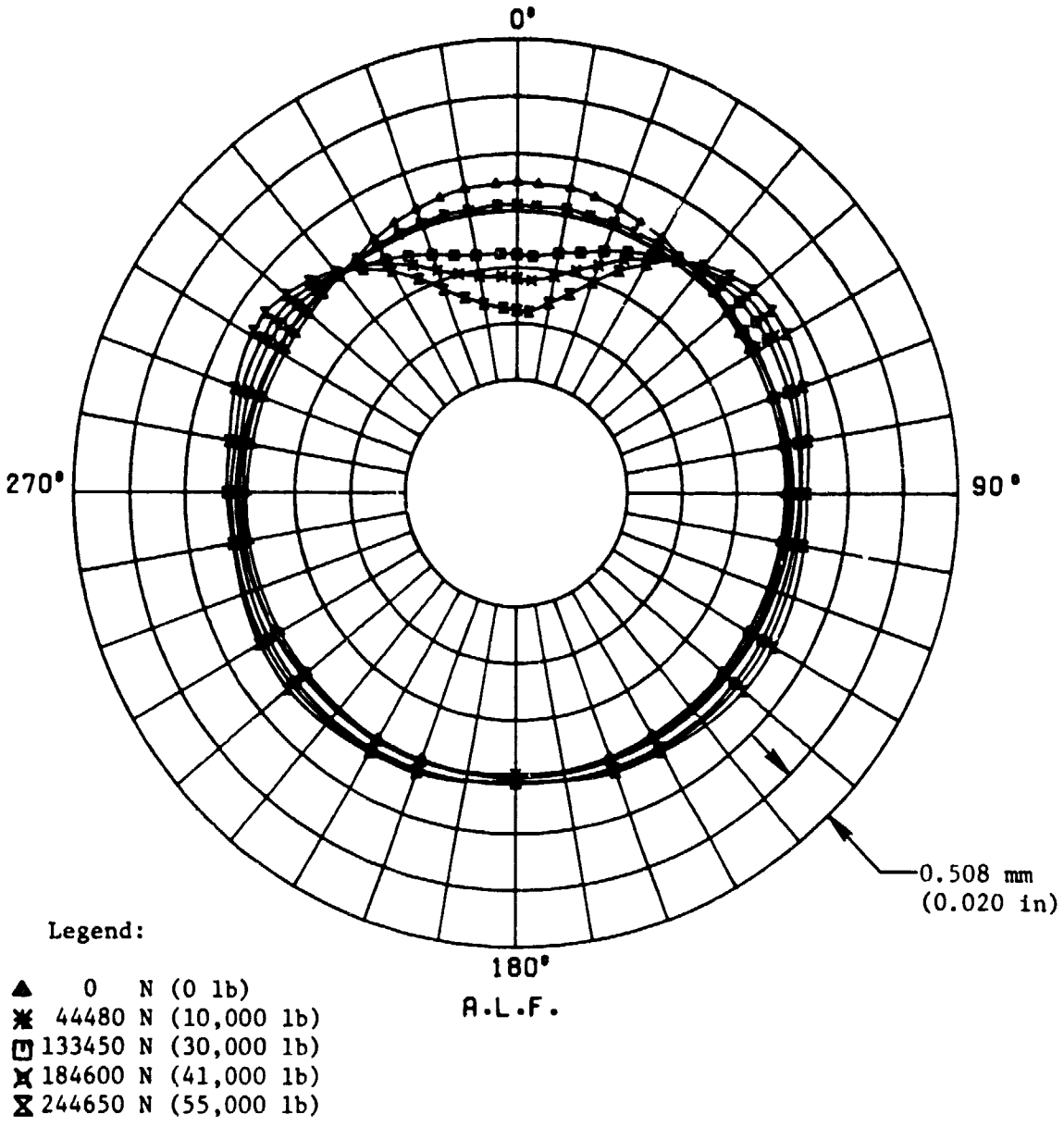

Figure 6.4. CF6-50 Original Front Mount - HPC Casing Stage 3 Radial Deflection, 0 to Maximum Static Thrust Condition (Including 1 G Down).

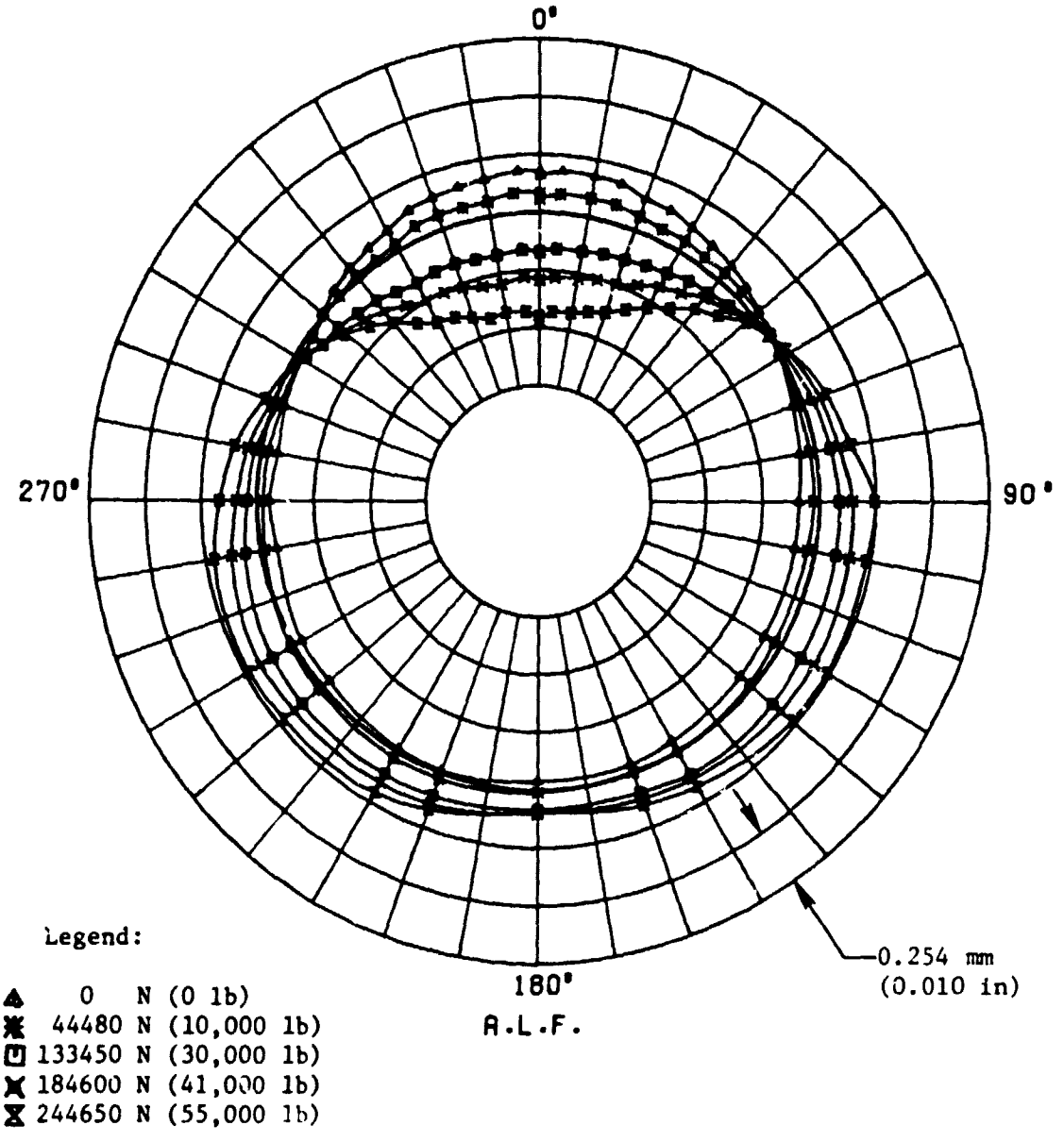

Figure 6.5. CF6-50 New Front Mount - HPC Casing Stage 3 Radial Deflection, 0 to Maximum Static Thrust Condition (Including 1 G Down).

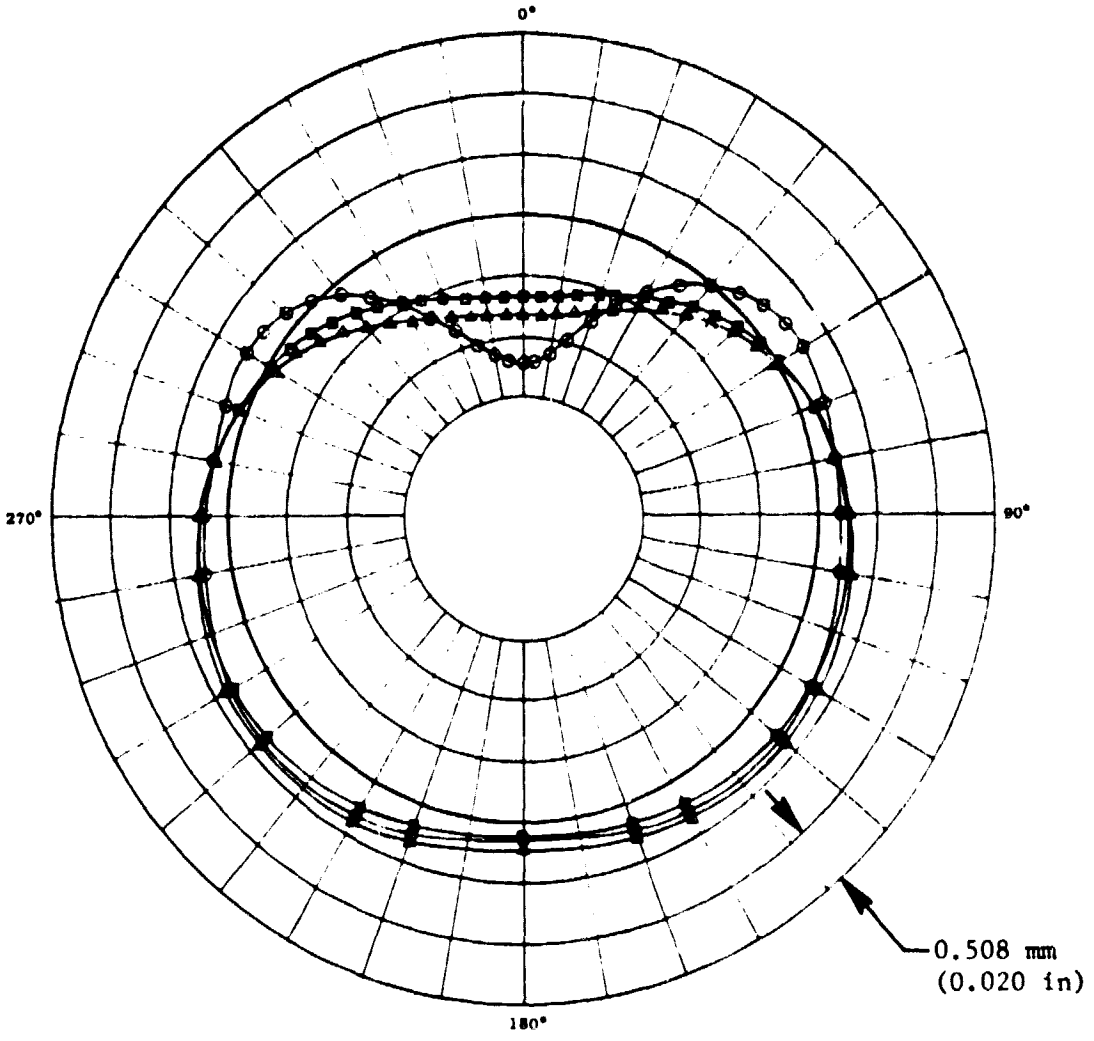

○ Original Front Mount, Titanium Casing

△ New Front Mount, Titanium Casing

□ New Front Mount, Steel Casing

Figure 6.6. CF6-50 Original and New Front Mount - HPC Casing Radial Deflection at Stage 3, Takeoff at Rotation Condition (Including 1 G Down).

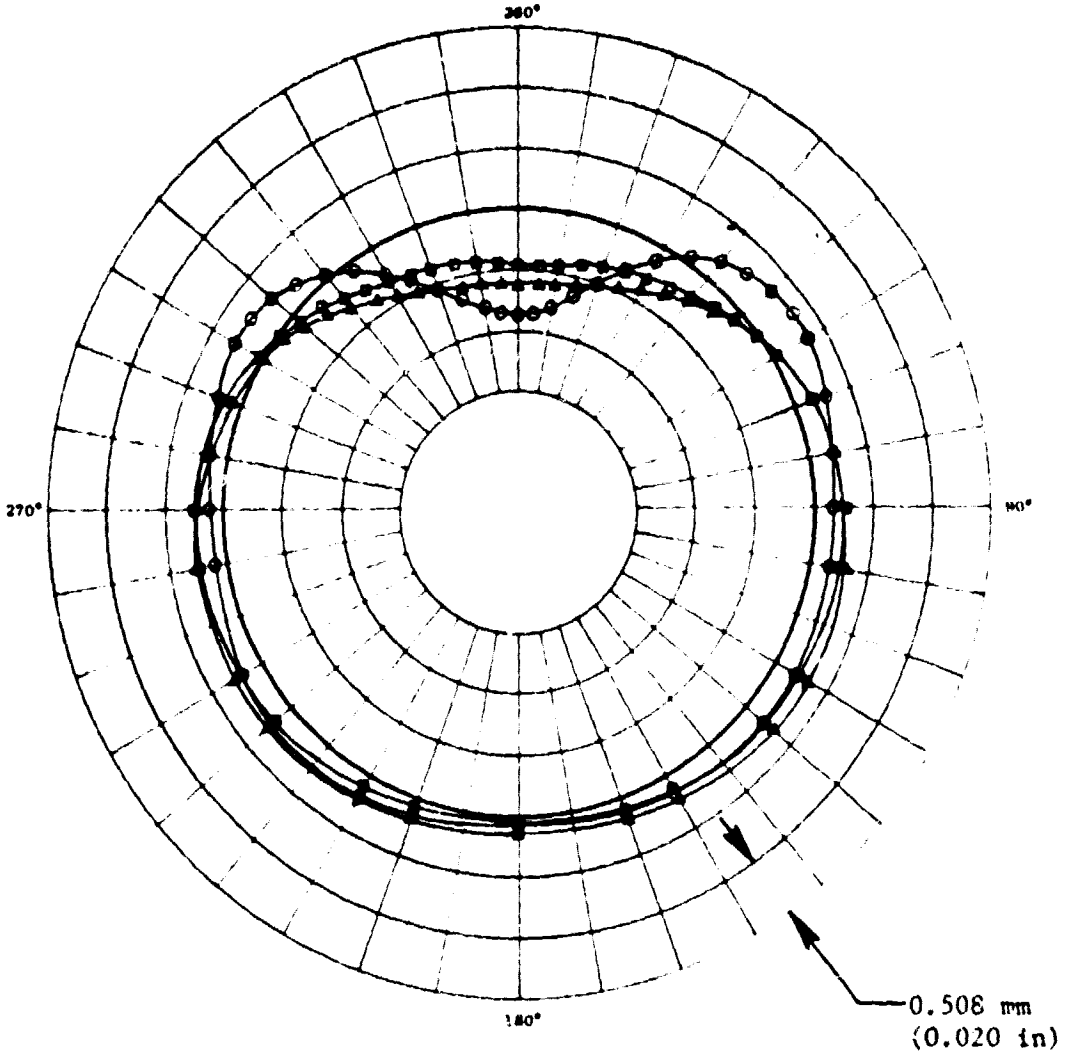

○ Original Front Mount, Titanium Casing

△ New Front Mount, Titanium Casing

□ New Front Mount. Steel Casing

Figure 6.7. CF6-50 Original and New Front Mount - HPC Casing Radial Deflection at Stage 3, Maximum Static Thrust Condition (Including 1 G Down).

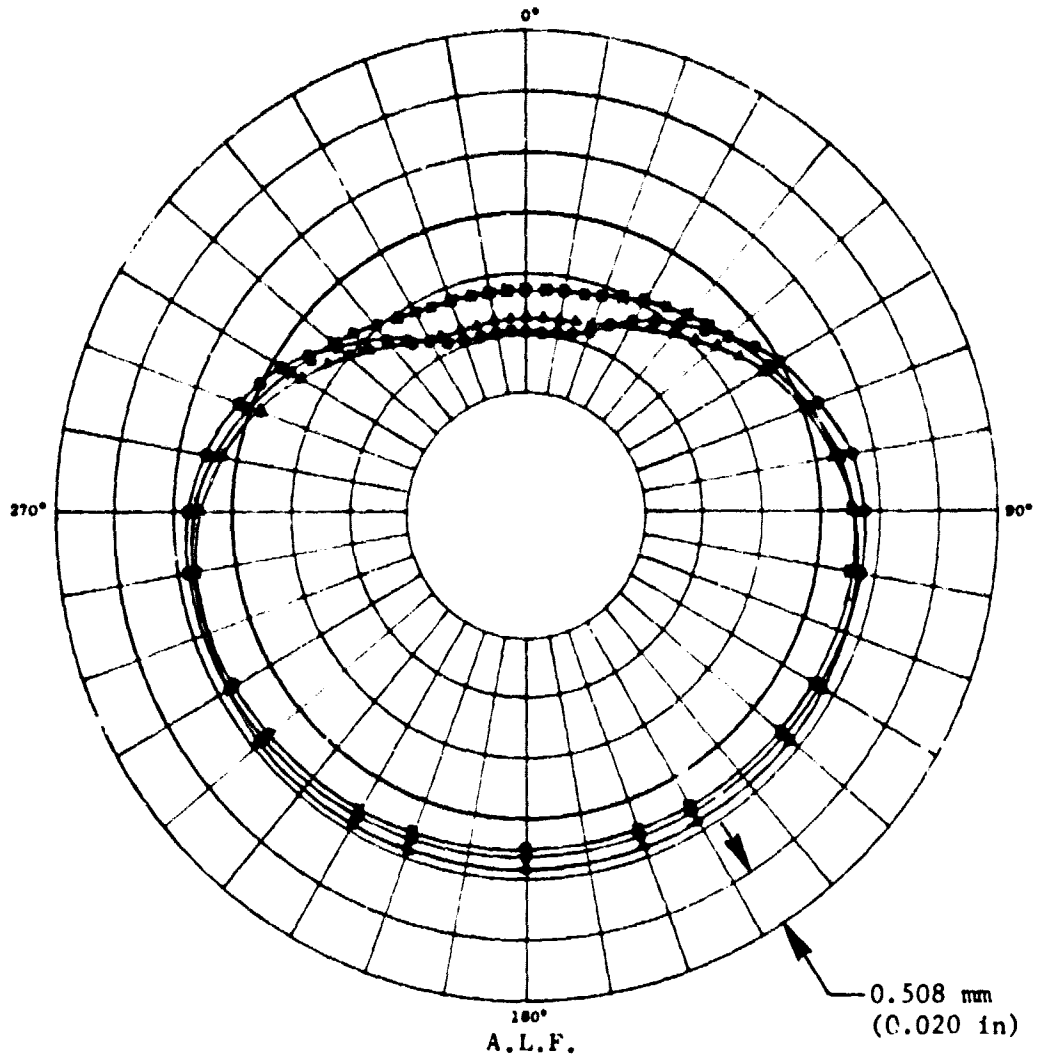

○ Original Front Mount, Titanium Casing

△ New Front Mount, Titanium Casing

□ New Front Mount, Steel Casing

Figure 6.8. CF6-50 Original and New Front Mount - HPC Casing Radial Deflection at Stage 7, Takeoff at Rotation Condition (Including 1 G Down).

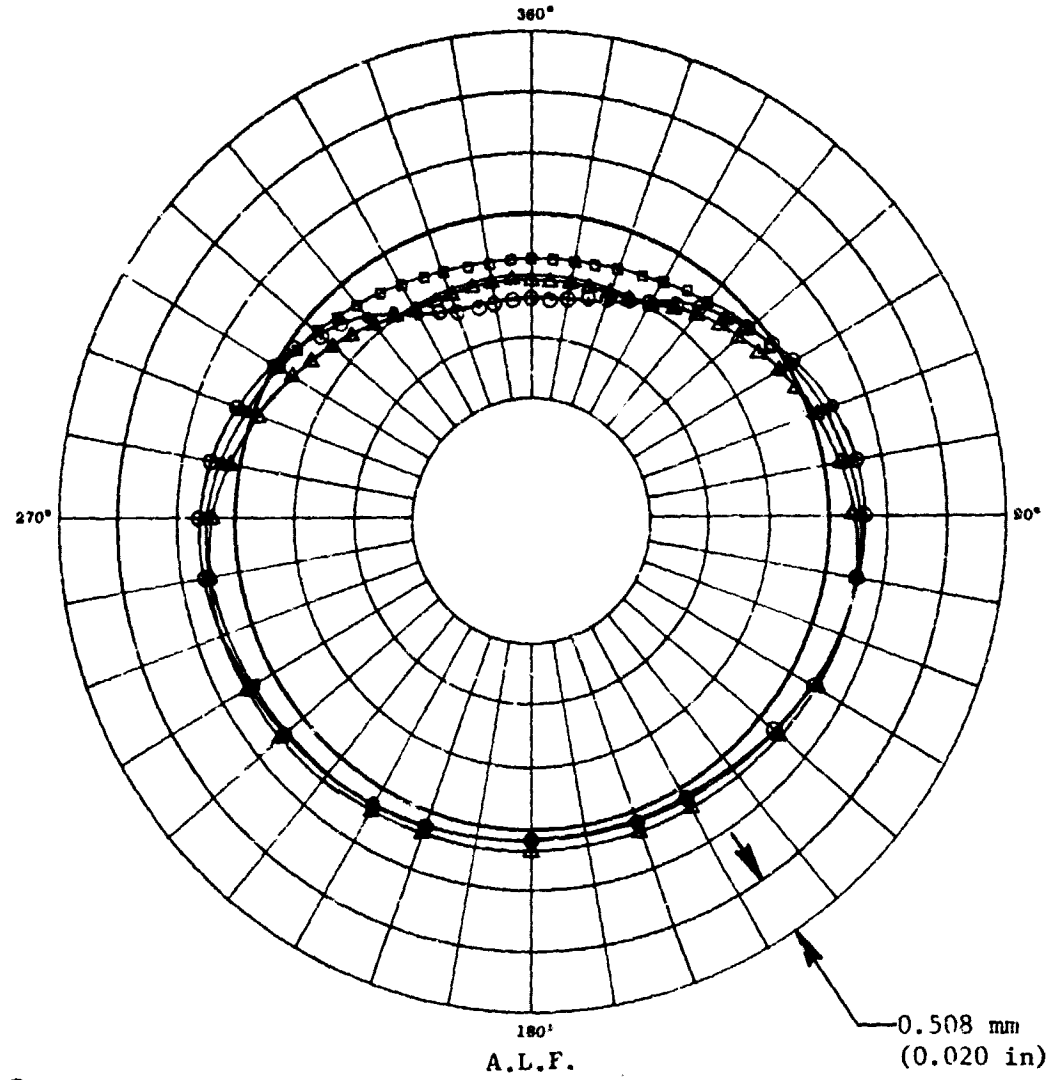

Figure 6.9. CF6-50 Original and New Front Mount - HPC Casing Radial Deflection at Stage 7, Maximum Static Thrust Condition (Including 1 G Down).

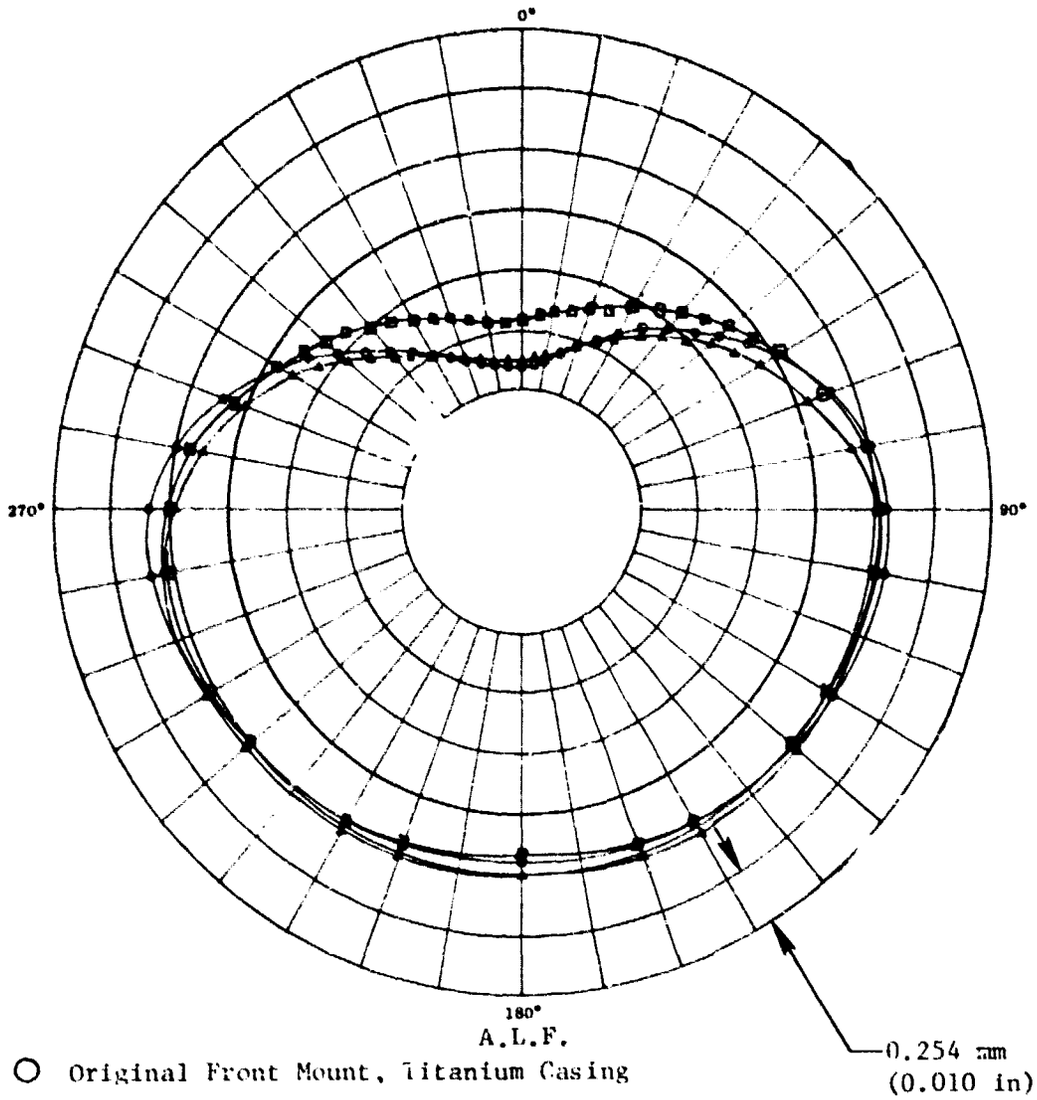

Figure 6.10. CF6-50 Original and New Front Mount - HPC Casing Radial Deflection at Stage 10, Takeoff at Rotation Condition (Including 1 G Down).

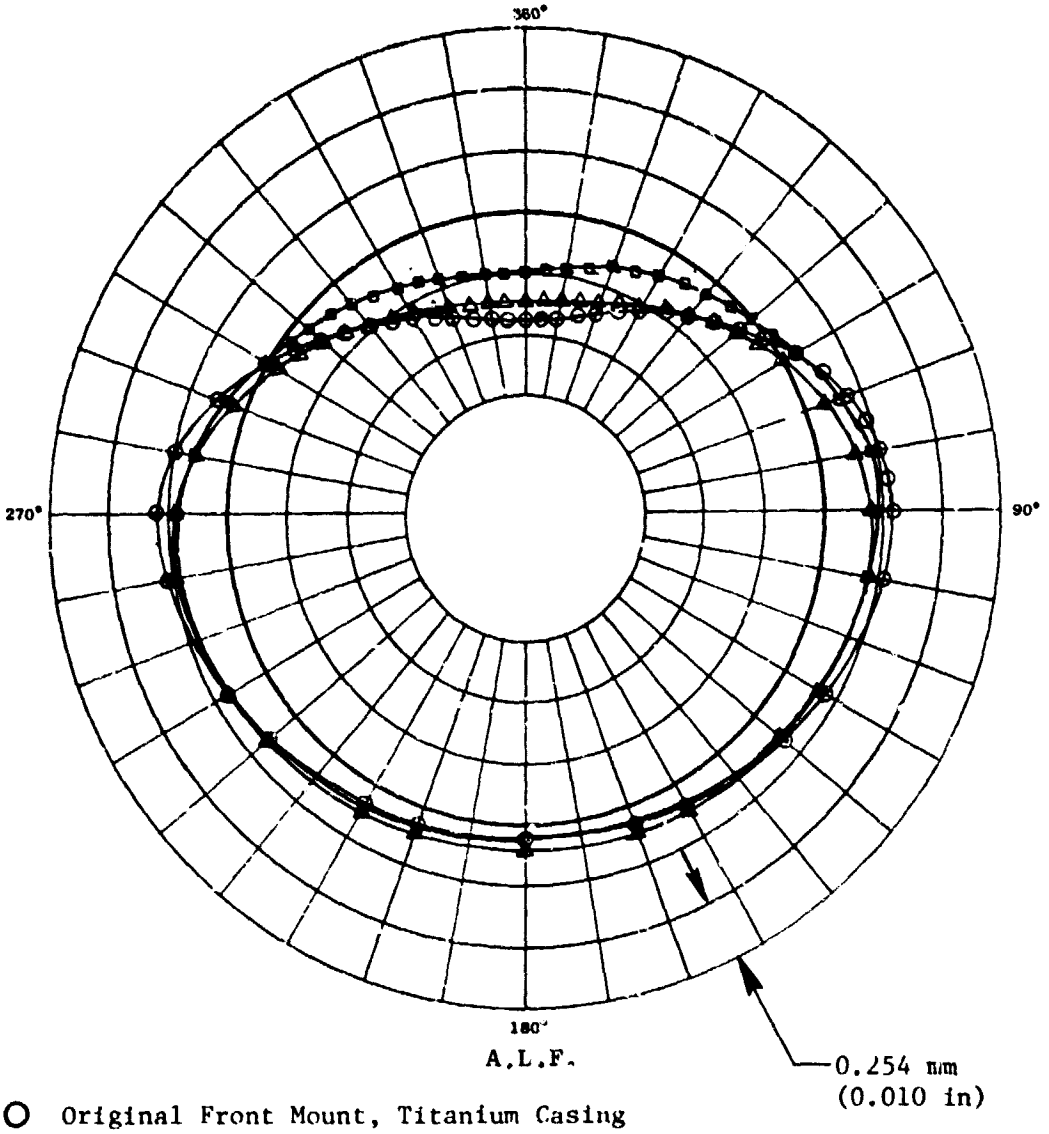

Figure 6.11. CF6-50 Original and New Front Mount- HPC Casing Radial Deflection at Stage 10, Maximum Static Thrust Condition (Including 1 G Down).

case was tested with the new front mount. The polar plots show the improvement due to the new front mount at Stages 3, 7, and 10 of the compressor casing. The new front mount reduced the radial deflection 0.010 to 0.020 in. in the forward HPC Stages 2 and 3, but in the later stages (7 and 10), only a slight improvement (0.001 to 0.007 in.) was observed. An additional reduction in the radial deflection of 0.006 to 0.010 in. was measured in the later Stages (7 and 10) with the new front mount and the steel HPC case.

The influence of the new front mount is apparent at compressor stages remote from the front mount. Figures 6.12 and 6.13 compare the 12 o'clock radial deflections along the length of the compressor casing, and illustrate that improvements are obtained along the complete length of the casing. For the 244,650 N (55,000 lb) max. static thrust plus 1G down applied load condition (Figure 6.12), the maximum radial deflection decreased 42% from 9.144 mm (0.036 in.) at Stage 3 with the original front mount to 5.334 mm (0.021 in.) at Stage 6 with the new front mount and the titanium HPC case.

For the takeoff at rotation load condition (Figure 6.13), the maximum radial deflection decreased 29% from 12.446 mm (0.049 in.) at Stage 3 with the original front mount to 8.890 mm (0.035 in.) at Stage 6 with the new front mount and titanium HPC case. With the new front mount and steel HPC case, the maximum radial deflection was decreased 45% as compared to the original front mount and titanium HPC case. The reduction in maximum radial deflection obtained by the use of the new front mount with the titanium HPC case is 29% for the takeoff at rotation condition and 42% for the maximum static thrust condition. With the steel HPC case, the new front mount reduced the maximum radial deflection 33% and 41% for the takeoff at rotation and maximum static thrust conditions, respectively.

Sensitivity of the radial deflection of the compressor casing to changes in stiffness of the fan casing is shown in Figure 6.14. Deflection obtained before and after the removal of the DC-10 inlet is plotted along the length of the compressor casing. The large change in fan casing stiffness can be seen to have a small but measurable effect on the radial deflection. Installation of the DC-10 inlet increased the stiffness of the fan casing assembly and reduced the HPC case maximum radial deflection by about 12%.

To determine the separate effects of compressor case backbone bending and the local vertical load on the front mount, a test was conducted in which a vertical load was applied to the fan casing to obtain the same vertical reactions at the front mount as the maximum static thrust provides. The compressor casing backbone bending effect, relative to the compressor shaft, was obtained by a harmonic analysis of the radial deflections at each compressor stage. Figure 6.15 illustrates the total radial deflection at 12 o'clock obtained from this test, the backbone bending curve calculated from the harmonic analysis, and the difference between the two which gives the distortion due to the vertical load on the new front mount (note low values of radial deflection).

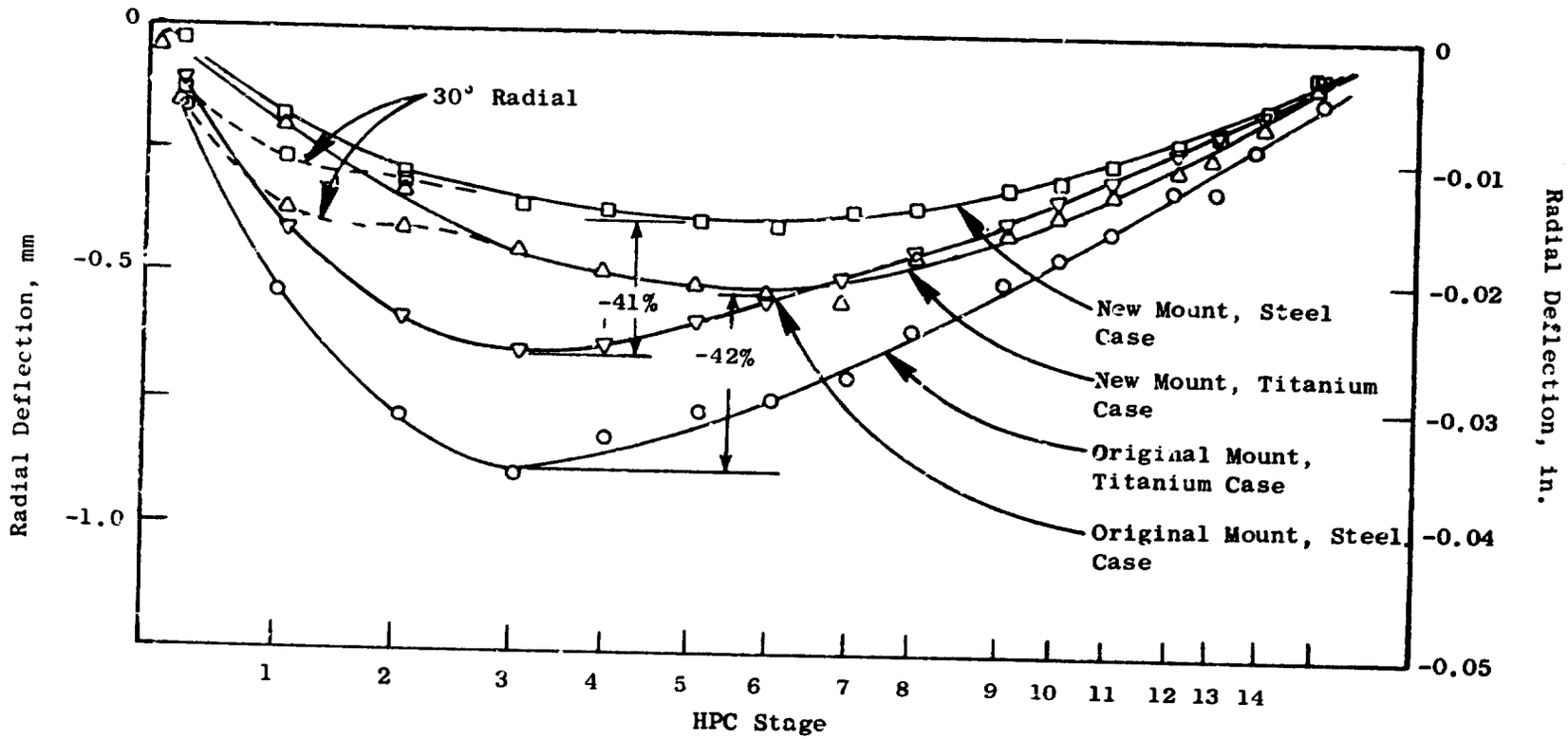

Figure 6.12. Original and New Front Mount - HPC Casing Backbone Radial Deflection, Maximum Static Thrust Condition (Including 1 G Down), DC-10 Inlet, DC-10 Wing Pylon.

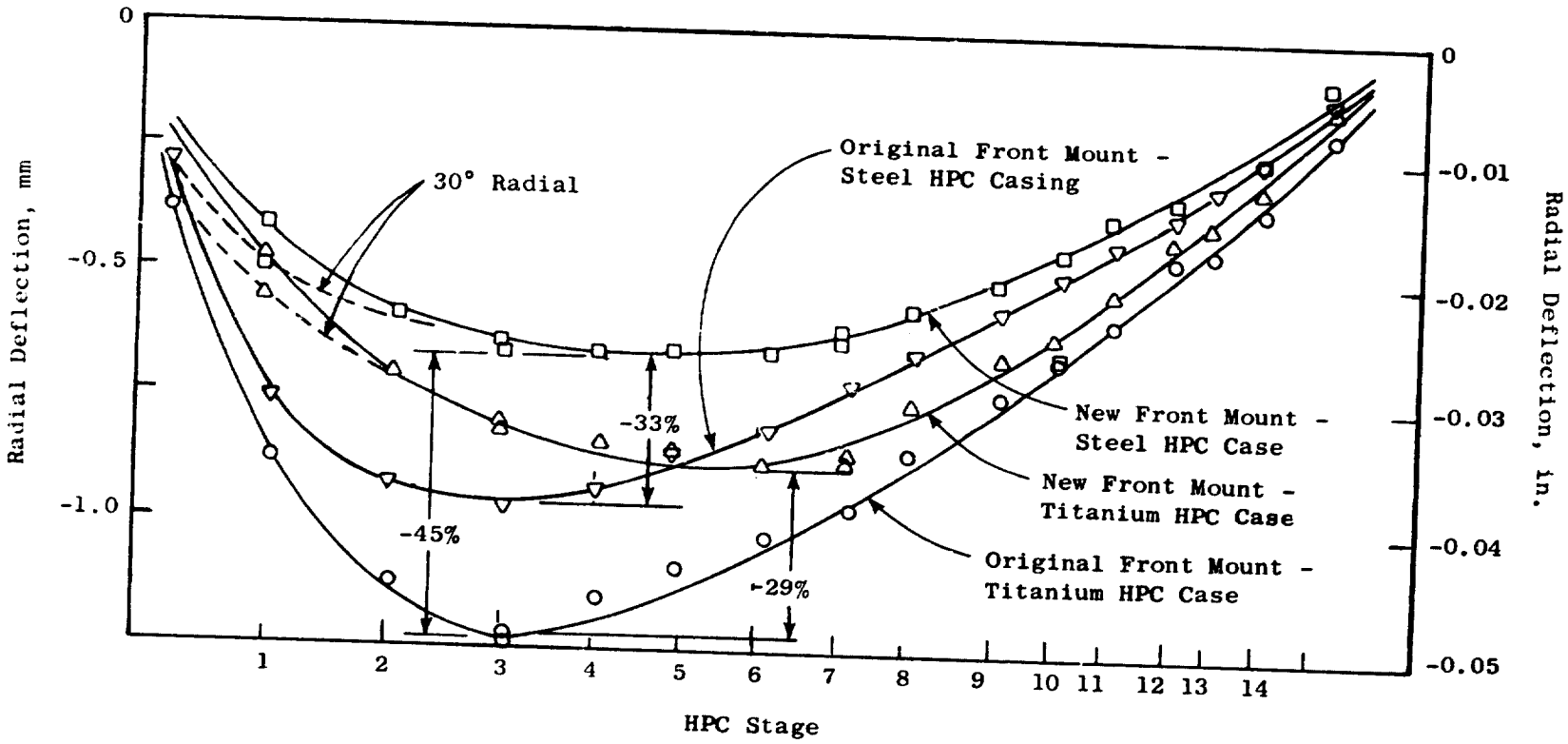

Figure 6.13. Original and New Front Mount - HPC Casing Backbone Radial Deflection, Takeoff at Rotation Condition (Including 1 G Down), DC-10 Inlet, DC-10 Wing Pylon.

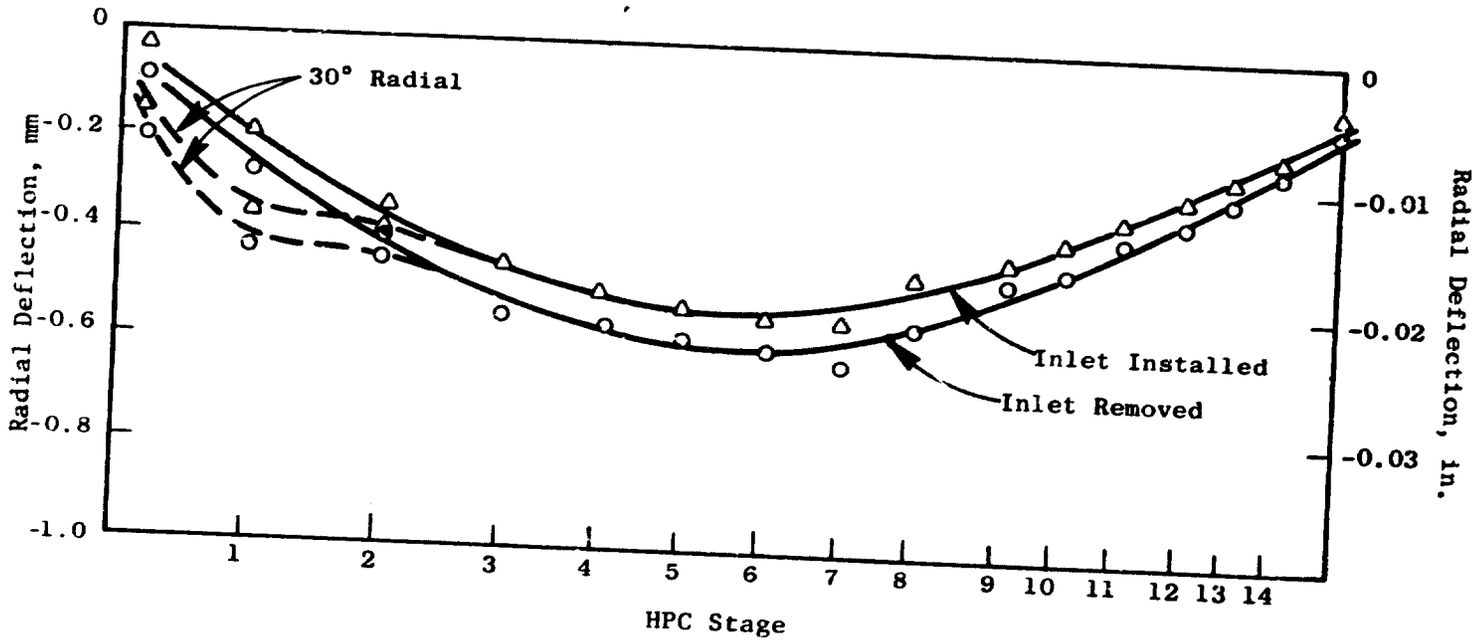

Figure 6.14. CF6-50 New Front Mount - Effect of DC-10 Inlet on HPC Casing Backbone Radial Deflection, Maximum Static Thrust (Including 1 G Down), DC-10 Wing Pylon, Titanium HPC Case.

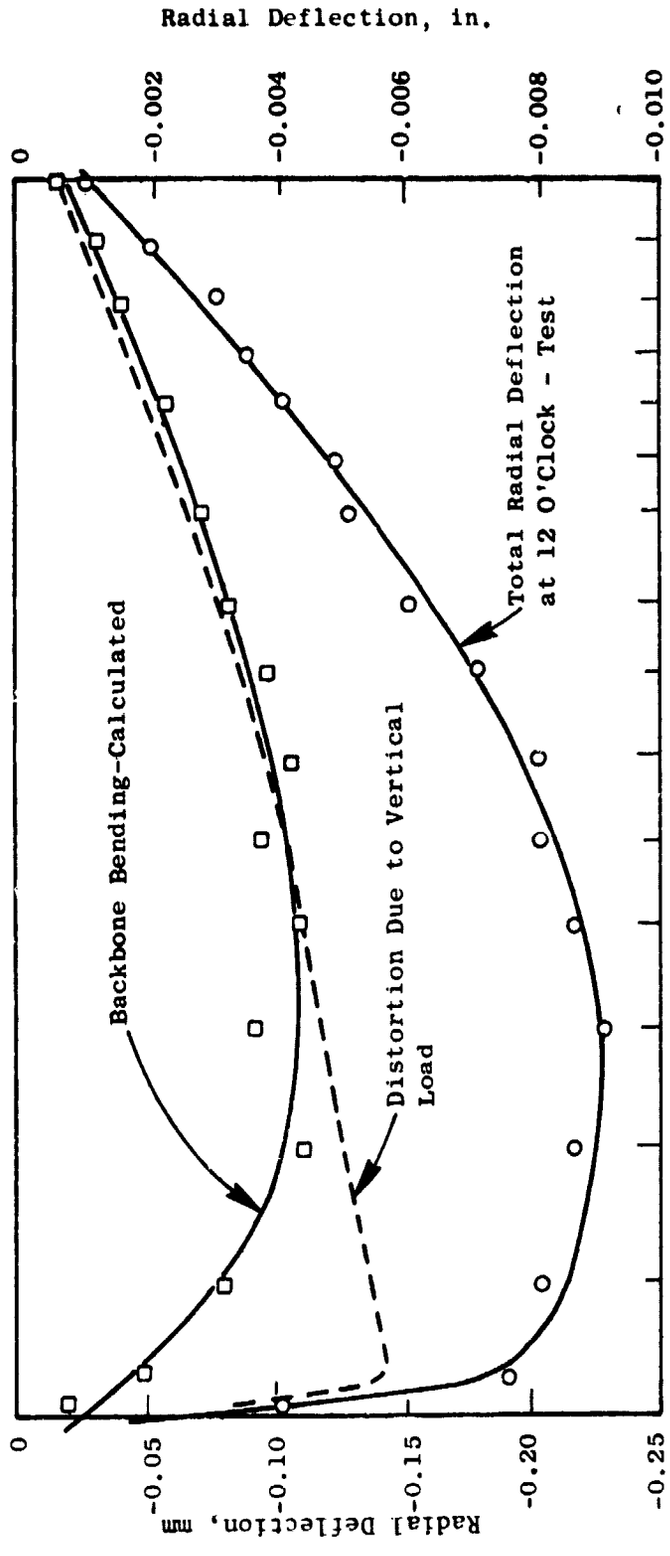

Figure 6.15. CF6-50 New Front Mount - HPC Casing Backbone Radial Deflection Due to Vertical Load on Mount.

All deflection/distortion testing demonstrated the improvement of the new over the original front mount in substantially reducing the distortion of the HPC casing.

Front Mount Component Loads and Stresses

Strain gage readings were obtained during these engine casing deflection/distortion tests, and were used to calculate stresses and internal loads in the front mount components for comparison with calculated values. Excellent agreement was obtained for the calculated and measured axial loads in the supporting side and thrust links, as may be seen from the curves in Figures 6.16 and 6.17. Calculated and measured stresses for the new front mount platform and link components during takeoff loading conditions are shown in Figure 6.18. Slight divergence occurs in some cases, which is attributed to the differences in the calculated and measured bending stresses in the components. The bending moment distribution is sensitive to the degree of assumed end restraint of the link components. However, both calculated and measured stresses are low and well within the fatigue allowable stresses for the material.

Discussion

The new front mount reduced the local deflection of the high pressure compressor casing for the takeoff conditions tested, permitting a reduction in core compressor clearances. However, other factors also affected the permissible minimum clearances and a detailed discussion of these results is given in Section 10.0, Performance Assessment.

Close agreement was obtained between the calculated and measured loads and stresses in the new front mount and the supporting links under conditions closely representing the actual engine/pylon installation. This confirms the calculated interaction loads between the pylon and front mount, which were used in the Low Cycle Fatigue Tests described in Section 7.0 and the Company-funded Certification Limit Load Tests described in Section 5.0, in which the test loads applied to the front mount interface were calculated from a computer structural analysis of the redundant engine/pylon configuration.

6.2 Failsafe Load Test

The objective of the Failsafe Load Test program was to examine the behavior of the new front mount and engine casings under several stipulated modes of partial failure of the front mount. During the testing, the failure of an element was simulated by the removal of that element from the front mount structure. Measurements of compressor casing radial distortion were made to ensure that these were acceptable with regard to compressor blade clearance. The behavior of the failsafe tongue, provided to reduce excessive motion and stress in the mount, was also studied, and comparisons were made between calculated and measured stresses in the front mount supports and backup structure.

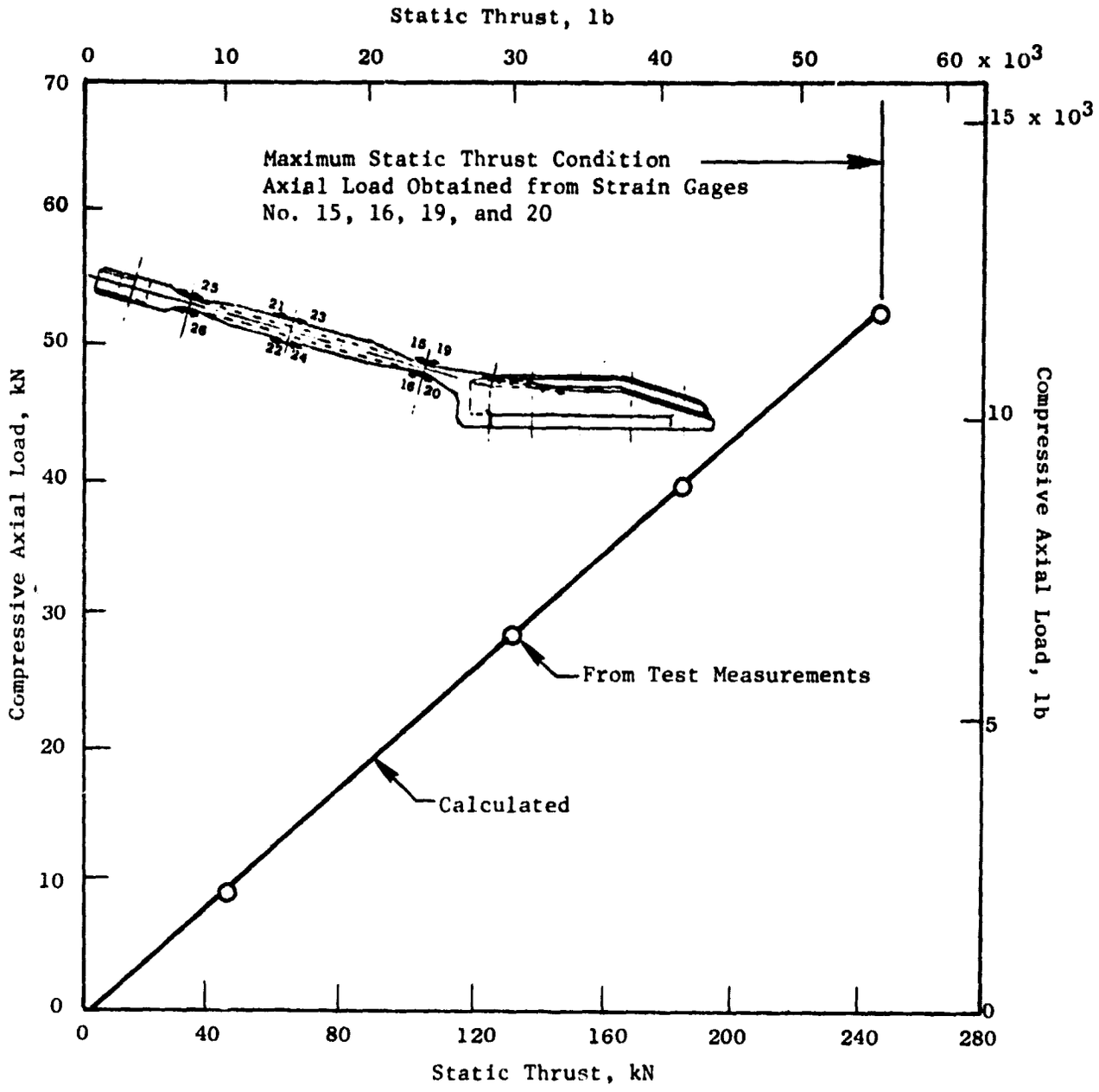

Figure 6.16. Calculated Versus Measured Compressive Axial Load in Side Link Due to Applied Static Thrust Loads.

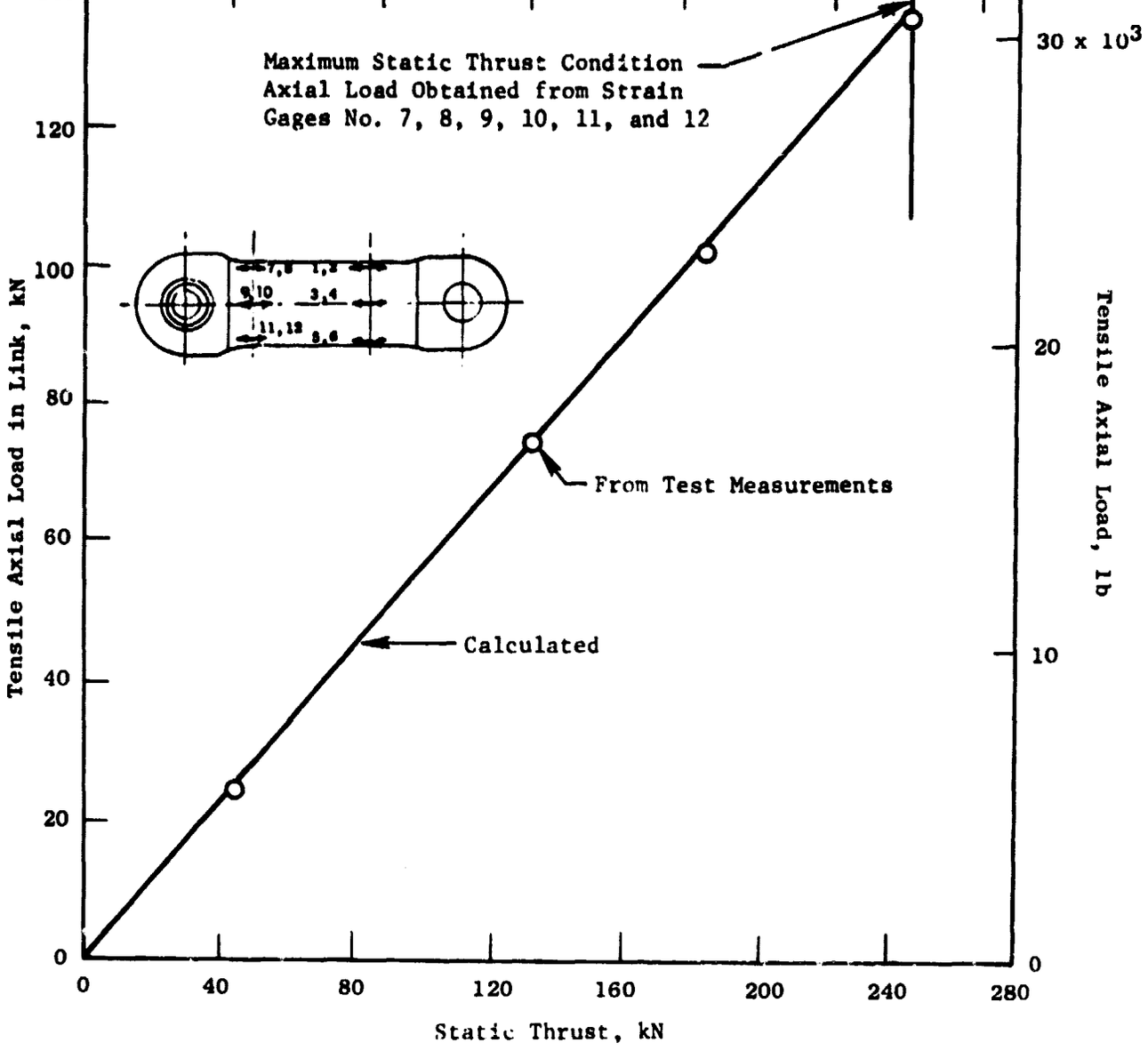

Figure 6.17. Calculated Versus Measured Tensile Axial Load in Thrust Link Due to Applied Static Thrust Loads.

MAXIMUM STATIC THRUST AND TAKEOFF AT ROTATION

COMPONENT	CALCULATED STRESS		MEASURED STRESS	
	MPa	psi x 10^{-3}	MPa	psi x 10^{-3}
Max Static Thrust Condition				
Thrust Link	384.8	86.5	424.4	95.4
Side Link	-260.2	-58.5	-195.3	-43.9
Sway Link	-31.3	-7.0	-93.2	-20.9
Mount Platform	222.8	50.1	235.31	52.9
Takeoff at Rotation				
Thrust Link	299.8	67.4	369.2	83.0
Side Link	-241.5	-54.3	-201.5	-45.3
Sway Link	-43.6	-9.8	-100.9	-22.7
Mount Platform	125.9	28.3	135.7	30.5

Figure 6.18. Comparison Between Calculated and Measured Stress During Takeoff Conditions for the New Front Mount.

6.2.1 Test Procedure

The failsafe test loads shown in Figure 6.19 provide the most severe axial, side, or vertical loads on the front mount from the failsafe conditions. Since there are no specific low cycle fatigue requirements for the failsafe condition, an objective of 5000 flight cycles was chosen to provide ample time for any failure to be observed during regular maintenance. The test load conditions of Figure 6.19 were compared with analysis to confirm the methods and analytical process. The most severe load occurs during the takeoff at rotation condition, and is one of the low cycle fatigue (LCF) spectra conditions. The remaining conditions are ultimate failsafe design loads and provide the maximum failsafe vertical and side loads.

Four failure modes were considered in addition to the unfailed base run for each of the three loading conditions. The four failure modes examined were:

a. left side link failure

b. left side link and left thrust link failure (left side of mount failed)

c. right thrust link failure

d. center link failure.

To provide a repeatable zero reference condition for the engine structure and to avoid initial sag due to disconnecting one or more load links to simulate their failures, the engine was supported with sufficient load at the fan frame ground handling pins and at the rear mount to balance the dead weight of the structure. Vertical inertia loads were simulated by distributed vertical loads along the engine (Figure 6.19). In each case, zero references were made in the "zero G" condition and the loads then increased in 20% increments to the maximum values of Figure 6.19. At each increment all stationary deflection pots and strain gages were recorded, and at the maximum value, the internal shaft-mounted pots were swept incrementally through a 360° arc.

During failsafe loading, stresses increase linearly in the mount and supporting links until contact is made between the failsafe link and the 12 o'clock clevis on the fan frame. After contact is made, additional side load and symmetrical vertical and axial loads are carried mainly by the failsafe link, and the mount and link stresses begin to build up. To determine the effect of the lateral assembly stack-up on the failsafe stress levels, tests were rerun with lateral contact between the failsafe tongue and the fan frame clevis, with shims introduced between the tongue and clevis to reduce the clearance and increase the stresses due to the contact.

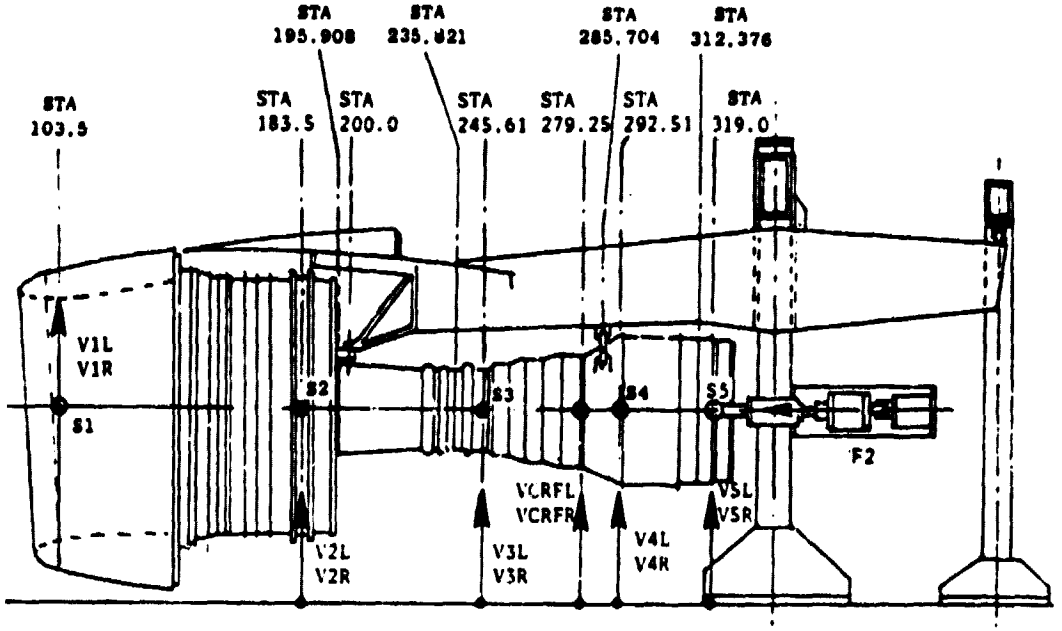

Test Loads	Case 1 T/O at Rotation		Case 2 Side Load Cond.		Case 3 Vertical Load Cond.	
	kN	lb	kN	lb	kN	lb
V1L	19.12	4300	- 8.2	-1850	-10.7	- 2400
V1R	19.12	4300	- 8.2	-1850	-10.7	- 2400
S1	0	0	20.5	4600	0	0
V2L	27.36	6150	-24.9	-5600	-59.6	-13400
V2R	-61.61	-13850	-24.9	-5600	-59.6	-13400
S2	5.78	1300	38.3	8600	0	0
V3L	58.3	13100	- 7.6	-1700	-16.0	- 3600
V3R	-66.3	-14900	- 7.6	-1700	-16.0	- 3600
S3	0	0	2.7	600	0	0
VCRFL	62.3	14000	0	0	0	0
VCRFR	-62.3	-14000	0	0	0	0
V4L	- 4.23	- 950	- 8.01	-1800	-16.9	- 3800
V4R	- 4.23	- 950	- 8.01	-1800	-16.9	- 3800
S4	0	0	2.89	650	0	0
V5L	-84.3	-18950	- 8.01	-1800	-16.9	- 3800
V5R	+84.3	+18950	- 8.01	-1800	-16.9	- 3800
S5	0	0	2.89	650	0	0
F2	200	45000	-28.9	-6500	0	0

Figure 6.19. CF6-50 New Front Mount Failsafe Test Loads.

6.2.2 Test Results and Discussion

The takeoff at rotation condition resulted in the largest radial distortion of the compressor casing during the tests of the complete new front mount. The failsafe tests demonstrated the additional radial deflections caused by simulated failures of new front mount components. Figures 6.20 and 6.21 illustrate the radial distortion on the high pressure compressor (HPC) casing at Stage 3 before and after the simulated link failures. Maximum inward radial deflection of the casing was 0.86 mm (0.034 in.) for the complete mount and for the left side link failed condition (Figure 6.20), 0.96mm (0.038 in.) with the right-hand side axial link failed, and 0.99 mm (0.039 in.) with the right-hand axial link and left-hand side link failed (Figure 6.21).

Figures 6.22 through 6.26 show the maximum stresses measured in the new front mount components for all the failsafe tests conducted. The corresponding calculated stresses are included, where available. Agreement is good except for stresses in the right side link for the right thrust link failed condition and the sway link failed condition. In each case the lack of agreement is due to an overestimation of the degree of fixity at the clamped connection between the link and the compressor casing flanges.

The compressor casing radial deflection increases slightly in the more severe failure simulation during the takeoff at rotation condition. This slight increase of 0.10-0.13 mm (0.004-0.005 in.) is acceptable considering the severity of the stipulated failure and loads. Stresses in the mount and supporting structure during takeoff at rotation are low enough to permit repeated application under the failure simulated. Stresses in the ultimate failsafe conditions are also acceptably low.

Stresses in the failsafe tongue, the clevis and backup structure of the fan frame are also acceptable and are generally lower than calculated stresses. Stresses in the side link were overestimated for the side loading condition. The major part of the side link stresses in these conditions are local bending stresses. Large bending stresses are calculated due to the relatively large transverse motion of the mount end of the link. In the computer structural model, the fan frame/compressor casing end of the side links were assumed to be completely restrained; the calculated bending stresses would be considerably reduced by a reduction in the stiffness of the connection.

6.3 Thermal and Assembly Stress Correlation Test

The new front mount system is a redundant structure in that all link end attachments, except the forward end of the thrust links, are clamped joints. Assembly stack and thermal growth in the casings will therefore induce stresses into the links and supporting structure. To give added confidence to the thermal growth and assembly misalignment stress calculations, the tests simulated the thermal and assembly stack conditions by the insertion of various thicknesses of shims between mount/engine and mount/pylon mating surfaces. Induced stresses were obtained from strain gage measurements taken before and after the insertion of the shims.

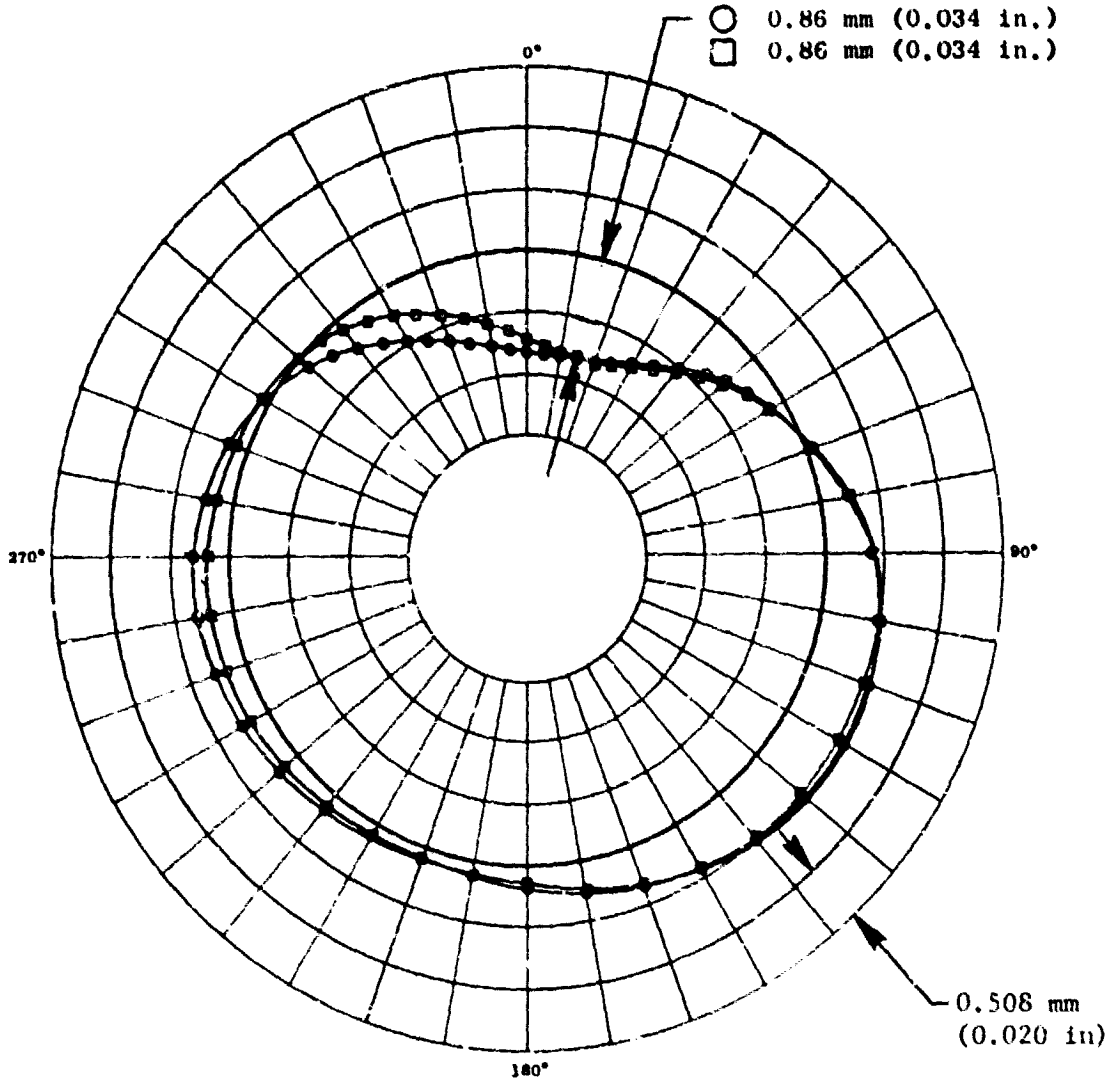

Figure 6.20. CF6-50 New Front Mount - HPC Casing Radial Deflection at Stage 3 Due to Simulated Failure of Left Side Link. Take-off at Rotation Condition (Including 1 G Down).

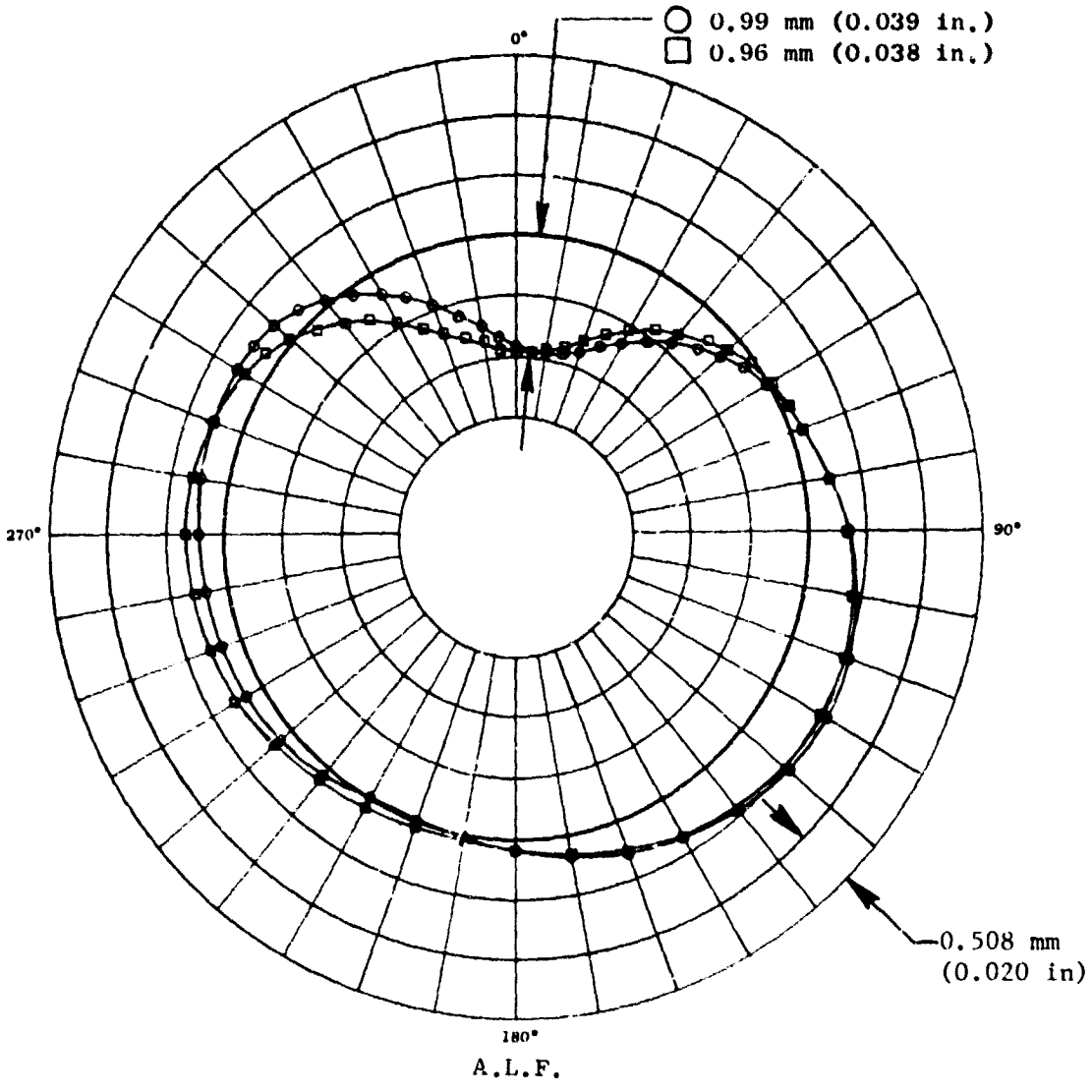

○ New Front Mount with Left Side and Left Axial Link Failed

□ New Front Mount with Right Side Axial Link Failed

Figure 6.21. CF6-50 New Front Mount - HPC Casing Radial Deflection at Stage 3 Due to Simulated Failure of Mount Links. Takeoff at Rotation Condition (Including 1 G Down).

Simulated Failure	LINK STRESSES MPa (psi x 10^{-3})					
	Takeoff Condition		Vertical Load Condition		Side Load Condition	
	Test Result	Analysis	Test Result	Analysis	Test Result	Analysis
No Failure	467.4 (67.8)	-	-177.2 (-25.7)		-346.8 (-50.3)	
Left Side Link failed	435.1 (63.1)	282.7 (41.0)	-482.6 (-70.0)		-377.2 (-48.9)	-186.2 (-48.9)
Left Side and Right Thrust Link Failed ▲	331.6 (48.1) 430.9 (62.5)	282.6 (41.0) 393.0 (57.0)	-475.7 (-69.0) -521.? (-75.6)		317.8 (46.1) 388.8 (56.4)	227.5 (33.0) 234.4 (34.0)
Right Thrust Link failed	208.2 (30.2)		-145.4 (-21.1)		144.1 (20.9)	
Sway link failed ▲					1020.4 (148.0) 717.1 (104.5)	896.3 (130.0) 799.8 (116.0)

▲ Shim added to reduce failsafe tongue to clevis side clearance to final design config.

Figure 6.22. New Front Mount - Failsafe Load Tests, Comparison Between Calculated and Measured Failsafe Stresses in Thrust Links.

Simulated Failure	LINK STRESSES MPa (psi x 10-3)					
	Takeoff Condition		Vertical Load Condition		Side Load Condition	
	Test Result	Analysis	Test Result	Analysis	Test Result	Analysis
No Failure	-288.2 (-41.8)	-	619.8 (89.8)	-	445.5 (64.6)	-
Left Side Link failed	-359.2 (-52.1)	-392 (-54.0)	897.0 (130.1)	-	579.8 (84.1)	723.9 (105.0)
Left Side and Right Thrust Link Failed ▲	-373.6 (-54.2) -301.3 (-43.7)	-441.3 (-64.0) -427.5 (-62.0)	943.0 (137.5) 948.0 (137.5)	- -	609.5 (88.4) 601.2 (87.2)	661.9 (96.0) 634.3 (92.0)
Right Thrust Link failed	810.1 (117.5)	-	507.5 (73.6)	-	598.5 (86.8)	1723.7 (250)
Sway link failed ▲	- -	- -	- -	- -	701.8 (101.8) 644.6 (93.5)	1461.6 (212.0) 1268.6 (184.0)

▲ Shim added to reduce failsafe tongue to clevis side clearance to final design config.

Figure 6.23. New Front Mount – Failsafe Load Tests, Comparison Between Calculated and Measured Failsafe Stresses in Side Links.

Simulated Failure	LINK STRESSES MPa (psi x 10^{-3})					
	Takeoff Condition		Vertical Load Condition		Side Load Condition	
	Test Result	Analysis	Test Result	Analysis	Test Result	Analysis
No Failure	-217.2 (-31.5)	-	117.8 (25.8)	-	-550.9 (-79.9)	-
Left Side Link failed	575.0 (83.4)	434.4 (63.0)	872.8 (126.6)	-	-890.1 (-129.1)	-1289.3 (-187.0)
Left Side and Left Thrust Link Failed ▲	-559.1 (-81.1) -540.5 (-78.4)	-951.4 (-138.0) -903.2 (-131.0)	1041.1 (151.7) 1023.4 (148.4)	- -	-965.3 (-140.0) -820.5 (-119.0)	-1151.4 (-167.0) -1310.0 (-190.0)
Right Thrust Link failed	-140.6 (-20.4)	-	217.2 (31.5)	-	-762.5 (-110.6)	-
Sway link failed ▲	- -	- -	- -	- -	- -	- -

▲ Shim added to reduce failsafe tongue to clevis side clearance to final design config.

Figure 6.24. New Front Mount - Failsafe Load Tests, Comparison Between Calculated and Measured Failsafe Stresses in Center Link.

Simulated Failure	LINK STRESSES MPa (psi x 10-3)					
	Takeoff Condition		Vertical Load Condition		Side Load Condition	
	Test Result	Analysis	Test Result	Analysis	Test Result	Analysis
No Failure	157.0 (22.8)	-	82.7 (12.0)	-	-81.4 (-11.8)	-
Left Side Link failed	-250.7 (-36.6)	-	718.4 (104.2)	-	273.0 (39.6)	-
Left Side and Thrust Link Failed ▲	368.8 (53.5) 565.4 (82.0)	- -	634.3 (92.0) 833.5 (120.9)	- -	-250.9 (-36.4) -543.9 (-78.8)	
Right Thrust Link failed	366.1 (53.1)	-	86.2 (12.5)	-	139.2 (20.2)	-
Sway link failed ▲	- -	- -	- -	- -	492.3 (71.4) 660.5 (95.8)	- -

▲ Shim added to reduce failsafe tongue to clevis side clearance to final design config.

Figure 6.25. New Front Mount - Failsafe Load Tests, Failsafe Stresses in Fan Frame Clevis.

Simulated Failure	LINK STRESSES MPa (psi × 10-3)					
	Takeoff Condition		Vertical Load Condition		Side Load Condition	
	Test Result	Analysis	Test Result	Analysis	Test Result	Analysis
No Failure	452.3 (65.6)	-	-184.1 (-26.7)	-	-87.6 (-12.7)	
Left Side Link failed	205.4 (29.8)	-	338.5 (49.1)	-	-251.6 (-36.5)	
Left Side and Left Thrust Link Failed ▲	369.5 (53.6) 375.0 (54.4)	- -	312.3 (45.3) 336.5 (48.8)	-	242.7 (35.2) 337.2 (48.9)	
Right Thrust Link failed	306.1 (44.4)	-	267.5 (38.8)	-	98.6 (14.3)	
Sway link failed ▲	-	- -	- -	- -	106.9 (15.5)	- -

▲ Shim added to reduce failsafe tongue to clevis side clearance to final design config.

Figure 6.26. New Front Mount - Failsafe Load Tests, Failsafe Stresses in Mount Structure.

6.3.1 Test Procedure

Thermal stresses and assembly stack stresses were obtained by taking zero readings of all strain gages and then relaxing various clamped joints in turn so that 0.127 mm (0.005 in.), 0.254 mm (0.010 in.) and 0.381 mm (0.015 in.) shims could be inserted in turn. After insertion of the shims, the joint fasteners were retorqued and the strain gages recorded once more. The conditions considered are shown in Figure 6.27.

6.3.2 Test Results and Discussion

As anticipated, stresses induced by the insertion of the shims into the mount and supporting links interface surfaces were very small. The maximum stresses obtained during the tests occurred in the thrust links during the simulated mount upper surface angular misalignment in the pitching direction. The calculated and measured bending stress correlated well, being 115.2 MPa (16,700 psi) and 118.6 MPa (17,200 psi), respectively.

Stresses induced in the new front mount system due to thermal growth and assembly stack misalignment are very small and close to the calculated values. Although small, the stresses are not negligible and have been included in the low cycle fatigue analysis calculations for the new front mount structure.

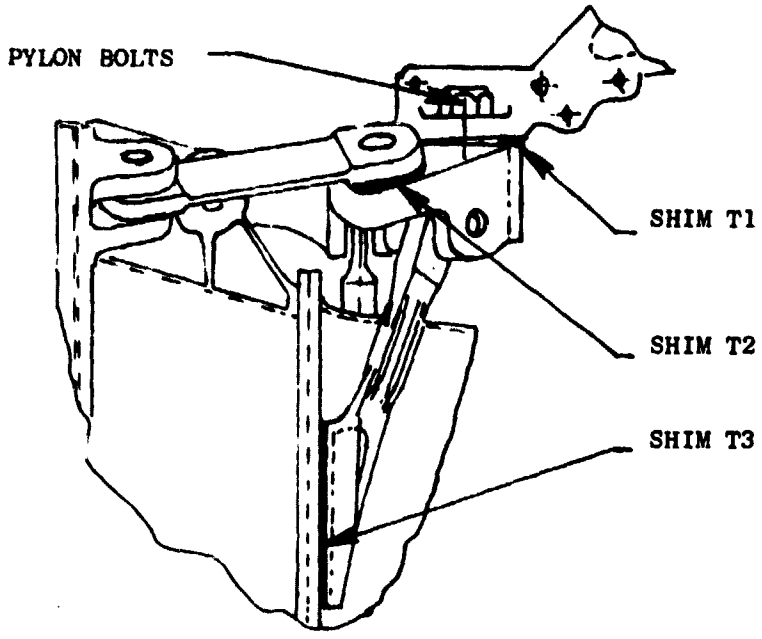

	TEST DESCRIPTION	SHIM T1	SHIM T2	SHIM T3	PYLON BOLT TORQUE
19	Thermal correlation Axial displacement	-	-	x	Tight *
20	Thermal correlation Vertical displacement	-	x	-	Tigh *
21	Assembly correlation Mount pitch rotation	x	-	-	Tight *
22	Assembly correlation Axial displacement	-	-	x	Loose **
23	Assembly correlation Vertical displacement	-	-	-	Loose **

* Loosen Mating Faces Sufficient to Insert Shim and then Retorque. Shim Sizes 0.127 mm (0.005 in.), 0.254 mm (0.010 in.) and 0.381 mm (0.015 in.)

** Lossen all Bolts, Insert Shims and Retorque All Except Pylon Bolts. Shim Sizes 0.127 mm (0.005 in.), 0.254 mm (0.010 in.) and 0.381 mm (0.015 in.)

Figure 6.27. Simulated Thermal and Assembly Stress Correlation Test.

7.0 LOW CYCLE FATIGUE TEST

The objective of the low cycle fatigue test was to demonstrate the ability of the new front mount structure to withstand 35,000 simulated flight load cycles, and to determine by what margin the structure would exceed this requirement. A description of the low cycle fatigue test setup with the engine outer structure in the load paths is presented in Section 4.1.

The simulated flight load cycle was based on the maximum loads obtainable for the flight mission sequence. Maximum static thrust-takeoff at rotation-landing with reversed thrust. One life cycle included 35,000 simulated flight load cycles. In addition, loading to simulate the cumulative effects of the design flight and gust loading spectrum was applied to the front mount. Using 80% of the maximum limit load condition as a constant amplitude test load, calculations based on the cumulative damage theory indicated that 100 cycles of the 80% maximum vertical load condition and 130 cycles of the 30% maximum side load condition would provide the equivalent cumulative damage of one life cycle. This is more severe than the predicted opeational life cycle and will substantiate the basic life capability for airline operation.

To cover the case of a mount having minimum material properties and assuming, on the basis of material certificates and the material fatigue tests designated in Appendix B, the test article was of average properties, the test loads for the second lifetime test were increased by a factor of 1.25. This factor was reduced to 1.20 for the maximum static thrust condition to account for normal derating of the engine by the airlines. The takeoff and landing spectrum and the 80% limit load conditions of Figure 7.1 for the second lifetime loads reflect these factors and also a more realistic reverse thrust condition. The relief provided by the redundancy of the pylon mounted fan reverser and core cowl were conservatively neglected.

7.1 TEST PROCEDURE AND LOADS

After first establishing the accuracy of the applied loads, by increasing the loads incrementally and reading all strain gages and load cells, the cycling was continued automatically at six cycles per minute. Load cells were monitored continuously on strip recorders throughout the test and after each 4,000 cycles, strain gages were recorded at the peak cyclic loads.

The test loads are tabulated in Figure 7-1 for the first and second lifetime load cycles.

7.2 TEST HISTORY AND DESCRIPTION

An initial problem of excess motion of the loading platform, caused by the difficulty in maintaining identical axial loads on each end of the loading

Life-time Test	Case	Cycles	Loading Condition	F1 - Side Load*		F2 - Axial (Thrust)*		F6 - Vertical*		M4 - Moment (Pitch)	
				kN	lbx10^{-3}	kN	lbx10^{-3}	kN	lbx10^{-3}	kN-m	in-lb x 10^{-3}
1		First Lifetime									
	1A	35000	Max Static Thrust		0	244.65	55.0	-12.90	-2.9	-293.7	-2.6
	1B	Cycle	Takeoff at Rotation		0	199.73	44.9	-78.73	-17.7	-1785.2	-15.8
	2	Spectrum	Landing-Rev Thrust		0	133.02	-29.9	77.84	17.5	1762.6	15.6
	3	130	Side load cond	146.35	(32.9)	195.72	44.0	-43.77	-9.84	262.1	2.32
	4	100	Vert load cond.		0	0	0	183.30	41.2	1977.2	17.5
2		Second Lifetime									
	1A	35000 Cycle	Max Static Thrust		0	289.13	65.0	-15.12	-3.4	-350.2	-3.1
	1B	Spectrum	Takeoff at rotation		0	249.10	56.0	-93.86	-21.1	-2231.4	19.75
	2		Landing-rev thrust		0	-93.43	-21.0	70.72	15.9	1615.7	14.3
	3	130	Side load cond.	18.24	(4.1)	244.65	55.0	-54.71	-12.3	327.6	2.9
	4	100	Vert load cond.		0	0	0	282.02	63.4	3039.3	26.9

* Reference Figure 4.2

Figure 7.1. First and Second Lifetime Low Cycle Fatigue Test Loads for New Front Mount System.

yoke, was solved by increasing the right-hand loading cyclinder force to provide a small constant yawing moment sufficient to overcome any out of balance occurring during the load cycles. A consequence of this problem were two failures, at 4,474 and 8,524 cycles in the first lifetime, of one of the two facility bolts attaching the loading yoke to the platform, and considerable fretting and galling of the mount platform upper interface surface.

The engine completed the first lifetime cyclic test with 35,000 cycles of the takeoff thrust - takeoff at rotation - landing with reverse thrust spectrum, 130 cycles at 80% of the maximum design limit side load condition, and 100 cycles at 80% of the maximum design limit vertical load condition. Examination of the mount platform after the first lifetime test showed little increase in the severe fretting of the mount platform interface surface which had occurred during the first 2,000 cycles. Examination of the links revealed cracks on one lip of the spherical ball of the left-hand thrust link. These cracks had not adversely affected the function of the link, and the ball was not replaced so that crack growth rate could be observed.

The second lifetime cycle test commenced with loads increased by approximately 20% to take into account the ratio of minimum to average material properties, assuming the mount to be of average properties. It was at these higher load levels that a failure occurred at cycle 47,360 (see Figures 7.2 and 7.3). The fatigue test program was concluded with the stress level tests of a second new front mount strain gaged to determine the stress levels in the failure region.

7.3 TEST RESULTS AND FAILURE INVESTIGATIONS

Stress levels measured at the maximum loads of cases 1A, 1B, 2, 3 and 4 (Figure 7.1) at the beginning of each lifetime test agreed well with the calculated values for these conditions.

Failure of the left thrust link lug on the mount platform occurred at a total of 47,360 cycles, or 12,130 cycles into the more severe second lifetime load spectrum. After failure of the left thrust link lug, the mount platform and links were dismantled for examination. A closeup photo of the failed lug (Figure 7.3) shows the location of the failure and shows fretting on the outer surface of the bushing lip which is in contact with the thrust link. Similar fretting was noted on the mating face of the link. On-site removal of the bushing revealed fretting on the mating surfaces of the bushing lip and front mount platform (Figure 7.2).

The previously noted cracks in the ball of the left thrust link had not propagated appreciably since first observed after 35,000 cycles. Fretting of the upper interface surface of the mount platform appeared to be unchanged since the previous examination.

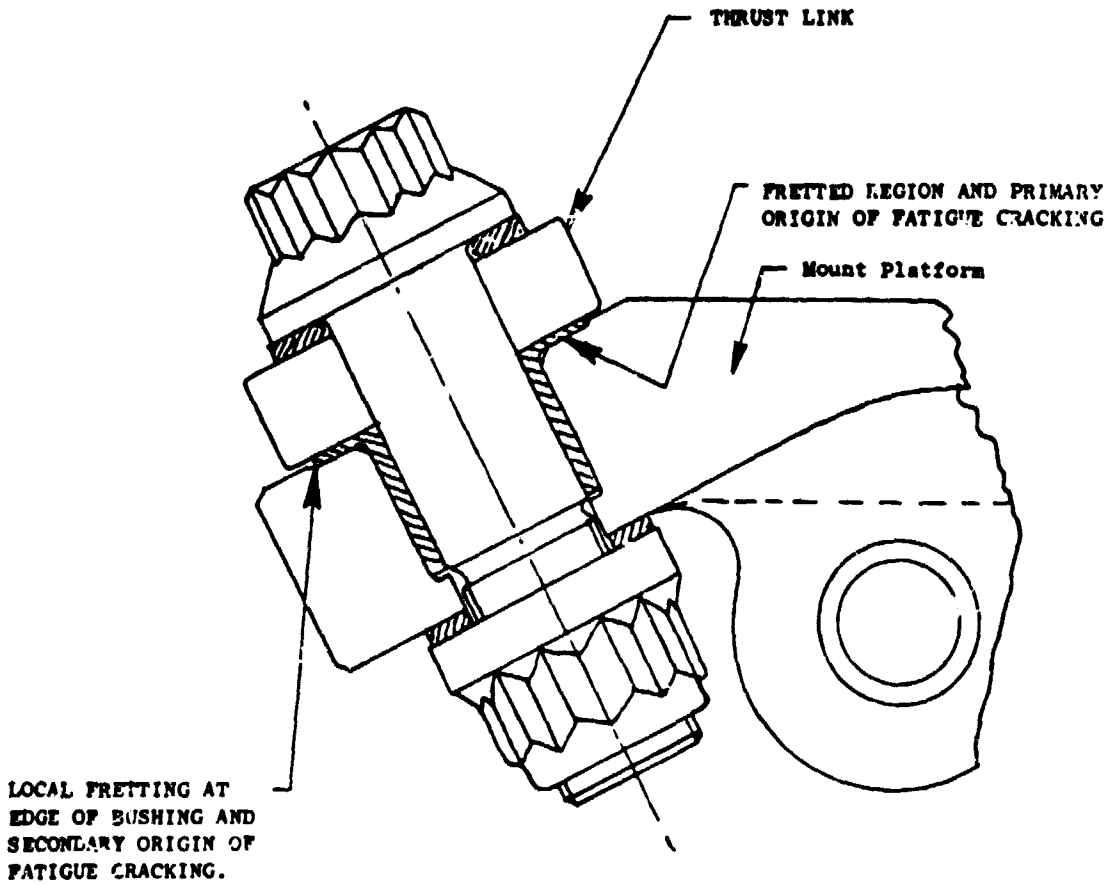

Figure 7.2. Cross Section of Left Lug of Mount Platform and Thrust Link Showing Origin of Fatigue Cracks.

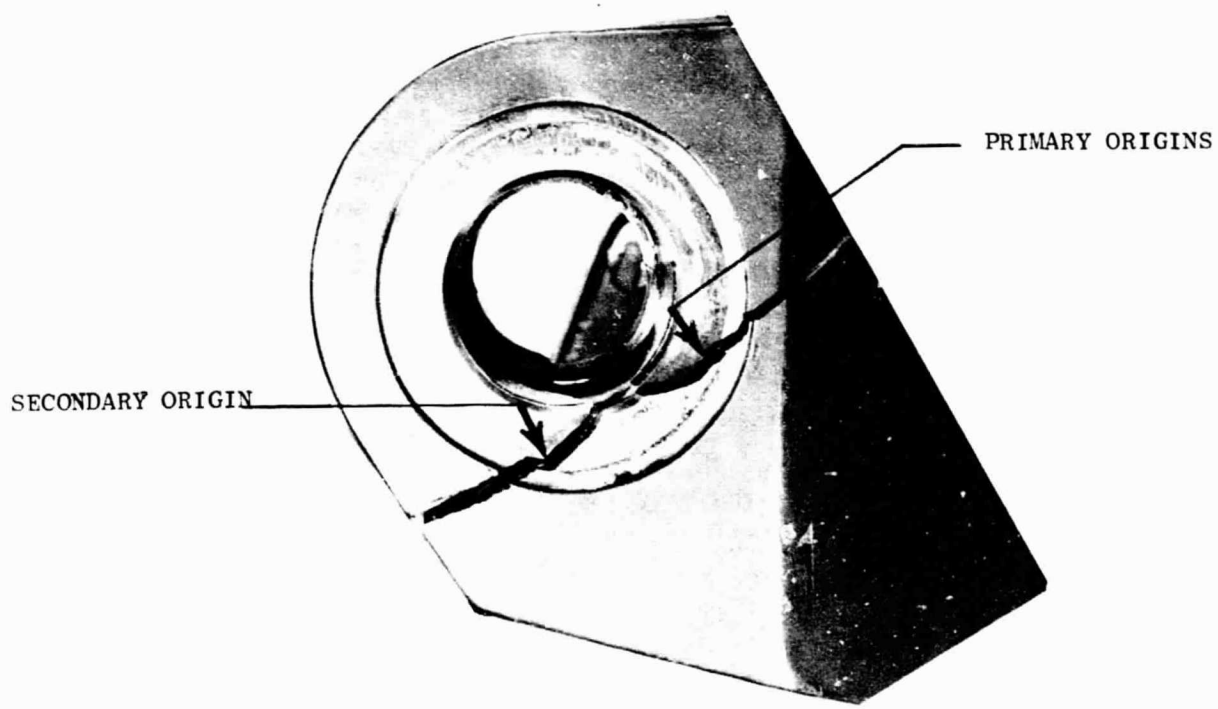

Figure 7.3. Origins of Fatigue Cracking in Left Hand Lug of New Front Mount Platform (Upper Surface) After 47,360 Simulated Flight Cycles, Hole Bushing Removed.

C-2

A failure investigation of the failed mount platform was conducted by the Materials Group with the following conclusions:

The failure was caused by low cycle fatigue cracks having multiple origins in the fretted surface of the mount lug under the lip of the hole bushing. The origins are shown in Figures 7.2 and 7.3 which shows the left lug upper surface with the bushing for the bolt hole removed so that the fretted region may be seen. The cracks propagated towards the edge of the hole and away from the hole as indicated in the photograph.

To continue testing the remaining front mount components and to evaluate the proposed procedure to eliminate the fretting problem, the following test plan was initiated: A new front mount was provided and strain gaged (see Figure 7.4) so that the surface stresses in the region of failure might be measured. Stress tests were conducted on the second new front mount in the same test facility. Following these stress tests, the mount was removed from the test facility for rework to eliminate the fretting problem. After removal of the bushings and strain gages, the surfaces were shot peened, and coated with a plasma spray of copper-nickel-indium. The surface was also coated with molybdenum disulphide lubricant before replacing the bushings.

Analysis of the results of the stress test on the second mount platform from strain gage rossette 506, 507 and 508 (see Figures 7.4 and 7.5) resulted in an effective low cycle fatigue stress of 170.65 MPa ± 216.75 MPa (24,750 psi ± 31,440 psi).

Fatigue testing of the mount was continued to complete the second lifetime cycles of the remainder of the mount system and complete one life cycle on the platform at the higher loads of the second lifetime cycles.

Discussion

The low cycle fatigue test demonstrated the life capability of the new front mount hardware to be in excess of the required 35,000 simulated flight cycles.

Stress levels in the failed area of the mount were sufficiently low that fatigue cracking would not have been initiated without the aggravated effects of local surface fretting.

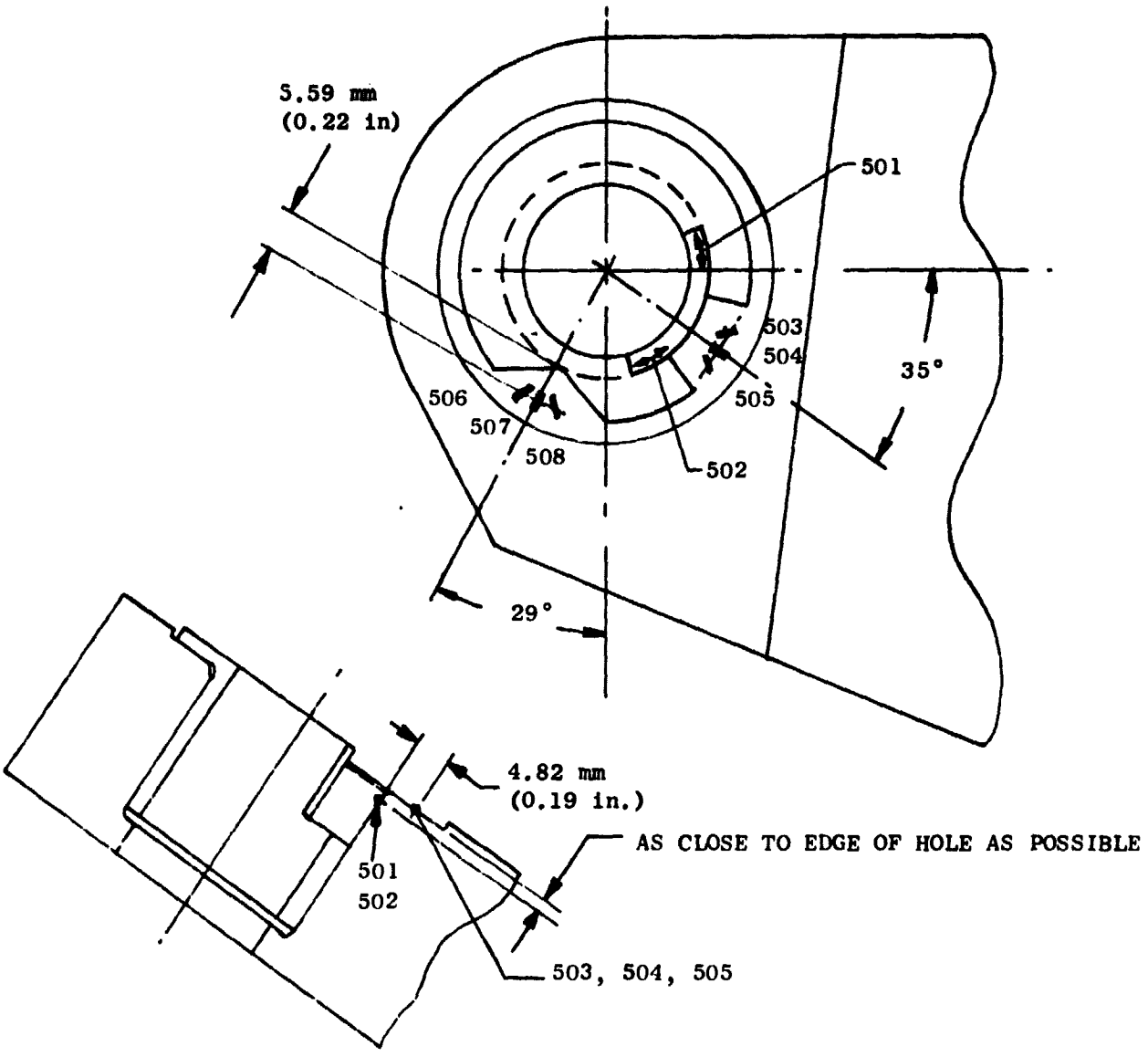

Figure 7.4. Strain Gages on Mount Platform for Stress Test with a Second New Front Mount.

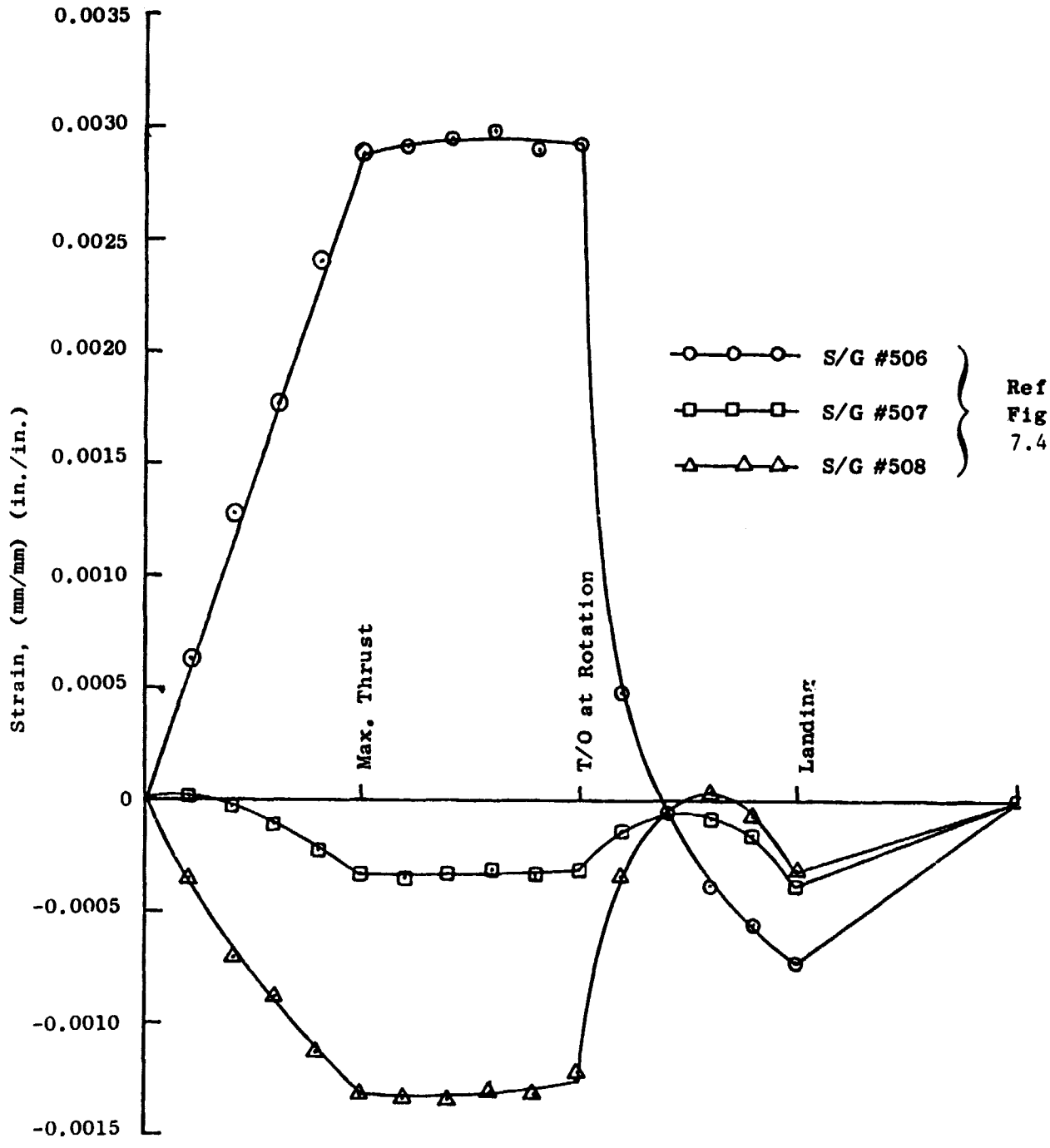

Figure 7.5. New Front Mount - Low Cycle Fatigue Test, Strain Variation on Mount Platform During Load Cycle.

8.0 ENGINE FACTORY AND FLIGHT TESTS

Factory and flight engine tests were conducted on engines having the new front mount with strain gaged links. Total accumulated time on all engines to date (3/27/79) is about 2,000 hours for factory engines and 1,227 hours for flight test engines. Figure 8.1 shows the time on the individual engines.

The condition of a prototype new front mount which had no protective coatings on the mount or links is shown in Figures 8.2 through 8.5 after about 204 hours of factory engine tests. There is very little evidence of galling of the mating surfaces. Production mounts have the titanium mating surfaces protected by a dry film lubricant while the steel links have a sealed aluminum spray corrosion protection coating.

Vibratory stress in the links were recorded during the factory tests and flight tests. The maximum stresses recorded were low, being 7,800 psi RMS total during the factory tests and 16,000 psi RMS total during flight testing. These max stresses occurred in the side links in the uniform portion of the link at S/G Station No. 15 (Figure 4.5).

Flight tests also provided strain gage records of steady-state strains and vibratory strains. Both of these are illustrated in the typical data taken during a takeoff run shown in Figures 8.6 a and b. The steady-state link loads obtained from the flight test are shown in Figure 8.7.

Engine	Time, hours	Flight Cycles
Total Factory		
455-115/4-6	882	2669
455-507/18	82	0
455-508/16 & 17	204	9
455-509/2-5	831	4554
	1999 hours	7232 Cycles
DC-10-30 Aircraft		
517-330	179	163
517-331	179	188
517-376	179	191
517-431	94	99
517-432	94	99
517-433	94	99
	819 hours	839 Cycles
B747-200 Aircraft		
517-373	102	59
517-375	102	59
517-401	102	59
517-408	102	59
	408 hours	236 Cycles
Total	3226 hours	8307 Cycles

Figure 8.1. CF6-50 New Front Mount Time on Flight and Factory Engines Up to March 27, 1979.

Figure 8.2. New Front Mount Platform from Engine 455-508 After 204 Hours.

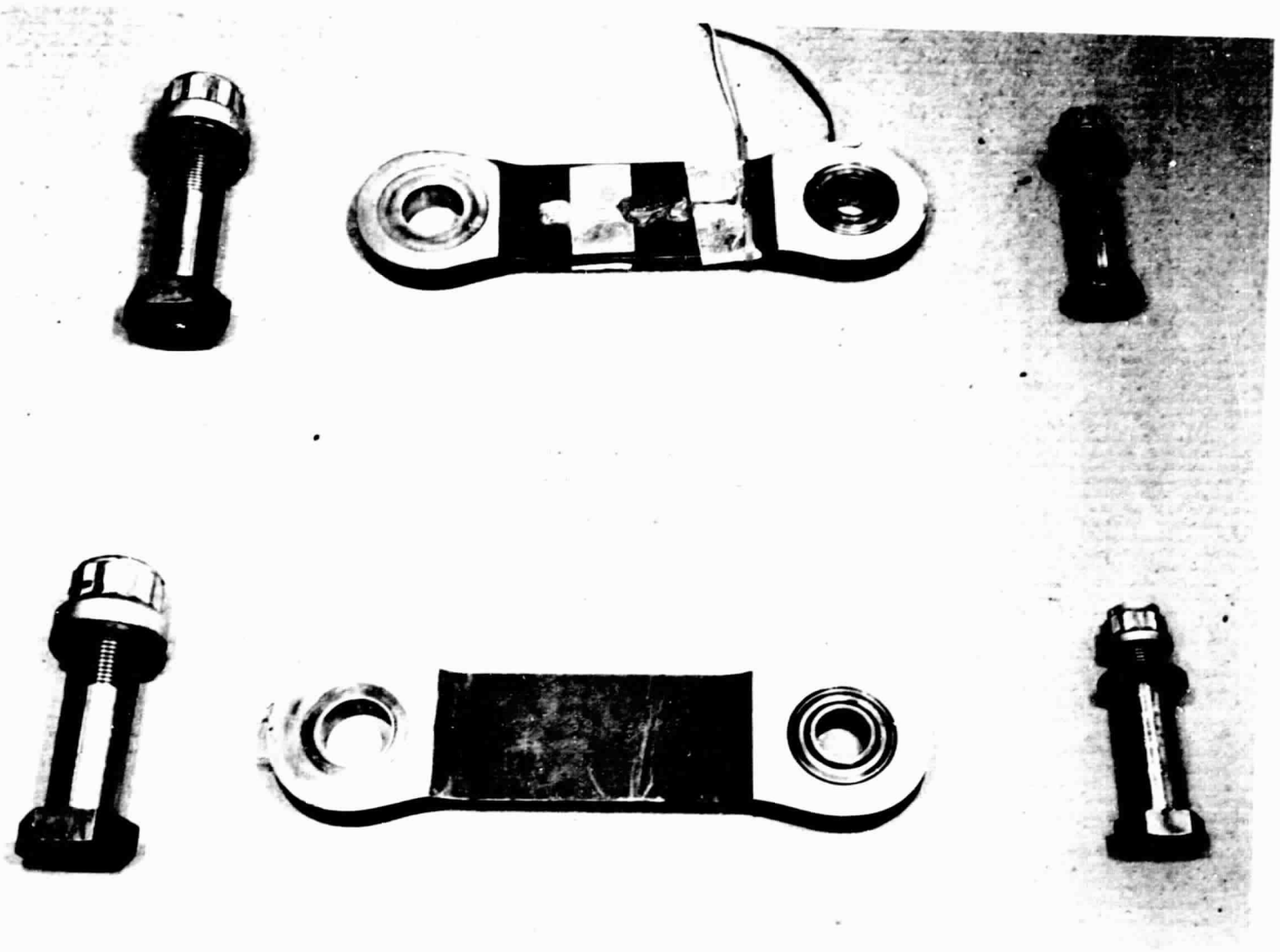

Figure 8.3. New Front Mount Left and Right Thrust Links and Attachment Bolts from Engine 455-508 After 204 Hours.

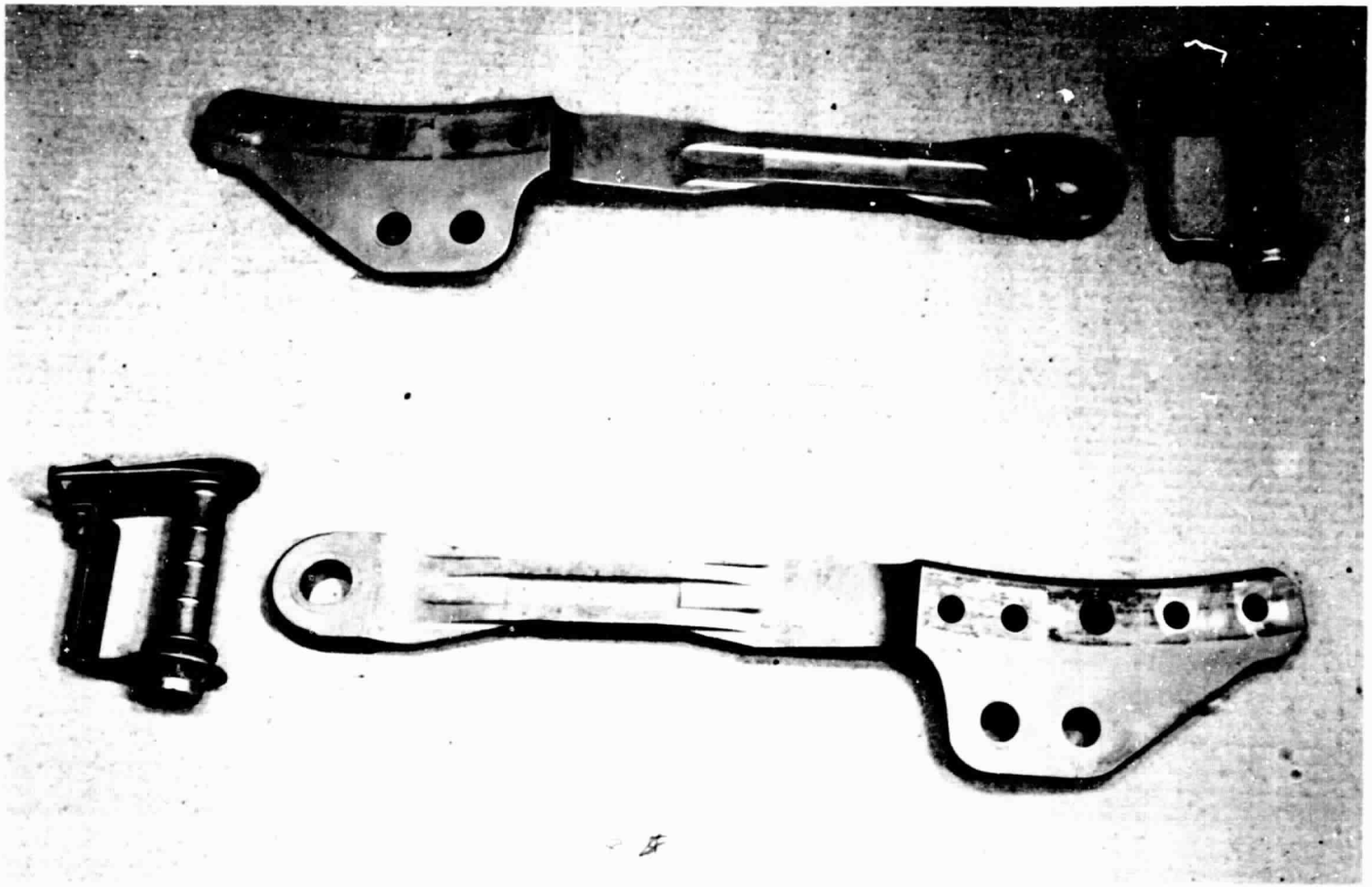

Figure 8.4. New Front Mount Left and Right Side Links and Attachment Bolts from Engine 455-508 After 204 Hours.

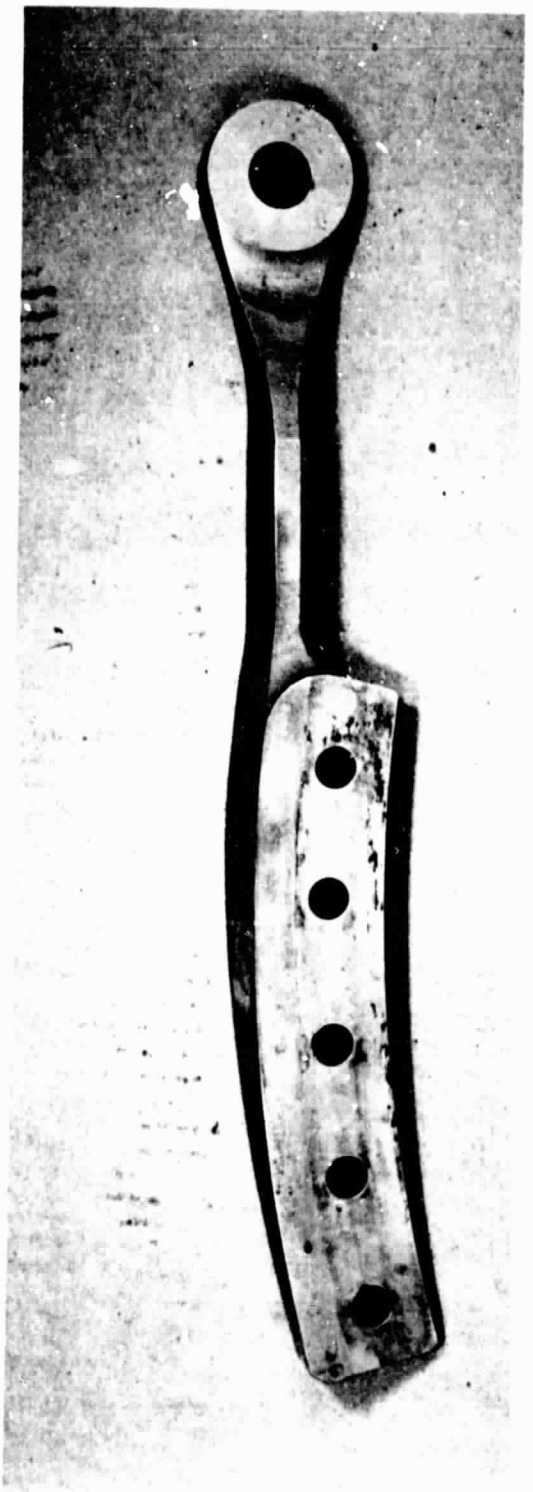

Figure 8.5. New Front Mount Sway Link from Engine 455-508 After 204 Hours.

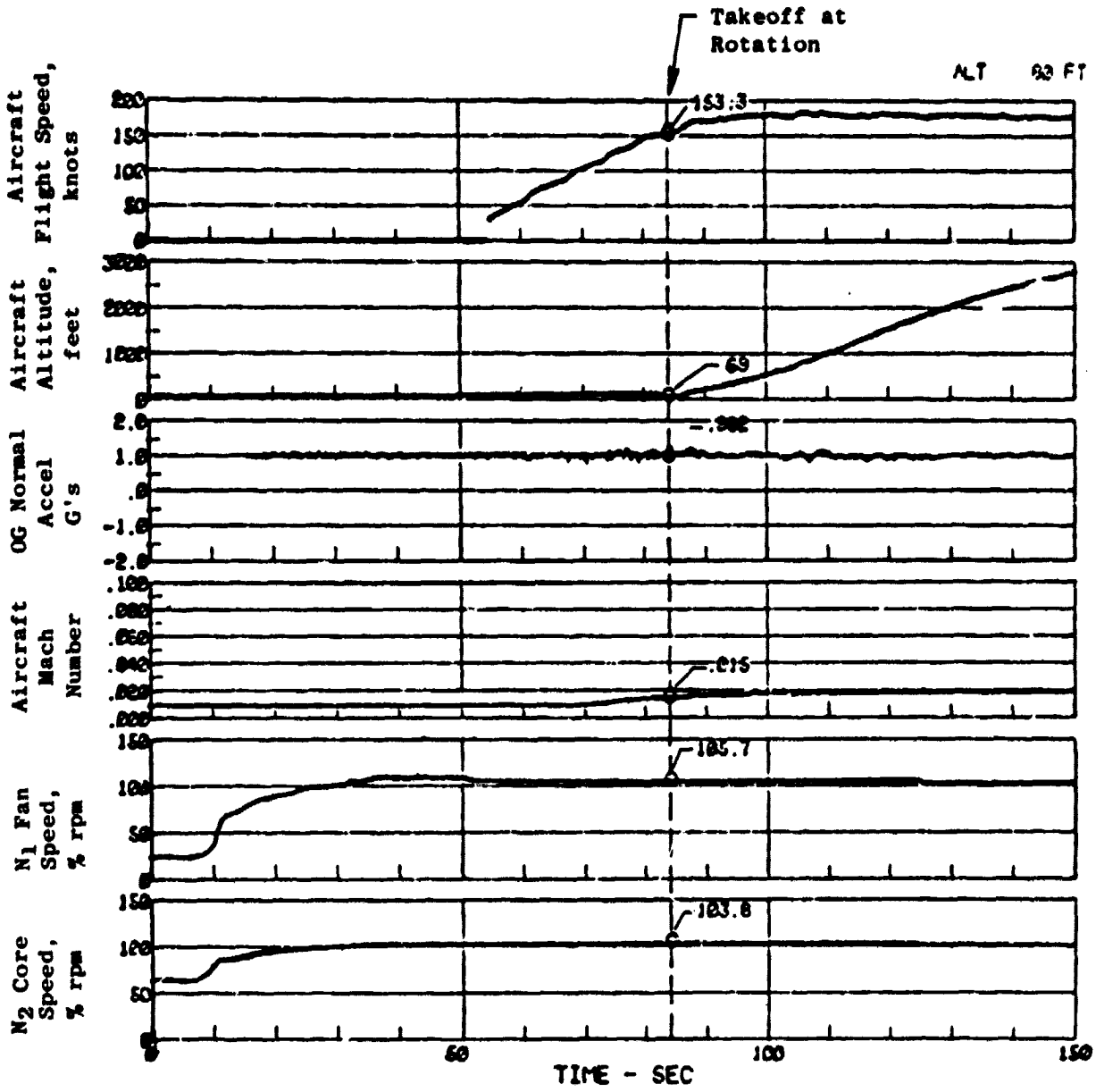

Figure 8.6a. Aircraft and Engine Data: DC-10-30 Flight Test Data During Takeoff Sequence.

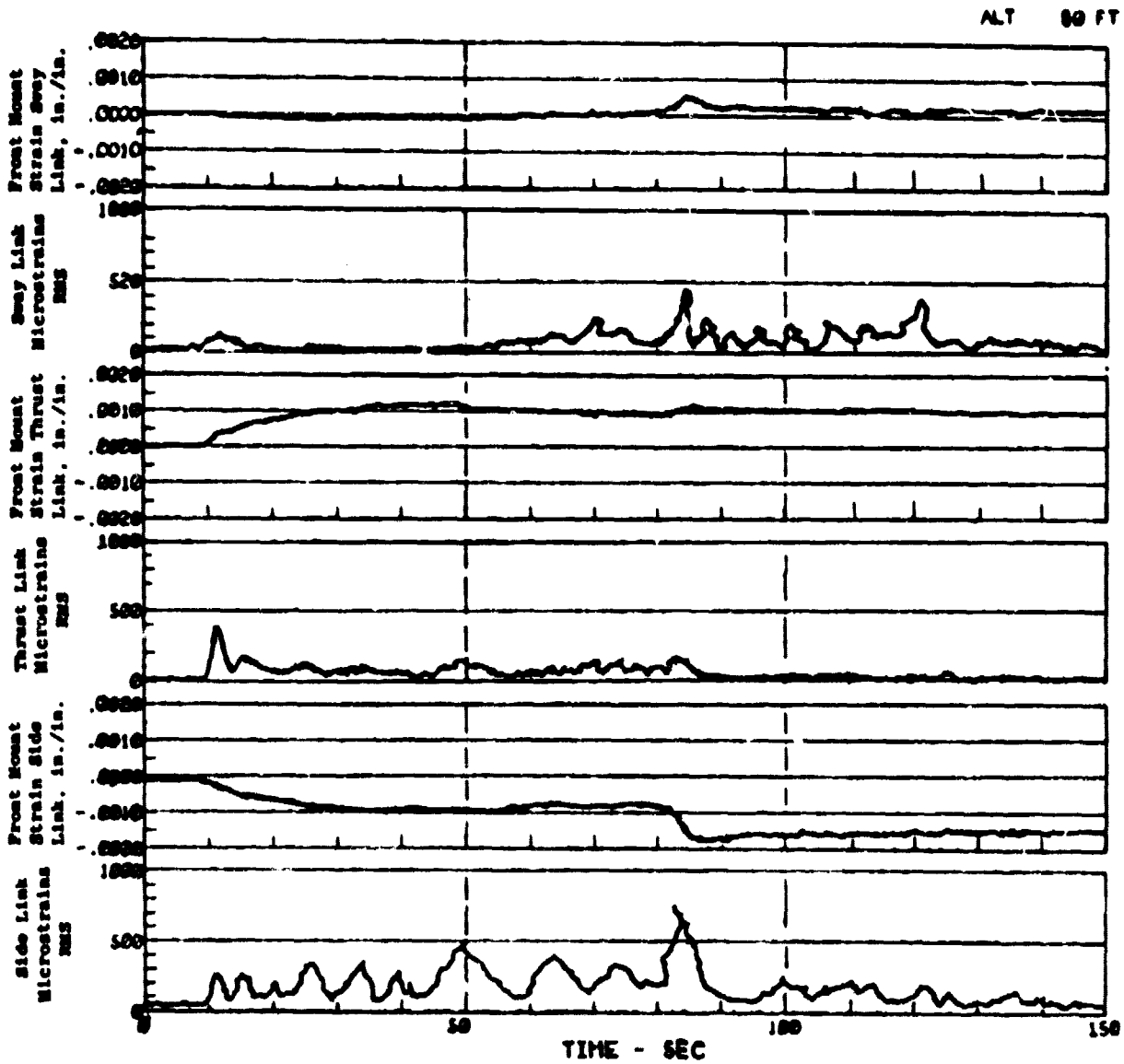

Figure 8.6b. New Front Mount Strain Survey, Engine 3: DC-10-30 Flight Test Data During Takeoff Sequence.

FRONT MOUNT SUPPORT LINK LOADS

FLIGHT CONDITION	THRUST LINK LOAD		SIDE LINK LOAD	
	kN	lb x 10^{-3}	kN	lb x 10^{-3}
STATIC T/O THRUST	102.3	23.0	-45.8	-10.3
▲	134.4	30.2	-54.3	-12.2
T/O AT ROTATION	89.0	20.0	-80.5	-18.1
▲	117.9	26.5	-91.7	-20.6
CLIMB	73.4	16.5	-55.1	-12.4
CRUISE	45.4	10.2	-31.6	- 7.1
LANDING APPROACH	18.2	4.1	-22.7	- 5.1
LANDING	27.1	6.1	-23.1	- 5.2
REVERSE THRUST	-17.8	-4.0	0	0
▲	-71.2	-19.0	-28.9	6.5

▲ CALCULATED MAXIMUM LOADS

Figure 8.7. CF6-50 New Front Mount Support Link Loads During DC-10-30 Flight Test Engine Position No. 3.

9.0 PERFORMANCE ASSESSMENT

An assessment of earlier tests and analysis had indicated that the introduction of a redesigned front mount to the CF6-50 series of engines would result in a performance improvement of 0.3% sfc. The improvement was to be realized by tightening the clearance between compressor rotor and casing and compressor vanes and spools, made possible by a reduction in compressor casing distortion.

Results of the tests, described in Sections 5.0 and 6.0 herein, confirm the ability of the New Front Mount to considerably reduce the compressor casing deformation. However, these results, and a more detailed examination of other influencing parameters, reduce the anticipated improvement resulting from the decrease in deformation.

In the discussion below a concentrically ground casing is assumed and the clearance between rotor and casing, and vanes and spools, is selected such that a slight tough or rub would occur under the most adverse condition.

The estimated maximum radial deflection improvement due to the New Front Mount over the original mount was thought to be as high as 0.79 mm (0.031 in.) for the takeoff-at-rotation condition (Figure 9.1, curve a). However, these levels were found to be optimistic for the following reasons.

Preliminary tests were conducted on a steel support with a Unibal universal joint at the front mount with the engine weight supported (Zero G). Final testing with the DC-10 pylon with the clamped interface resulted in a smaller improvement in radial deflection of 0.13 mm (0.005 in.). The installation of the DC-10 wing inlet resulted in a smaller improvement in radial deflection of 0.10 mm (0.004 in.). More realistic comparisons which included a 1G down load factor also lowered the improvement in radial deflection by 0.10 mm (0.004 in.). These effects are shown in Figure 9.1, curve b.

The fan reverser is a redundant installation, attaching to the pylon as well as the engine, which reduces the deflection an estimated 15%. See Figure 9.1, curve c.

The deflection improvement available at the forward stages of the compressor casing which may be utilized in reducing the clearances is therefore 0.41 mm (0.016 in.) rather than the earlier estimate of 0.79 (0.031 in.). Another feature which reduces the effectiveness of the deflection improvement is that aft of S[illegible]ge 10, clearances are established by the effects of a throttle chop wh[illegible]h exceed the local distortion effects of the casing (Figure 9.1).

Performance improvements have been recalculated for a concentrically ground casing, using semiempirical correlations based on General Electric experience of the effect of clearance on the efficiency and stall margin of

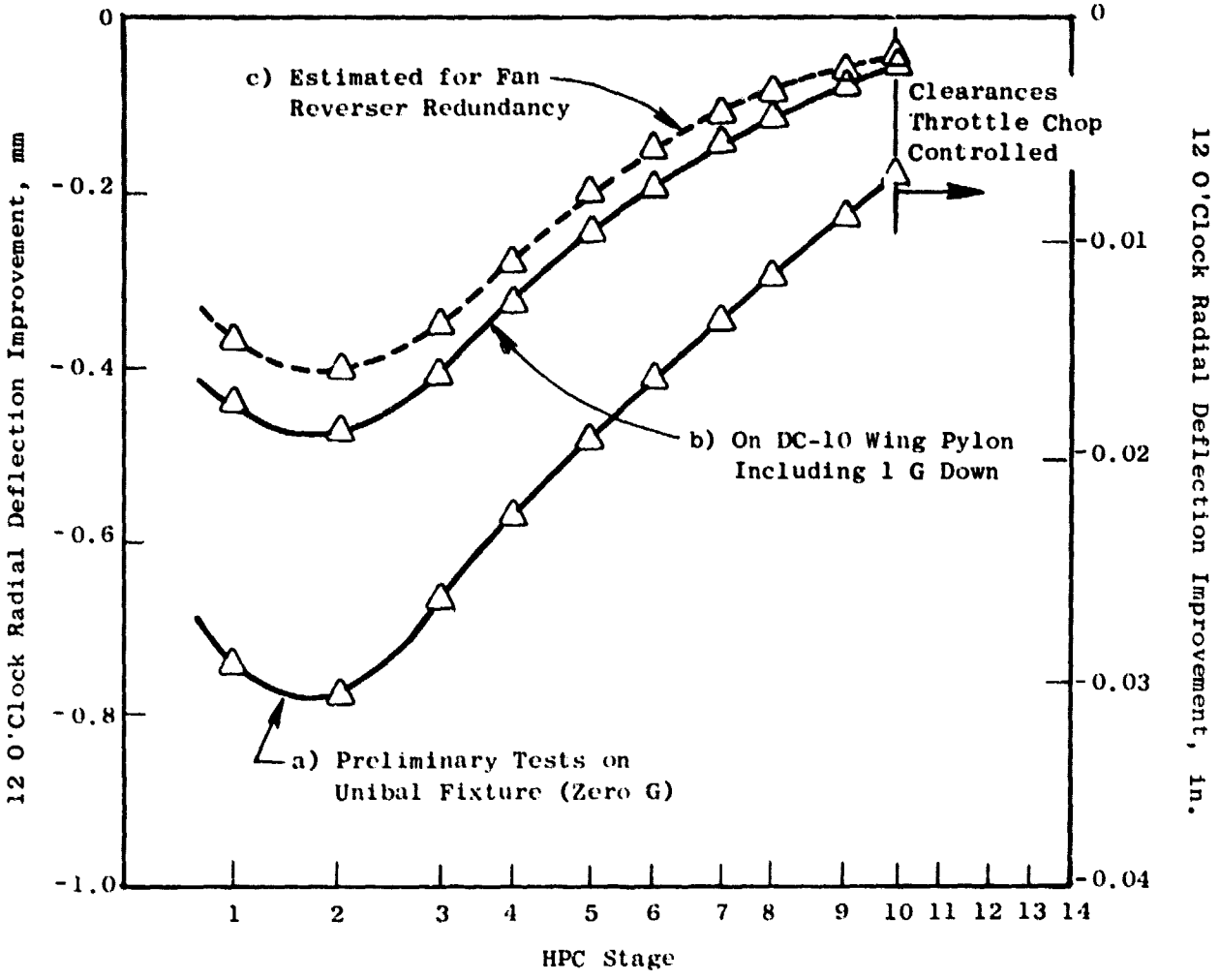

Figure 9.1. Titanium HPC Casing Backbone Radial Deflection Improvement Due to New Mount at Takeoff at Rotation Condition.

the CF6-50 high pressure compressor. The results of these calculations are as follows:

	Calculated (Based on Measurement)	Predicted
ΔSFC_{Cruise}	-0.1%	-0.3%
$\Delta EGT_{Takeoff}$	-1.5° C	-3.5° C
ΔStall Margin (Takeoff Flow)	+3.5 Pts. (16%)	
ΔStator Angle Margin (Takeoff)	+0.8 degree (10%)	
ΔEngine Weight	+4.5 kg (10 lb)	

The improvements in the stall margin are significant. For a new production high pressure compressor the baseline values are as follows:

	Stabilized	Cold Burst Transient
Stall Margin (Takeoff Flow)	22.0 Pts.	12.0 Pts.
Stator Angle Margin (Takeoff)	8.0 Degrees	5.0 Degrees

As can be observed, the above improvements provide a large percentage gain on the margins. All the above improvements will be even greater for a deteriorated engine.

10.0 ECONOMIC ASSESSMENT

The new front mount concept was evaluated by Boeing and Douglas during the Feasibility Analysis (Reference 1). A cruise specific fuel consumption improvement of 0.3 percent was predicted based on reduced HP compressor case distortion.

Deflection/distortion tests conducted under this program indicate that the sfc improvement for the new front mount amounts to 0.10 percent for a new engine as discussed in detail under Performance Assessment, Section 9.0. Further savings in the form of improved performance retention are predicted but not included in the economic assessment because of the difficulty of quantification.

A 0.10 percent cruise sfc reduction results in the block fuel savings per aircraft shown in Table 10.1 for the minimum fuel consumption mission analysis. The estimated annual fuel savings per aircraft for the above block fuel savings are shown in Table 10.2, and indicate an annual fuel savings up to 77,500 l (20,500 gal) per aircraft.

Economic assessment of Payback Period (PBP) and Return on Investment (ROI) for a new engine is summarized in Table 10.3 for the medium international fuel price of 14.53¢/l (55¢/ gal) for the DC-10-30, and for the medium domestic fuel price of 11.89¢/l (45¢/gal) for the DC-10-10 and the B747-200 (Reference 1.) Payback period for a new engine is about one year, and is economically attractive to the airlines. This does not include the effects of improved performance retention and reduced maintenance cost resulting from improved stall margin. As noted, even with the conservative assessment the new front mount is very attractive from both fuel savings and economic considerations.

The new front mount is physically interchangeable with the original front mount and requires rework of the fan frame and the HP compressor case forward flange for engine installation. Retrofit of existing deteriorated CF6 engines may be economically impractical, since new compressor blading and casing rub-strips would be required to obtain the tighter HP compressor tip clearances for improved performance.

Table 10.1. CF6 New Front Mount: Aircraft Block Fuel Savings: (Minimum Fuel Analysis for ΔSFC_{Cruise} = 0.1%).

Aircraft (Engine)	Range		Block Fuel Savings/Aircraft	
	km	miles	kg	%
DC-10-10 (CF6-6)	645	400	- 7.0	-0.10
	1690	1050	-15.7	-0.10
	3700	2300	-33.7	-0.10
DC-10-30 (CF6-50)	805	500	- 7.1	-0.07
	2735	1700	-24.5	-0.10
	6275	3900	-66.5	-0.10
B747-200 (CF6-50)	700	480	- 7.3	-0.07
	3460	2150	-41.0	-0.10
	6190	3850	-84.7	-0.10

Table 10.2. CF6 New Front Mount: Annual Fuel Savings Per Aircraft: (Minimum Fuel Analysis for ΔSFC_{Cruise} = 0.1%).

Aircraft (Engine)	Range		Annual Fuel Savings/Aircraft	
	km	mi	Liters/AC/Yr.	Gals/AC/Yr.
DC-10-10 (CF6-6)	645	400	23,610	6,238
	1690	1050	29,280	7,736
	3700	2300	33,330	8,806
DC-10-30 (CF6-50)	805	500	18,480	4,882
	2735	1700	29,890	7,897
	6275	3900	58,260	15,392
B747-200 (CF6-50)	770	480	21,740	5,744
	3460	2150	38,580	10,193
	6195	3850	77,480	20,470

Table 10.3. Economic Assessment (Payback and ROI) of New CF6 Engine with New Front Mount for ΔSFC_{Cruise} = 0.1%.

(Medium Range, Minimum Fuel Analysis, Medium Fuel Price)

Aircraft (engine)	Fuel Price ¢/l (¢/gal)	Payback Period (years)	ROI (%)
DC-10-10 (CF6-6)	11.89 (45) (Domestic)	1.15	87
DC-10-30 (CF6-50)	14.53 (55) (International)	1.01	99
B747-200 (CF6-50)	11.89 (45) (Domestic)	1.17	85

11.0 SUMMARY OF RESULTS

As part of the NASA-sponsored Engine Component Improvement Program, a new engine thrust mount has been developed which reduces fuel consumption and performance degradation in current CF6 turbofan engines for today's wide-bodied commercial aircraft. This new front mount reduced the induced point loads in the high pressure compressor (HPC) casing, resulting in a decrease in localized case distortion. This allows the compressor to operate with reduced blade-to-case tip clearances, which improves HPC efficiency and overall engine performance.

The New Front Mount Program included a fatigue life analysis, correlation of analytical and empirical stress and deflection data, material fatigue tests, and component stress, deflection/distortion, and low cycle fatigue (endurance) tests. Contractor-funded engine tests and aircraft flight tests with the new front mount were also monitored.

During the stress test, brittle lacquer crack development identified critical stress areas of the new front mount hardware, and indicated areas where additional strain gauges should be located.

In the deflection/distortion tests, the new front mount reduced the maximum radial deflection at each stage of the HPC case due to simulated flight loads. With the titanium HPC case the maximum radial deflection was reduced 29% for the takeoff at rotation condition and 42% for the maximum static thrust condition. With the new front mount and the steel HPC case, a 33% and 41% reduction in the maximum radial deflection were measured under the same corresponding loads. However, the predicted HPC clearance improvement of 0.66-0.78 mm (0.026-0.031 in.) due to the new front mount was not fully realized. Preliminary predictions were based on early back-to-back tests conducted with a high thrust load, a zero G down load, and with a rather flexible engine configuration. Subsequent tests reported herein were conducted with a lower applied maximum thrust load, a 1G down load, and the actual DC-10 wing pylon, inlet and fan reverser. This provided a stiffer and more realistic baseline engine installation, which reduced the radial deflection with the original front mount, and decreased the potential and measured improvement about 50% due to the new front mount.

Performance improvements due to the reduced HPC radial clearances have been recalculated for a concentrically ground HPC casing, using semiempirical correlations of the effect of clearance on the efficiency and stall margin of the CF6-50 high pressure compressor, and the results are presented below:

	Calculated (Based on Measurements)	Predicted
ΔSFC Cruise	-0.1%	-0.3%
ΔEGT Takeoff	-1.5° C	-3.5° C
ΔStall Margin (Takeoff Flow)	+3.5 Pts. (16%)	
ΔStator Angle Margin (Takeoff)	+0.8 Degree (10%)	

Improvements in the stall and stator angle margins are significant for a new compressor and are even greater for a deteriorated engine.

Low cycle fatigue testing demonstrated the life capability of the new front mount hardware to be in excess of 35,000 simulated flight cycles. A failure of the new front mount platform attachment lug occurred after 47,130 cycles, or 12,130 cycles into the second lifetime test with about 20% higher loads. Failure of the mount platform attachment lug was caused by low cycle fatigue cracking initiated by fretting between the lip of the bolt-hole bushing and the mating upper surface of the attachment lug. Stress levels measured in the same region on a second new front mount were sufficiently low such that fatigue cracking would not have been initiated without the adverse effect of local surface fretting. To eliminate the fretting problem, the upper surface of the mount platform lug at the bushing lip interface was shot peened and coated with a sacrificial protective layer of plasma sprayed copper-nickel-indium, followed by a coating of molybdenum disulfide dry film lubricant. The newly-coated mount platform was assembled with the hardware from the previous cyclic endurance test. Low cycle fatigue testing was continued to complete the second lifetime cycles (70,000 total cycles) on all remaining new front mount hardware, and to complete one lifetime (35,000 cycles) on the reworked mount platform at the 20% higher loads of the second lifetime cycle.

Factory engine and flight test results have indicated trouble-free operation with the new front mount, and showed that the link loads agree closely with the calculations. The new front mount system subsequently has been certified by the FAA and may be incorporated in all new CF6-50 production engines.

The new front mount performance improvement concept offers an annual fuel savings per aircraft of 18,500 to 77,500 liters (4900 to 20,500 gal.), depending on the aircraft application and mission range, plus reduced maintenance costs resulting from higher stall margins which will reduce unscheduled removals.

APPENDIX A

QUALITY ASSURANCE

INTRODUCTION

The quality program applied to this contract is a documented system throughout the design, manufacture, and repair, overhaul, and modification cycle for gas turbine aircraft engines. The quality system has been constructed to comply with military specifications MIL-Q-9858A, MIL-I-45208, and MIL-C-45662 and Federal Aviation Regulations FAR-145 and applicable portions of FAR-21.

The quality system and its implementation are defined by a complete set of procedures which has been coordinated with the DOD and FAA, and which has their concurrence. In addition, the quality system as described in the quality program for this contract has been coordinated with NASA-Lewis Research Center. The following is a brief synopsis of the system.

QUALITY SYSTEM

The quality system is documented by operating procedures which coordinate the quality-related activities in the functional areas of Engineering, Manufacturing, Materials, Purchasing, and Engine Programs. The quality system is a single-standard system wherein all product lines are controlled by the common quality system. The actions and activities associated with determination of quality are recorded, and documentation is available for review.

Inherent in the system is the assurance of conformance to the quality requirements. This includes the performance of required inspections and tests. In addition, the system provides change control requirements which assure that design changes are incorporated into manufacturing, procurement and quality documentation, and into the products.

Measuring devices used for product acceptance and instrumentation used to control, record, monitor, or indicate results of readings during inspection and test are initially inspected and calibrated and periodically are reverified or recalibrated at a prescribed frequency. Such calibration is performed by technicians against standards which are traceable to the National Bureau of Standards. The gages are identified by a control number and are on a recall schedule for reverification and calibration. The calibration functions maintains a record of the location of each gage and the date it requires recalibration. Instructions implement the provisions of MIL-C-45662 and the appropriate FAR requirements.

Work sent to outside vendors is subject to quality plans which provide for control and appraisal to assure conformance to the technical requirements. Purchase orders issued to vendors contain a technical description of the work to be performed and instructions relative to quality requirements.

Engine parts are inspected to documented quality plans which define the characteristics to be inspected, the gages and tools to be used, the conditions under which the inspection is to be performed, the sampling plan, laboratory and special process testing, and the identification and record requirements.

Work instructions are issued for compliance by operators, inspectors, testers, and mechanics. Components part manufacture provides for laboratory overview of all special and critical processes, including qualification and certification of personnel, equipment and processes.

When work is performed in accordance with work instructions, the operator/inspector records that the work has been performed. This is accomplished by the operator/inspector stamping or signing the operation sequence sheet to signify that the operation has been performed.

Various designs of stamps are used to indicate the inspection status of work in process and finished items. Performance or acceptance of special processes is indicated by distinctive stamps assigned specifically to personnel performing the process or inspection. Administration of the stamp system and the issuance of stamps are functions of the Quality Operation. The stamps are applied to the paperwork identifying or denoting the items requiring control. When stamping of hardware occurs, only laboratory approved ink is used to assure against damage.

The type and location of other part marking is specified by the design engineer on the drawing to assure effects do not compromise design requirements and part quality.

Control of part handling, storage and delivery is maintained through the entire cycle. Engines and assemblies are stored in special dollies and transportation carts. Finished assembled parts are stored so as to preclude damage and contamination, openings are covered, lines capped and protective covers applied as required.

Nonconforming hardware is controlled by a system of material review at the component source. Both a Quality representative and an Engineering representative provide the accept (use-as-is or repair) decision. Nonconformances are documented, including the disposition and corrective action if applicable to prevent recurrence.

The system provides for storage, retention for specified periods, and retrieval of nonconformance documentation. Documentation for components is filed in the area where the component is manufactured/inspected.

A buildup record and test log is maintained for the assembly, inspection and test of each major component or engine. Component and engine testing is performed according to documented test instructions, test plans, and instrumentation plans. Test and instrumentation plans are submitted to NASA for approval prior to the testing.

Records essential to the economical and effective operation of the quality program are maintained, reviewed, and used as a basis for action. These records include inspection and test results, nonconforming material findings, laboratory analysis, and receiving inspection.

APPENDIX B

MARAGE 300 STEEL LOW CYCLE FATIGUE TEST

OBJECTIVE

The objective of the low cycle fatigue test program was to provide high confidence fatigue properties of the Marage 300 steel (AMS 6514) in order to support the limited data available during the design of the front mount link components.

TEST SPECIMENS

Test specimens (Figure B1) were machined from two heat batches of Marage 300 steel obtained from Universal Cyclops Speciality Steel Division.

TEST FACILITY

Tests were conducted at the General Electric Company's Material and Process Technology Laboratory, Evendale, Ohio, using the low cycle fatigue test facility described in Figure B2.

TEST DESCRIPTION

All tests were conducted at 400° F and at three different ratios of alternating to mean stress (A Ratio). Test parameters were:

Control Mode	Load
Stress Ratio (A)	As noted
Cyclic Frequency	20 C.P.M.
Wave Form	Triangular
Test Temperature	400° F
Specimen Dwg.	As noted

A total of 56 specimens were tested.

TEST RESULTS AND DISCUSSION

Results of all specimens tested are shown in the tables of Figures B3 through B6.

A comparison with the data used during the design of the steel supporting links for the front mount indicates that the original data was conservative by approximately 5%.

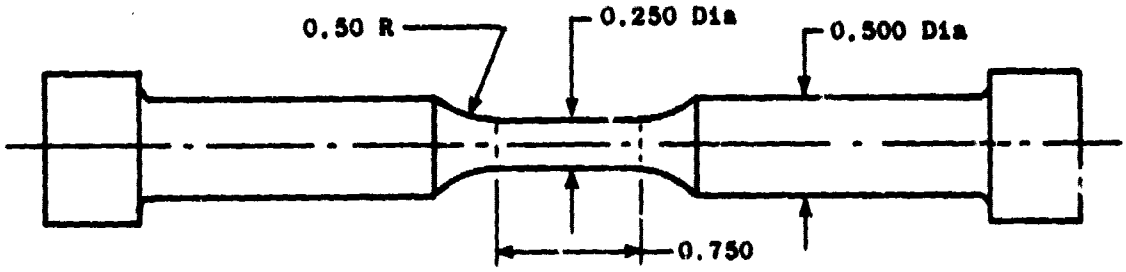

140P1 Smooth Specimen

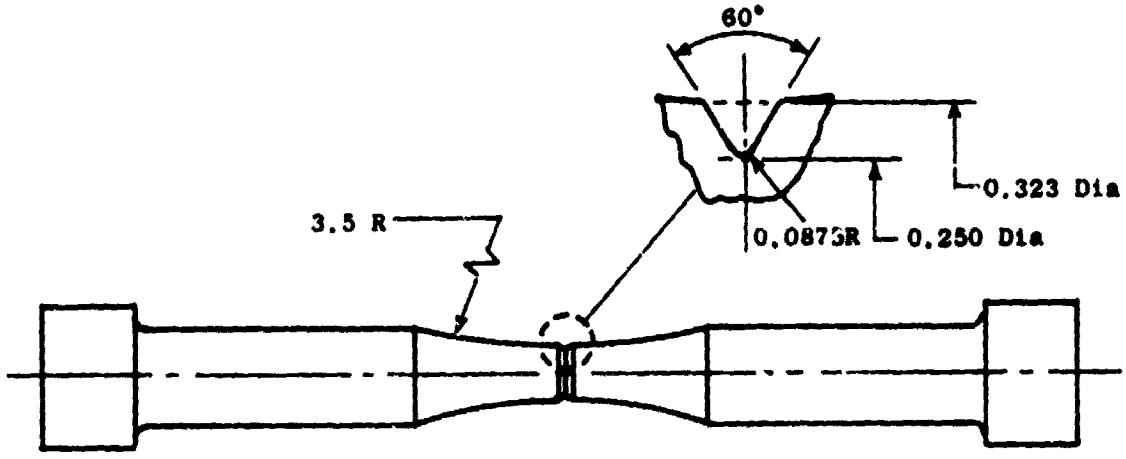

145P1 Notched Specimen

Dimensions in Inches

Figure B1. Fatigue Test Specimens.

Test Machine - M.T.S. Systems Corporation Fatigue Machine

Control Type - Closed-loop, servocontrolled, electrohydraulic

Control Modes - Constant load or strain amplitude (axial/axial, tension/compression)

Control Mode Waveform - Triangle, sine, ramp, square, trapezoidal

System Frequency Range - 0 to 1 Hz

Capacity:
- GE 1: +-20,000 lb. (2, 4, 10, 20,000 lb Ranges)
- GE 2: +-20,000 lb. (2, 4, 10, 20,000 lb Ranges)
- GE 3: +-10,000 lb. (1, 10,000 lb Ranges)

6-Inch Stroke
Maximum window opening - GE 1 & 2: 26" H x 24" W
GE 3: 6" H x 6 1/2" W

Test Temperature - R.T. and E.T., Induction or Resistance Heating

Special Features

1. Strip Chart recording of load and displacement.
2. Programmed stop at preset cycle count.
3. Crack initiation (N_i) is determined by various compliance change techniques.

Figure B2. Details of Test Facility.

Heat No.	Spec. No.	A Ratio	Stress, MPa (psi x 10^{-3}) Alternating		Maximum		Cycles to Initiation	Cycles to Failure	K_t	Dwg. No.
L3459K13	1	1.0	564.9	(127)	1334.5	(300)	Failed on Loading	255.2	1.0	140P1
	2	1.0	511.5	(115)	1023.1	(230)	7,618	7,970		
	3	1.0	444.8	(100)	889.6	(200)	N/A	126,854 →		
	4	1.0	489.3	(110)	978.6	(220)	18,292	19,048		
	5	1.0	476.0	(107)	951.9	(214)	9,660	10,318		
	6	2.5	489.3	(110)	685.0	(154)	21,776	22,568		
	7	2.5	511.5	(115)	716.2	(161)	16,254	17,254		
	8	2.5	522.7	(117.5)	731.7	(164.5)	18,290	19,070		
	9	2.5	476.0	(107)	666.3	(149.8)	27,178	27,820		
	10	.6	431.5	(97)	1150.7	(258.7)	6,832	7,460		
	20	"	533.8	(120)	533.8	(120)	N/A	137,746 →		
L3459K13	1	.6	400.4	(90)	1067.6	(240)	2,608	2,802	1.5	145P1
	2	.6	444.8	(100)	1186.3	(266.7)	1,549	1,929		
	3	.6	311.4	(70)	830.5	(186.7)	10,904	11,324		
	4	2.5	311.4	(70)	435.9	(98)	N/A	83,734 →		
	5	2.5	458.2	(103)	641.4	(144.2)	6,558	7,138		
	6	2.5	400.4	(90)	560.5	(126)	8,183	8,640		
	7	2.5	373.7	(84)	523.1	(117.6)	12,187	12,971		
	8	1.0	400.4	(90)	800.7	(180)	6,190	7,066		
	9	1.0	462.6	(104)	925.2	(208)	3,480	4,320		
	10	1.0	355.9	(80)	711.7	(160)	7,104	7,802		

Figure B3. Low Cycle Fatigue Test Results of Marage 300 Specimens at 400° F (Heat No. 1).

Heat No.	Spec. No.	A Ratio	Stress, MPa (psi x 10^{-3}) Alternating		Maximum		Cycles to Initiation	Cycles to Failure	K_t	Drawing Number
L4097	11	1.0	476.0	(107.0)	951.9	(214.0)	7,858	8,598	1.0	140P1
	12	1.0	524.9	(118.0)	1005.3	(226.0)	N/A	52,628→		
	13	2.5	556.0	(125.0)	778.4	(175.0)	16,406	17,528		
	14	2.5	467.1	(105.0)	653.9	(147.0)	N/A	117,743→		
	15	1.0	511.5	(115.0)	1023.1	(230.0)	N/A	24,150→		
	16	2.5	600.5	(135.0)	840.7	(189.0)	23,740	25,678		
	17	.6	378.1	(85.0)	1005.3	(226.0)	5,156	5,894		
	18	.6	355.9	(80.0)	947.5	(213.0)	6,326	6,566		
	19	.6	311.4	(70.0)	830.5	(186.7)	N/A	115,489→		
L4097	11	1.0	355.9	(80.0)	711.7	(160.0)	N/A	145,819→	1.5	145P1
	12	1.0	333.6	(75.0)	667.2	(150.0)	77,882	82,605		
	13	1.0	378.1	(85.0)	756.2	(170.0)	6,984	7,404		
	14	2.5	533.8	(120.0)	747.3	(168.0)	1,048	1,392		
	15	2.5	378.1	(85.0)	529.3	(119.0)	5,528	6,148		
	16	2.5	333.6	(75.0)	467.1	(105.0)	9,274	10,182		
	17	.6	311.4	(70.0)	830.5	(186.7)	2,500	2,669		
	18	.6	266.9	(60.0)	266.9	(160.0)	14,870	15,039		
	19	.6	244.7	(55.0)	652.6	(146.7)	9,336	9,770		
	20	2.5	311.4	(70.0)	435.9	(98.0)	N/A	9,558		

Figure B4. Low Cycle Fatigue Test Results of Marage 300 Steel at 400° F (Heat No. 2).

Heat No.	Spec. No.	A Ratio	Stress, MPa (psi x 10^{-3}) Alternating		Maximum		Cycles to Initiation	Cycles to Failure	K_t	Drawing Number
L4097	1	.6	400.3	(90.0)		--	*Failed in Button Head		1.0	104P1
	2	.6	422.6	(95.0)		--	*Failed in Button Head			
	3	.6	444.8	(100.0)		--	*Run at incorrect load	10,844		
	4	.6	425.2	(95.6)		--	*Mach. failed	62,862		
	5	.6	489.3	(110.0)		--	3,372	4,112		
	6	2.5	645.0	(145.0)	903.0	(203.0)	7,600	8,265		
	7	2.5	533.8	(120.0)	747.3	(168.0)	N/A	38,680→		
	8	2.5	711.7	(160.0)	996.4	(224.0)	5,149	5,859		
	9	1.0	511.5	(115.0)	1023.1	(230.0)	4,100	6,109		
	10	1.0	467.0	(105.0)		--	*Failed in Button Head			
	11	1.0	533.8	(120.0)	1067.6	(240.0)	25,431	26,894		
	12	.6	222.4	(50.0)	592.9	(133.3)		114,257→	1.5	145P1
	13	.6	231.3	(52.0)	617.0	(138.7)		138,820→		
	14	2.5	289.1	(65.0)	771.3	(173.4)		113,338→		
	15	1.0	444.8	(100.0)	889.6	(200.0)	4,900	5,158		
	16	1.0	378.1	(85.0)	756.2	(170.0)	9,550	10,867		
	17	2.5								
	18	2.5								

Figure B5. Low Cycle Fatigue Test Results of Marage 300 Specimens at 400° F (Heat No. 2).

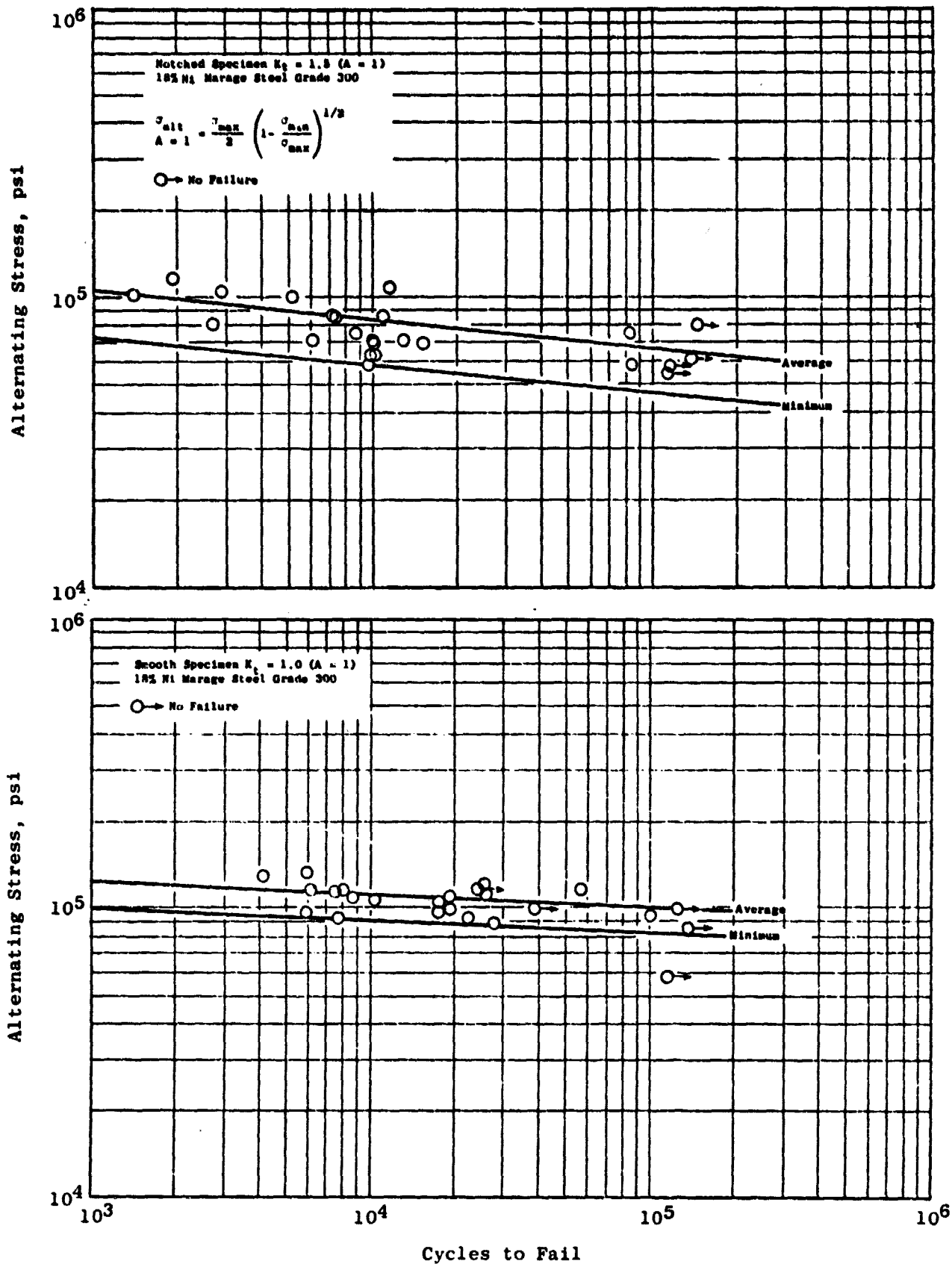

Figure B6. 400° F Fatigue Test Results.

APPENDIX C

REFERENCES

1. Fasching, W.A., "CF6 Jet Engine Performance Improvement Program, Task 1 - Feasibility Analysis," NASA Report CR-159450, March 1979.

APPENDIX D

SYMBOLS

EGT	Exhaust Gas Temperature (° C)
sfc	Specific Fuel Consumption kg/hrN (lb/hr lb)
HPC	High Pressure Compressor
PBP	Pay-Back Period
S/G	Strain Gage
ALF	AFT Looking Forward
RMS	Root Mean Square
ROI	Return on Investment

APPENDIX E

LIST OF ILLUSTRATIONS

LIST OF ILLUSTRATIONS (Continued)

LIST OF ILLUSTRATIONS (Continued)

LIST OF ILLUSTRATIONS (Continued)

LIST OF ILLUSTRATIONS (Continued)

LIST OF ILLUSTRATIONS (Continued)

LIST OF ILLUSTRATIONS (Concluded)